

EFFECT OF SKEW ON LIVE LOAD DISTRIBUTION IN INTEGRAL  
BRIDGES

A THESIS SUBMITTED TO  
THE GRADUATE SCHOOL OF NATURAL AND APPLIED SCIENCES  
OF  
MIDDLE EAST TECHNICAL UNIVERSITY

BY

MEHMET ALİ EROL

IN PARTIAL FULFILLMENT OF THE REQUIREMENTS  
FOR  
THE DEGREE OF MASTER OF SCIENCE  
IN  
ENGINEERING SCIENCES

DECEMBER 2009

Approval of the thesis:

**EFFECT OF SKEW ON LIVE LOAD DISTRIBUTION IN INTEGRAL  
BRIDGES**

submitted by **MEHMET ALİ EROL** in partial fulfillment of the requirements for  
the degree of **Master of Sciences in Engineering Sciences Department,**  
**Middle East Technical University** by,

Prof. Dr. Canan Özgen \_\_\_\_\_  
Dean, Graduate School of **Natural and Applied Sciences**

Prof. Dr. Turgut Tokdemir \_\_\_\_\_  
Head of Department, **Engineering Sciences Dept., METU**

Prof. Dr. Murat Dicleli \_\_\_\_\_  
Supervisor, **Engineering Sciences Dept., METU**

**Examining Committee Members:**

Prof. Dr. Turgut Tokdemir \_\_\_\_\_  
Engineering Sciences Dept., METU

Prof. Dr. Murat Dicleli \_\_\_\_\_  
Engineering Sciences Dept., METU

Prof. Dr. Zülfü Aşık \_\_\_\_\_  
Engineering Sciences Dept., METU

Assist. Prof. Dr. M. Tolga Yılmaz \_\_\_\_\_  
Engineering Sciences Dept., METU

Assoc. Prof. Dr. Oğuzhan Hasańçebi \_\_\_\_\_  
Civil Engineering Dept., METU

**Date:** \_\_\_\_\_

**I hereby declare that all information in this document has been obtained and presented in accordance with academic rules and ethical conduct. I also declare that, as required by these rules and conduct, I have fully cited and referenced all material and results that are not original to this work.**

Name, Last name : Mehmet Ali Erol

Signature :

# **ABSTRACT**

## **EFFECT OF SKEW ON LIVE LOAD DISTRIBUTION IN INTEGRAL BRIDGES**

Erol, Mehmet Ali

M.S., Department of Engineering Sciences

Supervisor: Prof. Dr. Murat Dicleli

December 2009, 145 pages

Structural analysis of highway bridges using complicated 3-D FEMs to determine live load effects in bridge components is possible due to the readily available computational tools in design offices. However, building such complicated 3-D FEMs is tedious and time consuming. Accordingly, most design engineers prefer using simplified 2-D structural models of the bridge and live load distribution equations (LLDEs) available in current bridge design codes to determine live load effects in bridge components. Basically, the live load effect obtained from a 2-D model is multiplied by a factor obtained from the LLDE to calculate the actual live load effect in a 3-D structure. The LLDE available in current bridge design codes for jointed bridges were also used for the design of straight and skewed integral bridges

by bridge engineers. As a result, these bridges are either designed conservatively leading to additional construction cost or unconservatively leading to unsafe bridge designs. Recently, LLDEs for integral bridges (IBs) with no skew are developed. To use these equations for skewed integral bridges (SIBs) a correction factor is needed to multiply these equations to include the effect of skew. Consequently, in this research study, skew correction factors for SIBs are developed. For this purpose, finite element models of 231 different three dimensional and corresponding two dimensional structural models of SIBs are built and analyzed under live load. The analyses results reveal that the effect of skew on the distribution of live load moment and shear is significant. It is also observed that skew generally tends to decrease live load effects in girders and substructure components of SIBs. Using the analyses results, analytical equations are developed via nonlinear regression techniques to include skew effects in the LLDEs developed for straight IBs. The developed skew correction factors are compared with FEAs results. This comparison revealed that the developed skew correction factors yield a reasonably good estimate of the reduction in live load effects due to the effect of skew.

Keywords: Skew, Skew Correction Factor, Integral Bridge, Live Load Distribution Factor

# ÖZ

## İNTEGRAL KÖPRÜLERDE VEREVİN HAREKETLİ YÜK DAĞILIMINA ETKİSİ

Erol, Mehmet Ali

Yüksek Lisans, Mühendislik Bilimleri Bölümü

Tez Yöneticisi: Prof. Dr. Murat Dicleli

Aralık 2009, 145 sayfa

Günümüzde köprü elemanlarındaki hareketli yük etkisinin üç boyutlu sonlu elemanlar modelleri ile yapılması tasarım ofislerindeki mevcut programlarla mümkündür. Fakat, bu tür üç boyutlu komplike modellerin yapılması zor ve zaman alıcı bir süreçtir. Bu sebeple, tasarım mühendislerinin çoğu köprü elemanlarındaki hareketli yük etkilerini belirlemek için sadeleştirilmiş iki boyutlu modelleri ve standartlarda yer alan hareketli yük dağılım katsayılarını tercih etmektedir. Bu yöntemde, basit iki boyutlu bir modelden elde edilen hareketli yük etkileri hareketli yük dağılım katsayısı ile çarpılarak üç boyutlu yapıdaki hareketli yük etkileri hesaplanır. Günümüz standartlarında klasik köprüler için bulunan bu hareketli yük dağılım denklemleri köprü mühendisleri tarafından düz ve vevli integral köprülerin tasarımında da kullanılmıştır. Sonuç olarak, bu formüllerle tasarlanan integral köprüler ya emniyetli tarafta

kalınarak aşırı maliyetli, ya da emniyetsiz tarafta inşa edilmiştir. Yakın zamanda, verevsiz integral köprüler için hareketli yük dağılım katsayıları geliştirilmiştir. Bu denklemleri verevli integral köprülerde kullanmak için verev etkisini bu formüllere dahil edecek bir düzeltme katsayısı gerekliliği ortaya çıkmıştır. Sonuç olarak, bu çalışmada verevli integral köprüler için düzeltme katsayıları geliştirilmiştir. Bu amaçla 231 farklı üç boyutlu ve aynı sayıda iki boyutlu verevli integral köprü modeli oluşturulmuş ve hareketli yük altında analiz edilmiştir. Analiz sonuçları, verevin hareketli yük momenti ve kesme kuvveti üzerinde kayda değer bir etkisinin olduğunu açığa çıkarmıştır. Aynı zamanda, verev etkisinin genel olarak verevli integral köprülerin elemanlarının hareketli yük momentini ve kesme kuvvetini azaltma eğiliminde olduğu gözlemlenmiştir. Analiz sonuçları kullanılarak lineer olmayan regresyon teknikleri ile integral köprüler için geliştirilen hareketli yük dağılım katsayılarına verev etkisini dahil etmek için analitik denklemler elde edilmiştir. Geliştirilen katsayılar sonlu elemanlar yöntemi ile elde edilen sonuçlar ile karşılaştırılmıştır. Bu karşılaştırma, geliştirilen formüllerin verevli integral köprü elemanlarındaki hareketli yük etkilerini yeterince iyi tahmin ettiğini göstermiştir.

Anahtar Kelimeler: Verev, Verev Düzeltme Katsayısı, İntegral Köprü, Hareketli Yük Dağılım Katsayısı

To My Parents

## **ACKNOWLEDGEMENTS**

I would like to express my gratitude to my supervisor Prof. Dr. Murat Dicleli for his guidance, support and encouragements throughout the work. This thesis would not have been possible without his guidance and persistent help.

I would like to thank Semih Erhan and Cengizhan Durucan for their kind support, criticism and advice on the thesis.

I owe my gratitude to my friends Elif Yurdanur Taşel and Erdiñç Taşel for their encouragement, support, criticism and advice on thesis.

I would like to thank all people who have helped and inspired me during this study. I would also like to thank my workfellows Ertuğrul Bozkurt, Emre Arlı and Meliha Ün for their patience and understanding.

My deepest gratitude goes to my family for their unflagging love and support throughout my life. I am indebted to my mother, Lütfiye Güler Erol and father, Muzaffer Erol for their patience and sensibility all through this work. I would also thank to my little brother Ender Erol for his patience at not playing games and moral support throughout this work.

# TABLE OF CONTENTS

ABSTRACT.....	iv
ÖZ.....	vi
ACKNOWLEDGEMENTS.....	ix
TABLE OF CONTENTS.....	x
LIST OF TABLES.....	xiii
LIST OF FIGURES.....	xiv
LIST OF SYMBOLS AND ABBREVIATIONS.....	xxi
CHAPTERS	
1. INTRODUCTION.....	1
1.1 Introduction.....	1
1.2 Research Objectives and Scope.....	4
1.3 Research Outline.....	6
1.4 Review of Previous Studies.....	7
1.4.1 Live Load Distribution Equations.....	7
1.4.2 Integral Bridges.....	9
1.4.3 Skewed Integral Bridges.....	10
1.4.4 Modeling.....	11
1.4.5 Soil-Bridge Interaction.....	13
2. SELECTION OF PARAMETERS AND MODELING.....	15
2.1 Selection of Parameters.....	15

2.2 Modeling.....	19
2.2.1 Superstructure Modeling for Integral Bridges .....	19
2.2.2 Substructure Modeling for Integral Bridges .....	25
2.2.3 Modeling of Soil-Structure Interaction for Integral Bridges .....	25
2.2.4 Two Dimensional Structural Model.....	32
3. LOADING .....	33
3.1 Live Load Model .....	33
3.2 Estimation of Most Critical Live Load Effects.....	33
3.3 Determination of the Most Critical Loading Pattern .....	40
3.3.1 General Information about Loading Patterns.....	40
3.3.2 Determination of Most Critical Loading Pattern .....	42
4. AUTOMATED ANALYSES PROCEDURE .....	53
4.1 General.....	53
4.2 Properties of the IO Worksheet .....	53
4.2.1 Parameters Used for Calculation .....	55
4.2.2 Calculation Procedure .....	56
4.3 Visual Basic Program .....	57
5. PARAMETRIC STUDY AND EVALUATION OF RESULTS .....	62
5.1 General.....	62
5.2 Calculation of Live Load Distribution Factors .....	62
5.3 Evaluation of Analyses Results with Respect to the Skew Angle ....	63
5.4 Evaluation of Analyses Results with Respect to the Other Parameters .....	70
6. SKEW CORRECTION FACTORS FOR SIBs.....	92

6.1 Determination of the Dominant Parameters for the Derivation of SCFs .....	92
6.2 Formulation of SCFs for SIBs.....	106
6.2.1 SCFs for Interior Girders .....	107
6.1.2 SCFs for Exterior Girders .....	111
6.2.3 SCFs for Substructure.....	111
6.2 Comparison and Verification of SCFs.....	113
7. CONCLUSIONS .....	132
REFERENCES .....	134
APPENDIX.....	142
A LLDEs for Straight Integral Bridges.....	142
A.1 LLDEs for Interior Girders .....	142
A.2 LLDEs for Exterior Girders .....	142
A.3 LLDEs for Substructure.....	143
A.4 An Example for the Calculation of LLDF Including Skew Effects ..	144

## LIST OF TABLES

### TABLES

Table 1: Parameters considered in the analyses .....	17
Table 2: Analysis sets considered in the analyses.....	18
Table 3: Difference of parallel and square modeling technique for constant model .....	23
Table 4: Comparison of frame results with frame and shell results for square and parallelogram modeling of deck slab.....	24
Table 5: Sample of transverse positions and number of trucks for the maximum live load effects of bridge with 50° skew where two or more design lanes are loaded .....	37
Table 6: Comparison of applicability of maximum live load effects for skew 30 with respect to pile spacing .....	51
Table 7: Comparison of applicability of maximum live load effects for skew 60 with respect to abutment height .....	52
Table 8: Comparison of applicability of maximum live load effects for skew 60 with respect to pile spacing .....	52
Table 9: Comparison of applicability of maximum live load effects for skew 60 with respect to abutment height .....	52
Table 10. Effect of skew and selected parameters on $R_s$ where two or more design lanes are loaded.....	106
Table 11. Averages and standard deviations for developed SCFs .....	114

## LIST OF FIGURES

### FIGURES

Figure 1. Integral and conventional bridge components (Dicleli and Erhan 2010).....	2
Figure 2. (a) A typical single span IB (Dicleli and Erhan 2008a), (b) Typical slab-on-girder bridge cross-section, (c) Plan view of a SIB.....	5
Figure 3. Finite element models of SIBs (a) 2-D (Dicleli and Erhan 2008a), (b) 3-D .....	21
Figure 4. FEMs of slab-on-girder bridge superstructures proposed by (a) Hays et al (Hays et al. 1986), (b) Imbsen and Nutt (Imbsen and Nut, 1978), (c) Brockenbrough (Brockenbrough 1986), (d) Tarhini and Frederick (Tarhini and Frederick 1992).....	22
Figure 5. Deformed shape of an IB under live load (Dicleli and Erhan 2008a) .....	26
Figure 6. (a) Idealization of a typical P-Y curve for soil modeling (Dicleli and Erhan 2008a), (b) $c_u$ versus $\epsilon_{50}$ plot (Evans 1982).....	30
Figure 7. Cross section of a four girder bridge and a strip used in 2-D modeling .....	32
Figure 8. (a) Minimum clearances for design truck loading for a typical slab-on-girder bridge cross-section (Dicleli and Erhan 2008a), (b) Truck loading considered in analyses .....	34
Figure 9. (a) Location of calculated maximum girder shear ( $V_g$ ) and moment ( $M_g$ ) for IB (Dicleli and Erhan 2008a), (b) A sample of transverse position of design trucks to produce maximum moment in the hatched girders for the cases where two- and three-lanes are loaded (Dicleli and Erhan 2008a)....	36

Figure 10. 3-D and 2-D models of bridges with truck loading (grey truck shows strip 1, black truck shows strip 2) (a) Straight (b) Skewed .....	39
Figure 11. Sample of two lane truck loading pattern for bottom, center, top and diagonal loading patterns (distance of trucks to bridge abutment for straight and diagonal loading patterns shown with d1, d2 and d3).....	39
Figure 12. Effect of skew on truck loading patterns for a sample bridge model .....	42
Figure 13. Girder moment comparison for 6 girder model with 30° skew and B-C-T-D loading patterns for different trucks .....	45
Figure 14. Abutment moment comparison for 6 girder model with 30° skew and B-C-T-D loading patterns for different trucks.....	46
Figure 15. Abutment shear comparison for 6 girder model with 30° skew and B-C-T-D loading patterns for different trucks .....	46
Figure 16. Pile moment comparison for 6 girder model with 30° skew and B-C-T-D loading patterns for different trucks .....	47
Figure 17. Pile shear comparison for 6 girder model with 30° skew and B-C-T-D loading patterns for different trucks.....	47
Figure 18. Maximum values of bottom, center, top and diagonal loading patterns for SIB with skew 30° .....	48
Figure 19. Maximum values of bottom, center, top and diagonal loading patterns for SIB with skew 50° .....	49
Figure 20. Maximum values of bottom, center, top and diagonal loading patterns for SIB where two or more design lanes are loaded 30° skew .....	50
Figure 21. Maximum values of bottom, center, top and diagonal loading patterns for SIB where two or more design lanes are loaded 50° skew .....	51
Figure 22. The IO worksheet formed for the calculation of values and coordinates of truck load.....	54
Figure 23. Reference point for different skews (dashed lines represents the skewed bridge deck for different skews) .....	55

Figure 24. Flowchart of Visual Basic program used for each analysis .....	59
Figure 25. Sample for stress averaging method .....	60
Figure 26. Section cut for frame and shell elements .....	61
Figure 27. Abutment moment for IBs (a) for straight IB (b) for SIB .....	64
Figure 28. Effect of skew on LLDFs of SIBs for Analysis Set 1 where two or more design lanes are loaded.....	65
Figure 29. Effect of skew on LLDFs of SIBs for Analysis Set 1 where one design lane is loaded .....	66
Figure 30. Effect of skew on LLDFs of SIBs for Analysis Set 9 where two or more design lanes are loaded.....	68
Figure 31. Effect of skew on LLDFs of SIBs for Analysis Set 9 where one design lane is loaded .....	69
Figure 32. Effect of skew on LLDFs of SIBs for Analysis Set 2 where two or more design lanes are loaded.....	74
Figure 33. Effect of skew on LLDFs of SIBs for Analysis Set 3 where two or more design lanes are loaded.....	75
Figure 34. Effect of skew on LLDFs of SIBs for Analysis Set 4 where two or more design lanes are loaded.....	76
Figure 35. Effect of skew on LLDFs of SIBs for Analysis Set 6 where two or more design lanes are loaded.....	77
Figure 36. Effect of skew on LLDFs of SIBs for Analysis Set 7 where two or more design lanes are loaded.....	78
Figure 37. Effect of skew on LLDFs of SIBs for Analysis Set 2 where one design lane is loaded .....	79
Figure 38. Effect of skew on LLDFs of SIBs for Analysis Set 3 where one design lane is loaded .....	80
Figure 39. Effect of skew on LLDFs of SIBs for Analysis Set 4 where one design lane is loaded .....	81

Figure 40. Effect of skew on LLDFs of SIBs for Analysis Set 6 where one design lane is loaded .....	82
Figure 41. Effect of skew on LLDFs of SIBs for Analysis Set 7 where one design lane is loaded .....	83
Figure 42. Effect of skew on LLDFs of SIBs for Analysis Set 5 where two or more design lanes are loaded.....	84
Figure 43. Effect of skew on LLDFs of SIBs for Analysis Set 5 where one design lane is loaded .....	85
Figure 44. Effect of skew on LLDFs of SIBs for Analysis Set 8 where two or more design lanes are loaded.....	86
Figure 45. Effect of skew on LLDFs of SIBs for Analysis Set 8 where one design lane is loaded .....	87
Figure 46. Effect of skew on LLDFs of SIBs for Analysis Set 10 where two or more design lanes are loaded.....	88
Figure 47. Effect of skew on LLDFs of SIBs for Analysis Set 10 where one design lane is loaded .....	89
Figure 48. Effect of skew on LLDFs of SIBs for Analysis Set 11 where two or more design lanes are loaded.....	90
Figure 49. Effect of skew on LLDFs of SIBs for Analysis Set 11 where one design lane is loaded .....	91
Figure 50. Effect of skew on $R_s$ for Analysis Set 1 where two or more design lanes are loaded .....	95
Figure 51. Effect of skew on $R_s$ for Analysis Set 2 where two or more design lanes are loaded .....	96
Figure 52. Effect of skew on $R_s$ for Analysis Set 3 where two or more design lanes are loaded .....	97
Figure 53. Effect of skew on $R_s$ for Analysis Set 4 where two or more design lanes are loaded .....	98

Figure 54.Effect of skew on $R_s$ for Analysis Set 5 where two or more design lanes are loaded .....	99
Figure 55.Effect of skew on $R_s$ for Analysis Set 6 where two or more design lanes are loaded .....	100
Figure 56.Effect of skew on $R_s$ for Analysis Set 7 where two or more design lanes are loaded .....	101
Figure 57.Effect of skew on $R_s$ for Analysis Set 8 where two or more design lanes are loaded .....	102
Figure 58.Effect of skew on $R_s$ for Analysis Set 9 where two or more design lanes are loaded .....	103
Figure 59.Effect of skew on $R_s$ for Analysis Set 10 where two or more design lanes are loaded .....	104
Figure 60. Effect of skew on $R_s$ for Analysis Set 11 where two or more design lanes are loaded.....	105
Figure 61. $R_s$ versus $\tan\theta$ .....	108
Figure 62. $R_2$ versus $S/N_b$ .....	109
Figure 63. Plot of FEAs results, proposed SCFs and AASHTO SCFs for interior girder moment of selected models where two or more lanes are loaded.....	115
Figure 64. Plot of FEAs results, proposed SCFs and AASHTO SCFs for interior girder moment of selected models where only one design lane is loaded.....	116
Figure 65. Plot of FEAs results, proposed SCFs and AASHTO SCFs for interior girder shear of selected models where two or more lanes are loaded .....	117
Figure 66. Plot of FEAs results, proposed SCFs and AASHTO SCFs for exterior girder shear of selected models where two or more lanes are loaded .....	118

Figure 67. Plot of FEAs results, proposed SCFs and AASHTO SCFs for exterior girder shear of selected models where only one design lane is loaded .....	119
Figure 68. Plot of FEAs results, proposed SCFs and AASHTO SCFs for abutment moment of selected models where two or more lanes are loaded .....	120
Figure 69. Plot of FEAs results, proposed SCFs and AASHTO SCFs for abutment moment of selected models where only one design lane is loaded .....	121
Figure 70. Plot of FEAs results, proposed SCFs and AASHTO SCFs for abutment shear of selected models where two or more lanes are loaded .	122
Figure 71. Plot of FEAs results, proposed SCFs and AASHTO SCFs for abutment shear of selected models where only one design lane is loaded	123
Figure 72. Plot of FEAs results, proposed SCFs and AASHTO SCFs for pile moment of selected models where two or more lanes are loaded .....	124
Figure 73. Plot of FEAs results, proposed SCFs and AASHTO SCFs for pile moment of selected models where only one design lane is loaded .....	125
Figure 74. Plot of FEAs results, LLDEs and LLDEs multiplied by SCFs for interior girder moment of selected models where two or more lanes are loaded .....	126
Figure 75. Plot of FEAs results, LLDEs and LLDEs multiplied by SCFs for interior girder shear of selected models where two or more lanes are loaded .....	127
Figure 76. Plot of FEAs results, LLDEs and LLDEs multiplied by SCFs for exterior girder shear of selected models where two or more lanes are loaded .....	128
Figure 77. Plot of FEAs results, LLDEs and LLDEs multiplied by SCFs for abutment moment of selected models where two or more lanes are loaded .....	129

Figure 78. Plot of FEAs results, LLDEs and LLDEs multiplied by SCFs for abutment shear of selected models where two or more lanes are loaded . 130

Figure 79. Plot of FEAs results, LLDEs and LLDEs multiplied by SCFs for pile moment of selected models where two or more lanes are loaded ..... 131

## LIST OF SYMBOLS AND ABBREVIATIONS

$A$	: Cross-sectional area of the girder
AASHTO	: Association State Highway Transportation Officials, 2007
$c_u$	: Undrained shear strength
$D$	: A constant which depends on the type of the bridge superstructure
$d_p$	: Pile width
$e_g$	: Distance between the centers of gravity of the girder and the slab
$E_s$	: Secant soil modulus
$\epsilon_{50}$	: Soil strain at 50% of ultimate soil resistance
FEA	: Finite Element Analysis
FEM	: Finite Element Model
GT	: Girder type
$h$	: Tributary length between the nodes along the pile
$H_a$	: Height of the abutment
$H_c$	: The abutment height measured from deck soffit
$I$	: The moment of inertia of the girder
$I_c$	: Moment of inertia of the composite slab-on-girder section

$I_g$	: Moment of inertia of girder
$I_s$	: Moment of inertia of the slab tributary to each girder
IB	: Integral Bridge
$k$	: Backfill pressure coefficient
$K_g$	: The parameter representing the longitudinal stiffness of the composite slab-on-girder section of the bridge
$k_{sh}$	: Coefficient of subgrade reaction modulus for the granular backfill
$L$	: Span length
LLDE	: Live Load Distribution Equation
LLDF	: Live Load Distribution Factor
$M_a$	: Abutment moment
$M_g$	: Girder moment
$M_p$	: Pile moment
$n$	: The ratio of the modulus of elasticity of the girder material to that of the slab material
$N_b$	: Number of beams
$N_T$	: Number of trucks
OAPI	: SAP2000 feature (Open Application Interface)
$P$	: Lateral soil resistance per unit length of pile
$Q_u$	: Ultimate soil resistance per unit length of pile

$R_s$	: The ratio of the LLDFs for various skews to that for zero skew angle
$S$	: Girder spacing
SCF	: Skew Correction Factor
SIB	: Skewed Integral Bridge
$S_p$	: Pile spacing
$t$	: Slab thickness
$V_a$	: Abutment shear
$V_g$	: Girder shear
$V_p$	: Pile shear
$w$	: Abutment width
$W$	: Bridge width
$x$	: Transverse position of first truck from the slab edge
$Y$	: Lateral deflection
$z$	: The distance from the top of the abutment
$\Delta_{50}$	: Deflection at 50% of the ultimate soil resistance
$\gamma$	: Backfill unit weight

# CHAPTER 1

## INTRODUCTION

### 1.1 Introduction

An integral bridge (IB) is one in which the continuous deck and the abutments are cast monolithically to form a rigid frame structure as shown in Figure 1. The main difference between a conventional jointed bridge (bridges with expansion joints) and an IB is at the abutments. In IBs, the abutments are generally thinner than those of conventional jointed bridges and are supported on a single row of steel H-piles to provide the required lateral flexibility for accommodating the longitudinal bridge movements due to daily and seasonal temperature variations. IBs have many advantages when compared to conventional jointed bridges. The main advantages of IBs are:

- i. The use of integral abutments eliminates the need for deck joints and expansion bearings which are expensive to buy and install. Elimination of these elements leads to significant cost savings for the construction of bridges.
- ii. Conventional jointed bridge abutments are generally supported by multiple rows of piles; on the other hand; IB abutments are supported by single row of piles. The reduction of number of piles lowers the construction costs considerably.

- iii. Presence of deck joints accelerates the deterioration of the bearings and the substructures by allowing water to leak through expansion joints. The expensive maintenance costs in conventional jointed bridges (Wolde-Tinsae, et al. 1988a, 1988b; Burke 1988, 1990a; Steiger, 1993) are reduced by the elimination of expansion joints in IBs.
- iv. Since the design of IBs is not as complex as conventional bridges, it is easier to make simple structural modifications like widening of the bridge.
- v. Stability, durability and life expectancy of bridges are improved by the elimination of joints.
- vi. Under seismic loading, IBs generally exhibit better overall structural performance (Khan, 2004; Sritharan, et al., 2005).

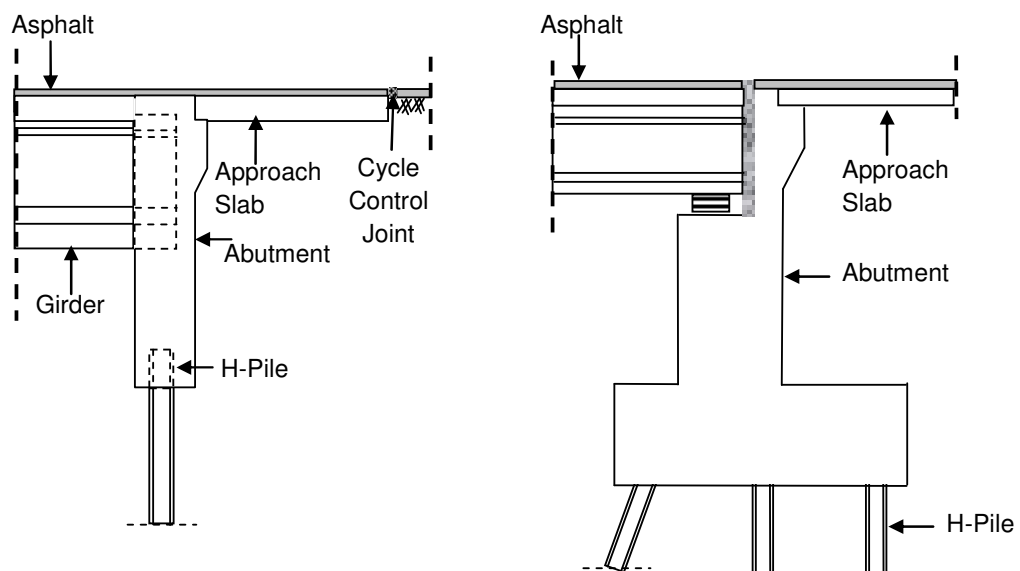


Figure 1. Integral and conventional bridge components (Dicleli and Erhan 2010)

As far as the stability, durability and economy of bridges are concerned, IB concept becomes a viable alternative to conventional jointed bridges. Consequently, IBs are becoming very popular and they are commonly used as an alternative to conventional jointed bridges in most parts of USA, Canada and Europe (Wolde-Tinsae, et al. 1988a, 1988b; Burke 1990a, 1990b, 1994; Soltani and Kukreti 1992; Dicleli 2000). When the geometry does not allow for building a straight IB, skewed IBs (SIBs) are designed. However, standard design methods for IBs have not been fully established yet. Thus, many practicing engineers use the provisions for regular jointed bridges in current bridge design specifications such as AASHTO LRFD (American Association State Highway Transportation Officials Load and Resistance Factor Design, 2007) to design IBs. This also includes using such provisions for the design of IB girders and substructure components such as abutments and piles under live load effects.

Most bridge engineers use simplified two-dimensional (2-D) structural models and live load distribution equations (LLDEs) readily available in bridge design specifications to determine live load effects in bridge girders. The LLDEs in AASHTO LRFD were basically developed for straight jointed bridge girders (skew correction factors (SCF) are used for SIBs) where the superstructure is separated from the abutments via expansion joints. Therefore, these LLDEs are not suitable for the design of substructure components of IBs under live load effects. Furthermore, in the case of IBs, the monolithic construction of the superstructure-abutment joint forces the superstructure and the abutments to act together under live load effects. The continuity of the superstructure-abutment joint in IBs is found to improve the distribution of live load moment among the girders especially for short spans (Dicleli and Erhan 2008a). Accordingly, using the LLDEs in AASHTO LRFD Specifications for the design of IB girders may result in incorrect estimates of live load effects.

To address these problems, recently, Dicleli and Erhan (2009a) conducted an extensive research study where they obtained LLDEs for the design of IB girders and substructure components. In the LLDEs developed by Dicleli and Erhan, the effect of skew was totally neglected. Therefore, these LLDEs are not suitable for SIBs. Accordingly, SCFs that will be used with the LLDEs developed by Dicleli and Erhan (Dicleli and Erhan 2008a, 2009a) are urgently needed to estimate live load effects in SIB components.

## **1.2 Research Objectives and Scope**

The objective of the present research study is to develop SCFs for LLDEs of IBs. This research study is focused on symmetrical, single span slab-on-girder IBs (Figure 2 (a)) with skews varying from 0 to 60 degrees. IB girders are assumed to be commonly used AASHTO type prestressed concrete girders. A typical single-span IB cross-section with such girders is shown in Figure 2 (b). End-bearing steel H-piles, which are typically used in IB construction, are used to support the abutments of IBs. A moment connection is assumed between the piles and the abutment as well as between the superstructure and the abutment per current state of design practice (Husain and Bagnariol 1996). Granular material typically used in IB construction is assumed for the backfill behind the abutments while cohesive soil (clay) is assumed for the pile foundations (Figure 2 (a)).

Moreover, the scope of this research study is limited to short to medium length IBs where the superimposed dead load and thermal effects are assumed to be less significant compared to live load effects. Consequently, yielding of the piles is not anticipated under total load effects and the behavior of the backfill and foundation soil remains within the linear elastic range as proven by an earlier research study (Dicleli and Erhan 2008b) due to the small lateral displacements of the abutments and piles under live load

effects. This also ensures that potential formation of a gap behind the abutment due to cyclic thermal movements is negligible.

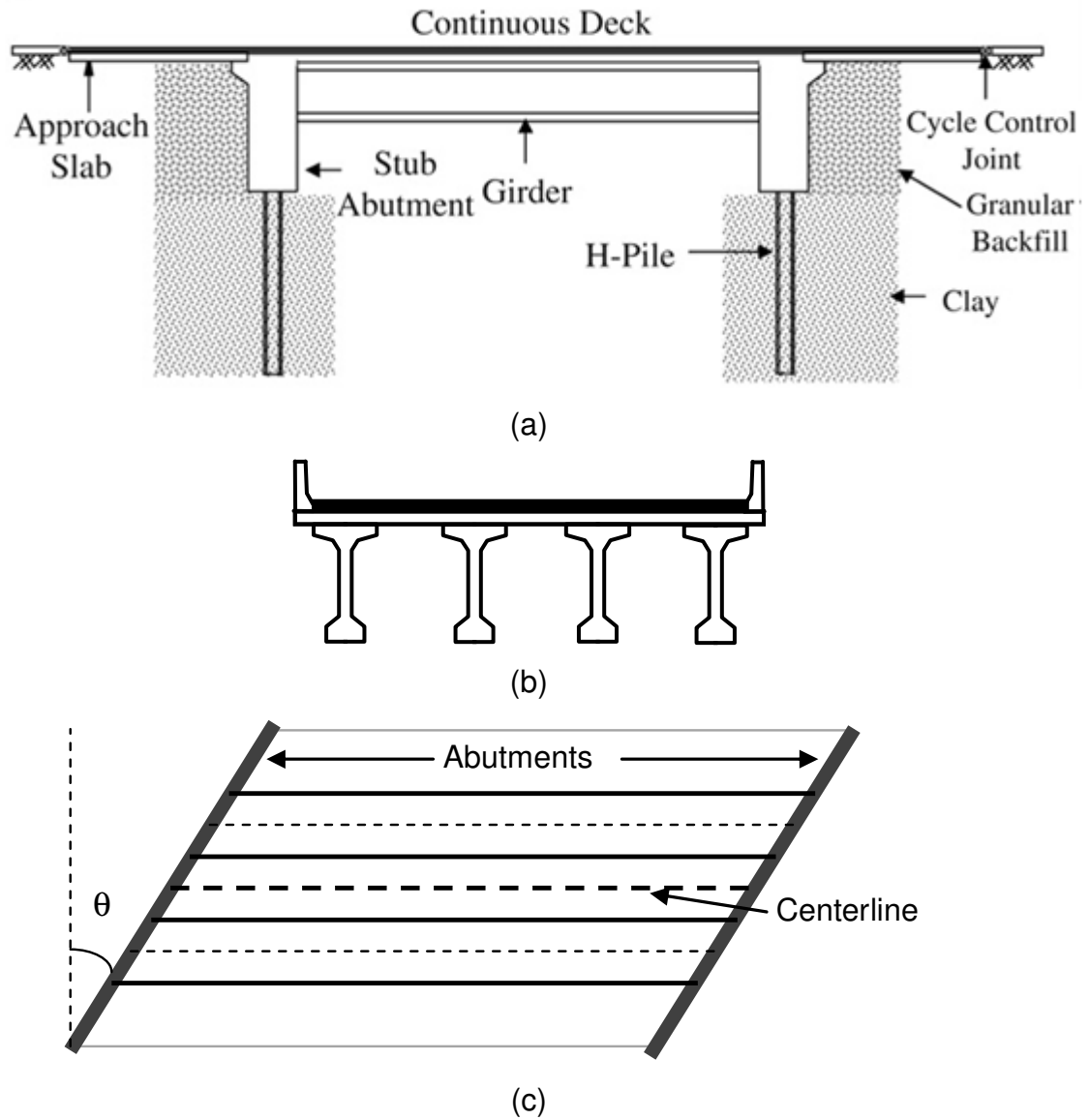


Figure 2. (a) A typical single span IB (Dicleli and Erhan 2008a), (b) Typical slab-on-girder bridge cross-section, (c) Plan view of a SIB.

### **1.3 Research Outline**

This research is composed of six main phases:

- i. In the first phase of the study, an extensive literature review on the development of the LLDEs for conventional jointed bridges and IBs is carried out. Next, a literature review on finite element modeling techniques for standard and skewed bridges is also carried out. The knowledge gathered from this literature review is used to built finite element models (FEMs) of SIBs to determine the live load effects in the components of such bridges as precisely as possible.
- ii. In the second phase of the research study, sensitivity analyses are performed to investigate the effect of finite element modeling techniques on the accuracy of the analyses results under AASHTO live load. This phase also includes the determination of geometric, structural and geotechnical parameters, which are used in finite element analyses (FEAs), to obtain SCFs to accurately estimate live load effects in the components of SIBs. A set of 2-D and three dimensional (3-D) SIB models is then built using the finite element based program SAP2000 with regards to the determined parameters to obtain SCFs.
- iii. This phase of the research study includes the determination of the truck positions and loading patterns to estimate the maximum live load effects in SIB components.

- iv. In the fourth phase of this research study, a visual basic program is developed to prepare input data for the FEMs and extract output data from the FEAs of the same models of SIBs.
- v. In the fifth phase of this research study, 3-D and 2-D FEAs of the aforementioned SIB models with respect to the selected parameters are analyzed under AASHTO live load. From the analysis results the maximum live load moments and shears in the components of SIBs are determined. The live load effects obtained from 3-D models are then divided by the values obtained from the corresponding 2-D models to calculate the live load distribution factors (LLDFs).
- vi. In the sixth phase of the research study, SCFs are formulated for the LLDEs developed by Dicleli and Erhan to accurately determine live load effects in SIB components.

## **1.4 Review of Previous Studies**

### ***1.4.1 Live Load Distribution Equations***

Structural analysis of highway bridges using complicated 3-D FEMs to determine live load effects in bridge components is possible due to the readily available computational tools in design offices. However, building such complicated 3-D FEMs is tedious and time consuming. Accordingly, most design engineers prefer using simplified 2-D structural models of the bridge and LLDEs available in current bridge design codes to determine live load effects in bridge components. The maximum moment and shear of an individual bridge member is then determined by multiplying the maximum

moment and shear obtained from 2-D frame analysis of the bridge under truck load by the LLDEs available in design codes (AASHTO 2007).

The AASHTO Standard Specifications for Highway Bridges' simple  $S/D$  formulae have been used for an extended period of time as LLDFs in most common cases for calculating the live load bending moment and shear in bridge girder design; where  $S$  is the girder spacing and  $D$  is a constant which depends on the type of the bridge superstructure. The AASHTO Standard Specifications for Highway Bridges have contained LLDFs since 1931. The earlier versions of LLDFs were based on the work done by Westergaard (1930) and Newmark (1948), but the factors were modified as new research results became available (Barr et al. 2001). The traditional  $S/D$  formulae are easy to apply, although they can be overly conservative for some ranges of span lengths while unconservative for others (Cai 2005; Puckett et al. 2005). The applicability of these formulae in the AASHTO Standard Specifications is limited by the fact that they were developed considering only non-skewed, simply supported bridges. However, the  $S/D$  formulae are also used by some bridge designers even in bridges with complicated geometries such as high skew, curved alignment, as well as continuous and IBs (Mourad and Tabsh 1999) since design guidelines for such bridges do not exist. Therefore, these bridges may either be designed in a conservative way which involves the additional cost or in an unconservative way which leads to unsafe bridge designs (Zokaie et al. 1993). The studies on the development of LLDFs before 90's were based on the determination of new  $D$  values in the AASHTO load distribution formula ( $S/D$ ) (Hays et al. 1986; Bakht and Moses 1988). Bakht and Moses (1988) presented a procedure to calculate the constant  $D$  which was expressed as a function of the span length. The span length was found to be an important parameter in calculating the distribution factor.

After 90's, additional geometric and structural parameters such as slab thickness, bridge span, girder stiffness etc., were included in the new AASHTO LRFD Specifications which uses live load distribution formulae to get more accurate results. The specifications additionally require the application of SCFs when the bridge supports are skewed. More precise but complex LLDFs were developed under National Cooperative Highway Research Program (NCHRP) Project 12-26 (Zokaie et al. 1991). These new equations have been published in the AASHTO LRFD Specifications (1994) then modified in more recent editions of AASHTO LRFD Specifications (1998, 2007). The LLDFs in AASHTO LRFD Specifications are more accurate than those provided in AASHTO Standard Specifications (Cai 2005; Mabsout et al. 1997). However, designers are concerned mainly about the complexity of the AASHTO LRFD distribution factor equations. The AASHTO LRFD procedure includes SCFs, a different set of equations for moment and shear, different sets of equations for interior and exterior girders as well as limited ranges of applicability due to the bridge structural and geometric properties imposed on the equations. Therefore, simpler and less complex LLDEs would be welcomed by the bridge design community. As a result, a new study under project NCHRP 12-62 was initiated for this purpose and is on-going (Cai 2005).

#### ***1.4.2 Integral Bridges***

The IB concept is defined as the practice of constructing bridges without deck joints. Arch bridges, rigid-frame bridges and culverts can be classified as IBs (Diciceli 2000). IBs were first considered after observing the successful performance of older bridges with inoperative joints (Mourad and Tabsh 1999). Subsequently, bridge engineers started to eliminate the deck joints at piers and abutments after the moment distribution method (cross method)

was first developed by Cross (1930) in early 1930s since this method allowed for the analysis of statically indeterminate structures such as rigid frame bridges. Therefore, concrete rigid frame bridges became very popular and a standard type of construction for many transportation departments by the mid of 20<sup>th</sup> century. Currently a number of state departments of transportation provide limited in-house design guidelines for IBs based on past experience and performance of older IBs.

Most recent research publications on IBs are related to the effect of thermal (Dicleli and Albhaisi 2003, 2004; Dicleli 2005) and seismic (Khan 2004; Sritharan et al. 2005; Steinberg et al. 2004) loading on the performance of IBs. Only few studies on live load analysis of IBs have been found in the literature (Dicleli and Erhan 2008b; Mourad and Tabsh 1999, 1998). Recently, Dicleli and Erhan (2008a, 2009a) conducted an extensive research study where they obtained LLDEs for the design of IB girders and substructure components. However, in the LLDEs developed by Dicleli and Erhan the effect of skew was totally neglected. Accordingly, SCFs that will be used with the LLDEs developed by Dicleli and Erhan (2009a, 2009b) are urgently needed to estimate live load effects in SIB components.

### ***1.4.3 Skewed Integral Bridges***

When the geometry and conditions does not allow designing straight bridges, skewed bridges are designed. Skewed bridge is a bridge, where the abutments are not perpendicular to bridge centerline. The angle between the abutment and a line perpendicular to the centerline of the bridge deck is defined as skew angle ( $\theta$ ) as shown in Figure 2 (c). Currently, two-thirds of bridges constructed in the U.S. are skewed (AASHTO 2007). Although skew generally decreases extreme force effects due to live load, it produces

negative moments at the corners, torsional moments within the end zones and redistribution of reaction forces at the supports (AASHTO 2007). Therefore, AASHTO LRFD specifications require the application of SCFs to the LLDFs obtained for straight bridges when the bridge is skewed. There is also a similar need to estimate live load effects in SIB girders and substructure components. Due to the absence of provisions for the calculation of live load effects in SIBs, most design engineers use the AASHTO LLDEs which are actually developed for skewed conventional jointed bridges. Consequently, most design engineers generally calculate the live load effects in the abutments and piles of SIBs by using the AASHTO LLDEs developed for the girders of jointed bridges. This approach is based on the assumption that the same rotations about a transverse axis perpendicular to the longitudinal direction of the bridge occur both in the abutments and the girders under live load due to the monolithic construction of the superstructure-abutment joint in SIBs. However, it is anticipated that the concentrated rigidity of a particular girder combined with those of the adjacent girders connected to the abutment having a smeared rigidity, may produce a live load distribution within the abutment and piles different than that calculated using the LLDEs developed for the girders of jointed bridges (Diciceli and Erhan 2009b). Therefore, using AASHTO LLDEs may result in either conservative or unconservative estimates of the live load effects in the piles and abutments of SIBs.

#### ***1.4.4 Modeling***

The finite element method is a well-accepted method of analysis. However, any method of analysis or modeling technique requires some degree of approximation when applied to a real structure. Therefore, a realistic FEM is required for an accurate determination of LLDFs. For this purpose, many

researchers have developed FEMs to obtain accurate predictions of LLDFs for bridge girders. One of these models developed by Hays et al. (1986) for the Florida Department of Transportation, which predicts the lateral load distribution of bridges with single span under flexural bending, is not only simple but also accurate. In the FEM, linear elastic behavior was assumed. The concrete slab was idealized as quadrilateral shell elements with five degrees of freedom at each node and steel girders and diaphragms were modeled as standard frame elements.

A study was performed on deck slab stresses in IBs using a finite element program called ALGOR to simulate the bridge features (Mourad and Tabsh 1999). In this study, the deck slab and beam web were modeled with four node rectangular shell elements, flanges and piles were modeled with two node space beams and the abutments were modeled with eighth node brick elements. In this study, the deck stresses determined from the FEA were about 40% less than those calculated using AASHTO LRFD equations.

Mabsout (1997) conducted an extensive research study to compare four finite element modeling techniques reported in the literature used in evaluating the wheel load distribution factors of steel girder bridges. In the first model, the concrete slab was idealized as quadrilateral shell elements with five degree of freedom at each node and steel girders were idealized as space frame members (Hays et al. 1986). In the second model, the concrete slab and girders were modeled as quadrilateral shell elements and eccentrically connected space frame members respectively (Imbsen and Nut 1978). In the third one, the concrete slab and steel girders were modeled as quadrilateral shell elements and girder flanges were modeled as space frame elements (Brockenbrough 1986). In the last one, the concrete slab was modeled using isotropic eight node brick elements with three degree of

freedom at each node and the steel girder flanges and webs were modeled using quadrilateral shell elements.

Faraji et. al. (2001) used a 3-D FEM to simulate the behavior of a three-span IB under thermal loading. In this model, the deck slab is modeled using bending and stretching plate elements while the steel stringers and diaphragms are modeled as beam elements. Abutment walls are modeled as plate elements. The piers are modeled as beam elements. The soil response behind the abutment walls is modeled using uncoupled nonlinear springs. HP-Piles are modeled using beam elements. Soil response next to each pile is modeled with 15 nonlinear springs.

The information gathered from the literature study on modeling of bridges is used to build a simple, yet accurate model of SIBs.

#### ***1.4.5 Soil-Bridge Interaction***

Soil-Bridge interaction is one of the most important factors that affect the IB behavior especially under thermal loading. In the FEMs built for the determination of LLDFs, these effects seem to be negligible especially for the girders (Dicleli and Erhan 2009a).

In the literature, the interaction between the abutment and backfill soil as well as pile and foundation soil in IBs are considered only under thermal effects (Duncan and Arsoy 2003; Dicleli and Albhaisi 2003, 2004; Dicleli 2005). The backfill pressure distribution behind the abutment is inherently nonlinear and depends on depth, amount and mode of wall displacement (Clough and Duncan 1991; Faraji et al. 2001; Khodair and Hassiotis 2005). Clough and Duncan (1991) obtained the variation of the backfill pressure coefficient (K)

as a function of the abutment displacement from the experimental data and FEAs. This relationship was used recently by Dicleli (2000, 2005) and Dicleli and Albhaisi (2003, 2004) to model abutment-backfill behavior under thermal-induced displacements of IBs. Such thermal-induced displacements are large and hence require a fully defined pressure-distribution versus abutment displacement relationship over a complete range of active to passive state. However, for live load analysis, since the lateral displacement of the abutment results from the deck-abutment joint rotation, it is anticipated to be very small. As a result a linear approximation of abutment-backfill interaction may be adequate using linear springs under compression and no springs under tension. The linear properties of these springs may be obtained from the initial slope of abutment-backfill interaction relationship provided by Clough and Duncan (1991). Dicleli and Erhan's (2008b) recent research study has proved the applicability of linear soil behavior for the live load analysis of IBs.

Generally, the soil pile interaction for a particular point along the pile is defined as a nonlinear load (P) – deformation (Y) curve, where P is the lateral soil resistance per unit length of pile and Y is the lateral deflection (Faraji et al. 2001; Dicleli and Albhaisi 2004) under lateral loading. Several nonlinear models for P-Y curves are available (Clough and Duncan 1991; Husain and Bagnariol 1996) in the literature. Load-deformation relationship can be modeled as elastoplastic (Dicleli and Albhaisi 2004) as well as a nonlinear parabolic curve (Faraji et al. 2001). However, under live load, the initial linear portion of the P-Y curve is anticipated to be adequate due to smaller lateral displacement of the piles. Accordingly, an analysis that incorporates the linear response of the soil to pile movement may be adequate when studying the live load distribution in IBs.

## CHAPTER 2

### SELECTION OF PARAMETERS AND MODELING

#### 2.1 Selection of Parameters

In earlier research studies (Dicleli and Erhan 2008b, 2009a, 2009b), the IB superstructure and substructure properties that affect the distribution of live load moment and shear in the components of IBs are identified. These parameters are; span length, girder size and spacing for the superstructure and abutment height, pile size, pile spacing and foundation soil stiffness for the substructure. Using these superstructure and substructure parameters, a number of SIB models are built and analyzed to develop SCFs for SIB components. For the superstructure, the span lengths of the SIBs considered in the analyses are assumed as 10, 15, 20, 25, 35, 40, 45 m. Furthermore, as AASHTO prestressed concrete girders are commonly used in IB construction, AASHTO prestressed concrete girder types; II, IV and VI spaced at 1.2, 2.4, 3.6 and 4.8 m are considered in the analyses. Overhanging slab length for the SIBs considered in this study is assumed to be 1.2 m excluding the cases where the effect of girder spacing is studied. For the cases where the effect of girder spacing is studied overhanging slab length is taken as 0.6 m since a larger overhanging slab length may not be suitable for the case of 1.2 m girder spacing (generally the overhanging slab length is limited to %60 of the girder spacing (Canadian Highway Bridge Design Code). For the slab, the thickness is assumed to be 0.15, 0.2, 0.25,

0.3 m. The strength of the concrete used for the prestressed concrete girders is assumed to be 50 MPa while those of the slab and abutments are assumed to be 30 MPa. For the substructure, the abutments are assumed to be 2.5, 3, 4 and 5 m tall and supported by 12 m long end-bearing steel HP piles. The spacing of the piles is assumed to be 1.2, 1.8, 2.4 and 3 m. In addition, the foundation soil surrounding the piles is assumed to be soft, medium, medium-stiff and stiff clay with an undrained shear strength ( $C_u$ ) of 20, 40, 80 and 120 kPa, respectively. The granular backfill behind the abutments is assumed to have a unit weight of 18, 20, 22 kN/m<sup>3</sup> to study the effect of backfill compaction level on live load distribution in SIB components. The range of values considered for each parameter is given in Table 1. For each parameter, a commonly used design value is selected as a reference value. When studying the effect of a certain parameter, the value of the parameter is changed within the given range while the rest of the parameters are assigned their reference values. Accordingly, eleven sets of analyses are conducted as shown in the first column of Table 2. In each analysis set, one of the parameters is considered to be dominant. For instance, in Analysis Set 1 while the number of beams is the main parameter, in Analysis Set 2 the foundation soil stiffness is the main parameter. For the main parameter, the full range of values considered is included in the analyses while the remaining parameters assume constant values. To highlight the effect of skew, each analysis set includes the full range of skews considered. For instance, in Analysis Set 1 while the number of girders is selected as a dominant parameter, each number of girder parameter also includes six skews considered in these analyses.

*Table 1: Parameters considered in the analyses*

<b>Parameters</b>	<b>Constants</b>	<b>Variables</b>
Number of Girders	4	6, 8, 10
Skew (Degree)	-	0, 10, 20, 30, 40, 50, 60
Undrained Shear Strength (kPa)	40	20, 80, 120
Pile Size	250x85	310x125
Pile Spacing (m)	2.4	1.2, 1.8, 3
Abutment Height (m)	3	2.5, 4, 5
Abutment Thickness (m)	1	1.5
Backfill Unit Weight (kN/m <sup>3</sup> )	20	18, 22
Span Length (m)	30	10, 15, 20, 25, 35, 40, 45
Girder Spacing (m)	2.4	1.2, 3.6, 4.8
Girder Size	Type IV	Type II, Type VI
Slab Thickness (cm)	20	15, 25, 30

This resulted in a total of 231 different 3-D and corresponding 2-D structural models of IBs and more than 25,000 analyses cases. Analyses cases include the analyses of both 2-D and 3-D models, the analyses for various longitudinal positions of the truck for shear and moment and the analyses for various transverse positions of two or more trucks in the analyses of 3-D models. Note that the combination of various parameters presented above may not always be realistic (e.g. the combination of girder type IV and a span length of 10 m). Although such unrealistic combinations may result in biased interpretations of analysis results for LLDFs due to the combination of unrealistic girder sizes with various span lengths, this was done deliberately to solely study the effect of a certain parameter on the distribution of live load moment and shear among the girders and substructure components of SIBs by keeping the other parameters constant and to have adequate data covering the full range of possible variation of the parameters to incorporate all possible cases of scenarios. A similar approach was also used in the development of AASHTO LLDFs.

Table 2: Analysis sets considered in the analyses.

Set	$\theta$	$N_b$	$c_u$	Pile Size	$S_p$	$H_a$	$w$	$\gamma$	L	S	GT	t
1	10, 20, 30, 40, 50, 60	4, 6, 8, 10	40	250x85	2.4	3	1	20	30	2.4	Type IV	20
2	10, 20, 30, 40, 50, 60	4	20, 40, 80, 120	250x85	2.4	3	1	20	30	2.4	Type IV	20
3	10, 20, 30, 40, 50, 60	4	40	250x85 310x125	2.4	3	1	20	30	2.4	Type IV	20
4	10, 20, 30, 40, 50, 60	4	40	250x85	1.2, 2.4, 1.8, 3	3	1	20	30	2.4	Type IV	20
5	10, 20, 30, 40, 50, 60	4	40	250x85	2.4	2.5, 3, 4, 5	1	20	30	2.4	Type IV	20
6	10, 20, 30, 40, 50, 60	4	40	250x85	2.4	3	1, 1.5	20	30	2.4	Type IV	20
7	10, 20, 30, 40, 50, 60	4	40	250x85	2.4	3	1	18, 20, 22	30	2.4	Type IV	20
8	10, 20, 30, 40, 50, 60	4	40	250x85	2.4	3	1	20	10, 15, 20, 25, 30, 35, 40, 45	2.4	Type IV	20
9	10, 20, 30, 40, 50, 60	4	40	250x85	2.4	3	1	20	30	1.2, 2.4, 3.6, 4.8	Type IV	20
10	10, 20, 30, 40, 50, 60	4	40	250x85	2.4	3	1	20	30	2.4	Type II, IV, VI	20
11	10, 20, 30, 40, 50, 60	4	40	250x85	2.4	3	1	20	30	2.4	Type IV	15, 20, 25, 30

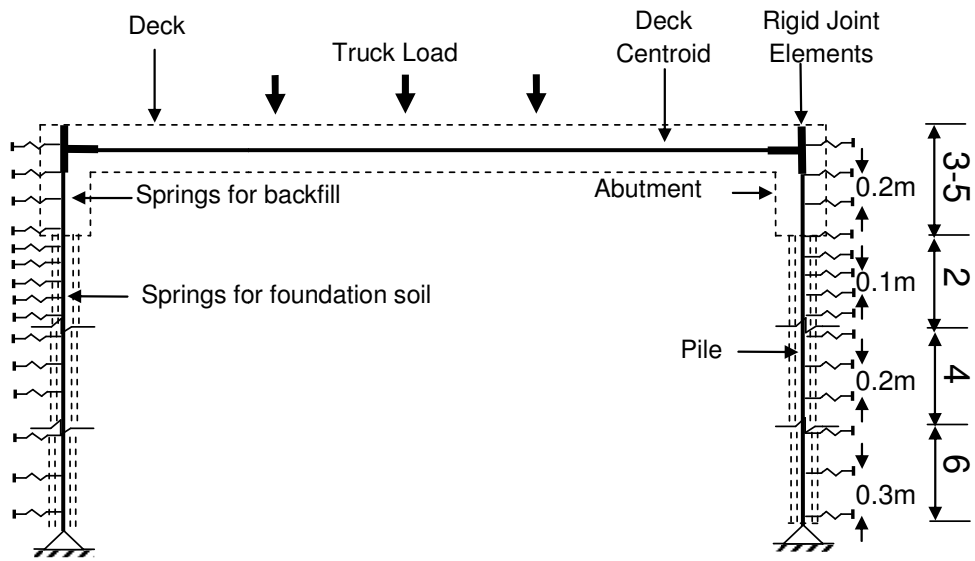
## **2.2 Modeling**

Structural models of the SIBs considered in this study are built and analyzed using the finite element based software SAP2000 (2007). The 2-D and 3-D structural model of a typical SIB used in the analyses are shown in Figure 3 (a) and (b) respectively. The verification of similar IB models have already been performed by Dicleli and Erhan (2009c) using the finite element based program ANSYS (2007).

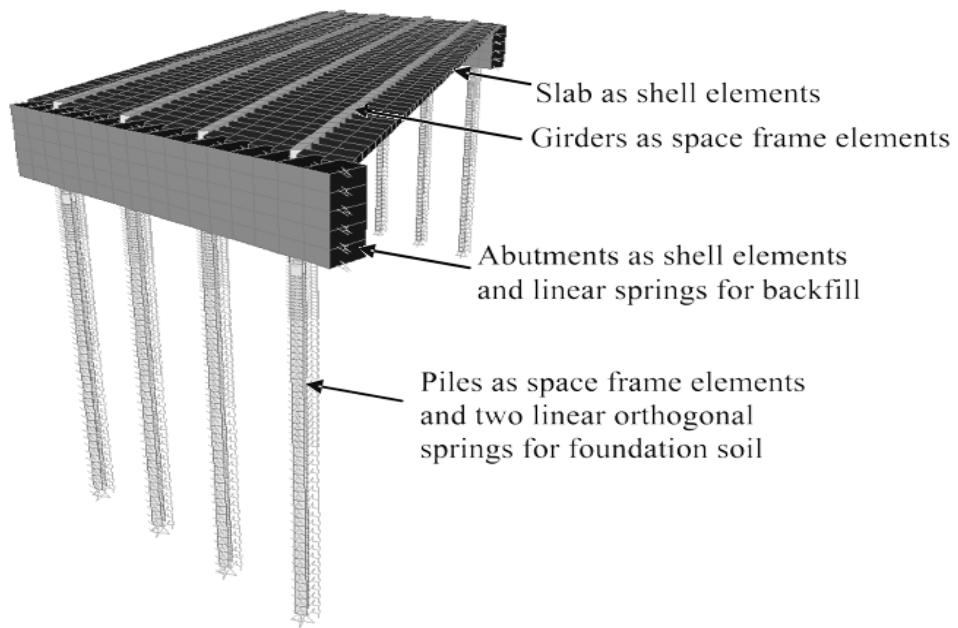
### ***2.2.1 Superstructure Modeling for Integral Bridges***

Mabsout et al. (1997) and Hindi and Yousif (2006) performed a comparative study on FEMs of slab-on-girder bridges to select an accurate and practical FEM. Four FEMs of slab-on-girder bridges, which are available in the literature, are compared in these studies. The first model is based on a study conducted by Hays et al (1986) where the concrete slab is idealized as quadrilateral shell elements with five degrees of freedom (DOF) at each node and the steel girders are idealized as space frame members with six degrees of freedom at each node. The center of gravity of the slab coincides with the girders' center of gravity and the girder properties are transformed to the deck center of gravity. The model is shown in Figure 4 (a). The second FEM is based on the research study of Imbsen and Nutt (1978). The concrete slab is idealized as quadrilateral shell elements and the girders are idealized using eccentrically placed space frame members. This model is similar to the first one but, rigid links are imposed to accommodate for the eccentricity of the girders with respect to the slab as illustrated in Figure 4 (b). The third FEM is based on the research reported by Brockenbrough (1986). The concrete slab and the steel girder web are modeled as quadrilateral shell elements; the girder flanges are modeled as space frame elements while the

flange to deck eccentricity is modeled by imposing a rigid link as shown in Figure 4 (c). The fourth and the most complicated FEM is based on the research study of Tarhini and Frederick (1992). The concrete slab is modeled using isotropic eight node brick (solid) elements with three DOF at each node. The steel girder flanges and webs are modeled using quadrilateral shell elements as demonstrated in Figure 4 (d).



(a)



(b)

Figure 3. Finite element models of SIBs (a) 2-D (Dicleli and Erhan 2008a), (b) 3-D

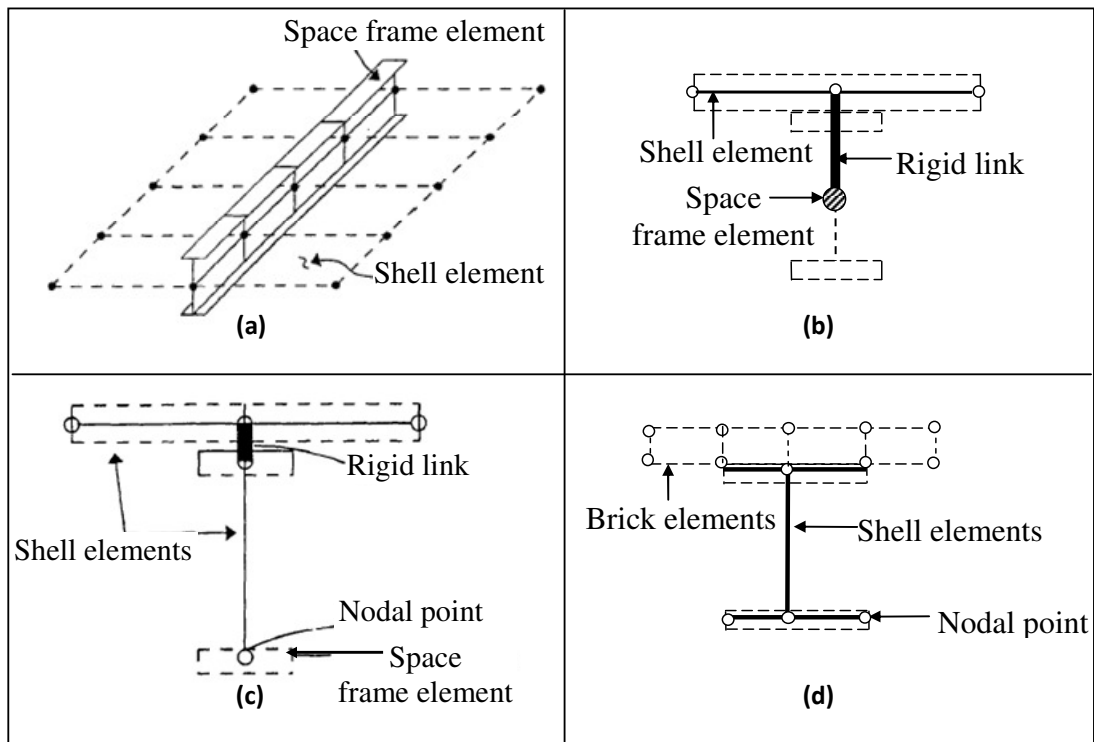


Figure 4. FEMs of slab-on-girder bridge superstructures proposed by (a) Hays et al (Hays et al. 1986), (b) Imbsen and Nutt (Imbsen and Nut, 1978), (c) Brockenbrough (Brockenbrough 1986), (d) Tarhini and Frederick (Tarhini and Frederick 1992)

The studies conducted by Mabsout et al. (1997) and Hindi and Yousif (2006) have concluded that the model proposed by Hays et al. (1986) although simple, gives comparable results to those of the other more complicated three models. For the slab on steel girder bridge analyzed by Mabsout et al. (1997) (bridge length=56 feet, bridge width=30 feet, girder spacing=8 feet, slab thickness=7.5 inches and girder size=W36x160), the maximum girder moments are calculated as 5.396, 5.396, 4.968 and 5.206 kip-in, for the models proposed by Hays et al. (1986), Imbsen and Nutt (1978), Brockenbrough (1986) and Tarhini and Frederick (1992) respectively. Thus, a finite element modeling technique similar to that proposed by Hays et al. (1986) is used to model the slab-on-girder deck of SIBs used in this study.

Accordingly, the bridge slab is modeled using quadrilateral shell elements with six DOF at each node and the girders are modeled as 3-D frame elements with six DOF's at each node as shown in the 3-D structural models presented in Figure 3 (b). Slab of the bridges with no skew is divided into equal square elements with 0.6m width for each model under consideration. For the skewed bridge models two options are available for constructing the FEM of the slab. The slab can be modeled using either square or parallelogram shell elements where the sides of the parallelogram shell elements are parallel to the skewed abutments. Automatic generation of the shell elements for the slab becomes difficult when using square shell elements (For the case of parallelogram shell elements, automatic generation becomes easier due to the uniform element geometry). In addition, parallelogram shell elements facilitate the placement of the truck wheel loads especially for the case of girder shear. Therefore, shell elements, in the shape of a parallelogram, is used for the finite element modeling of the slab. However, to test the effect of using parallelogram shell elements on the accuracy of analysis results sensitivity analyses are conducted. For this purpose, two 30 m long SIBs with skew angles of 30° and 60° are considered. Both bridges are modeled using rectangular and parallelogram shell elements for the slab. The analyses results are presented in Table 3. There is a slight difference between pile moment and shears in favor of the diagonal modeling technique (responses of square model is smaller). It is observed that the difference between the two modeling techniques is negligible.

*Table 3: Difference of parallel and square modeling technique for constant model*

<b>Skew</b>	<b>M<sub>g</sub></b>	<b>M<sub>p</sub></b>	<b>V<sub>p</sub></b>	<b>M<sub>a</sub></b>	<b>V<sub>a</sub></b>
30	0.04%	-0.92%	-0.65%	0.12%	-0.18%
60	-0.24%	-1.64%	-0.80%	0.32%	-0.14%

Full composite action between the slab and the girders is assumed in the models. For that reason, the moment of inertia,  $I_g$ , of the girder used in the FEM is calculated as the moment of inertia,  $I_c$ , of the composite slab-on-girder section minus the moment of inertia,  $I_s$ , of the slab tributary to each girder (i.e.  $I_g = I_c - I_s$ ). Table 4 shows the contribution of the girders and the girder+slab to the total girder moment. As observed from the table the difference is negligible. In spite of this negligible difference, the full contribution of girder+slab is considered in the analyses.

*Table 4: Comparison of frame results with frame and shell results for square and parallelogram modeling of deck slab*

<b>Modeling Technique</b>	<b>Skew</b>	<b>Model</b>	<b>Mg Girder</b>	<b>M<sub>g</sub> Girder+Slab</b>	<b>Difference</b>
Parallel	30	Constant	1032.388	1038.554	0.60%
Square	30	Constant	1029.993	1038.944	0.87%
Parallel	60	Constant	906.820	911.474	0.51%
Square	60	Constant	903.511	909.270	0.64%

Furthermore, in order to improve the accuracy of the analysis results for the bridges with the AASHTO type prestressed concrete girders; an exact solution for the torsional constant of the girders is used in the FEM (Chen and Aswad 1996). In addition, the abutment-deck joint is assumed to be rigid. Accordingly, the abutment-deck joint is modeled by assigning a large modulus of elasticity to the deck shell elements and part of the girders located within the joint area. This modeling technique has already been verified by Dicleli and Erhan (2008a).

### ***2.2.2 Substructure Modeling for Integral Bridges***

The literature study conducted on the finite element modeling of abutments and piles has revealed that the piles are modeled using 3-D beam elements (Mourad and Tabsh 1999; Faraji et al. 2001) while the abutments are generally modeled using either 8-node brick elements (Mourad and Tabsh 1999) or shell elements (Faraji et al. 2001). Modeling the abutments using 8-node brick elements requires the integration of stresses to calculate the shears and moments. Accordingly, in this study, the abutments are modeled using Mindlin shell elements (Cook 1995) with six DOF at each node to accurately simulate shear and bending deformations with minimal computational effort and the piles are modeled using 3-D beam elements. Rectangular shell elements are used to model the behavior of the skewed abutment. In addition, to model the rigidity of the deck-abutment joint, the abutment shell elements located within the joint area are assigned a large modulus of elasticity.

### ***2.2.3 Modeling of Soil-Structure Interaction for Integral Bridges***

For modeling the soil-structure interaction in SIBs, although the behavior of the backfill and foundation soil is nonlinear in nature, a linear elastic behavior is assumed due to the small lateral displacements of the abutments and piles under live load. The linear soil behavior under live load has already been validated in an earlier research study by Dicleli and Erhan (2008b). The linear backfill-abutment and soil-pile interaction modeling is summarized below. A more detailed description of soil-structure interaction modeling for IBs can be found elsewhere (Dicleli and Erhan 2008b).

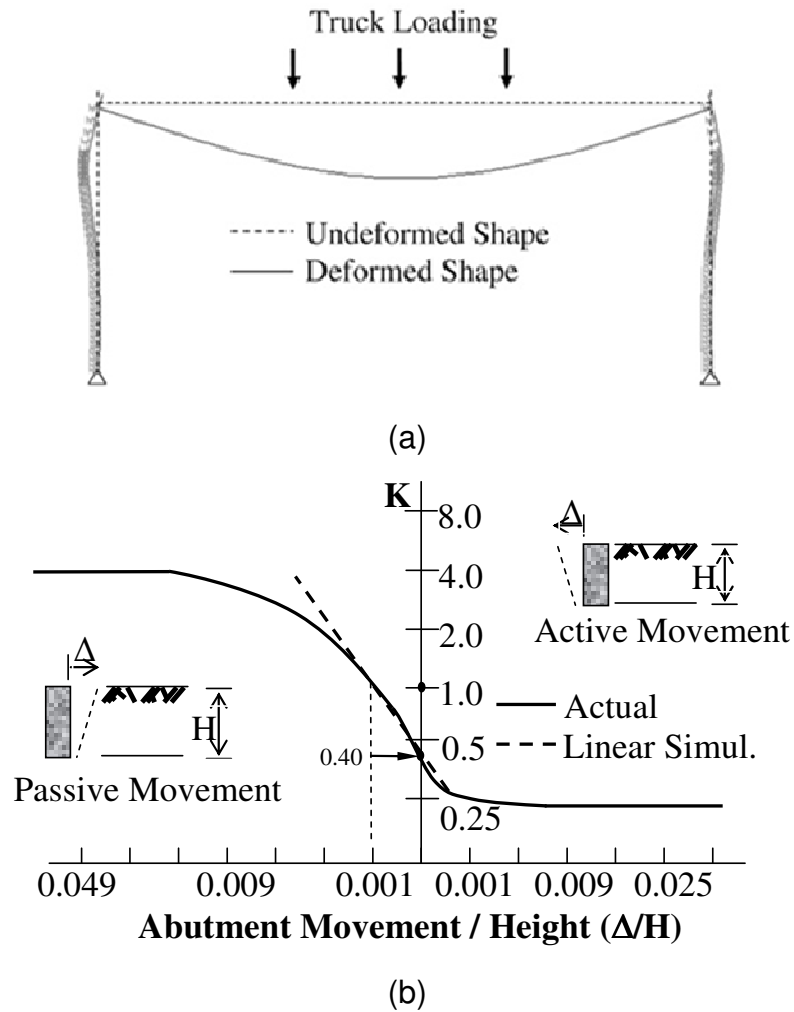


Figure 5. (a) Deformed shape of an IB under live load (Dicleli and Erhan 2008a), (b) Variation of the backfill pressure coefficient as a function of the ratio of the abutment movement to abutment height (actual and linear simulation) (Dicleli and Erhan 2008a)

Under live load effects while the portion of the abutment below the superstructure centroid moves towards the backfill, the portion of the abutment above the deck centroid moves away from the backfill as observed from Figure 5 (a). When the abutment moves towards the backfill as a result of the rotation at the deck-abutment joint under live load effects, the intensity

of the backfill pressure depends on the magnitude of the abutment displacement. The actual earth pressure coefficient,  $K$ , may change between at rest,  $K_0$ , and passive,  $K_p$ , earth pressure coefficients depending on the amount of displacement. Clough and Duncan (1996) modeled the variation of the lateral earth pressure coefficient,  $K$ , as a function of the ratio,  $\Delta/H$ , of abutment movement to abutment height using experimental data and finite element analyses.

To model backfill-abutment interaction, a set of linear springs connected at the abutment-backfill interface nodes below the superstructure centroid along the height and width of the abutment are used as illustrated in Figure 3. To calculate the stiffness of these springs, first the coefficient of subgrade reaction modulus for the granular backfill is calculated using the following equation (Dicleli and Erhan 2008b).

Assuming small lateral abutment displacements due to live load effects, the secant slope of the solid curve shown in Figure 5 (b), between  $\Delta/H=0$  and  $\Delta/H =0.001$  is used to obtain a subgrade reaction modulus,  $k_{sh}$ , representing the relationship between the abutment movement and passive resistance of the backfill soil (The dashed line in Figure 5 (b)). For this reason, first, the variation of earth pressure,  $\Delta P$ , from at rest ( $\Delta/H =0$ ) to passive state at  $\Delta/H =0.001$  is formulated for an arbitrary location,  $z$ , measured from the top of the abutment as;

$$\Delta P = (K_p - K_0) \cdot \gamma \cdot z \quad (1)$$

The above equation is divided by the displacement of the wall at  $\Delta/H =0.001$  to obtain  $k_{sh}$  as;

$$k_{sh} = \frac{(K_p - K_0) \cdot \gamma \cdot z}{0.001 \cdot H_a} \quad (2)$$

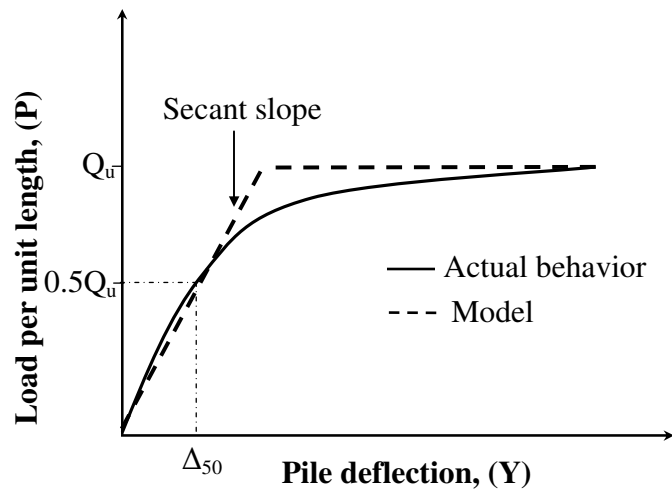
The values of  $K_p$  at  $\Delta/H = 0.001$  and  $K_0$  for the backfill are obtained from Figure 5 (b) as 1.125 and 0.4 respectively. Assuming a unit weight of 20 kN/m<sup>3</sup> for the backfill,  $k_{sh}$  is computed as;

$$k_{sh} = \frac{14500}{H_a} \cdot z \quad (3)$$

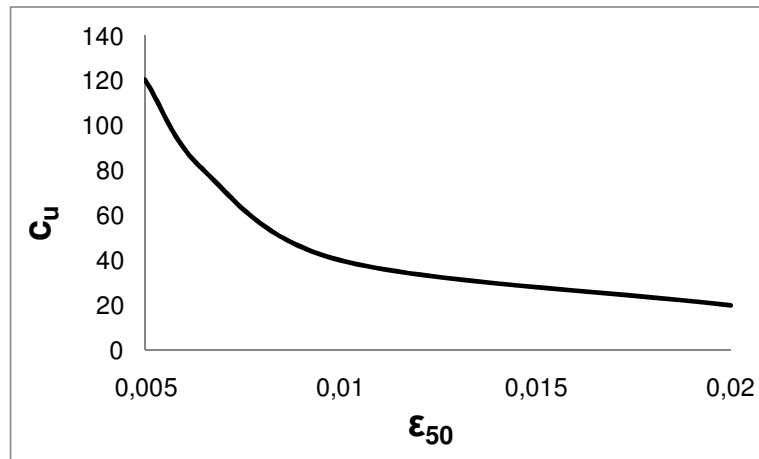
The stiffness of the linear springs connected at the abutment-backfill interface is then calculated by multiplying  $k_{sh}$  by the area tributary to the node in the 3-D structural model. The backfill stiffness model described above considers only the passive resistance of the backfill to the movement of the abutment below the superstructure centroid (Figure 5 (a)) and excludes the at-rest portion of the backfill pressure which is not directly related to the loading on the bridge. Consequently, only the resistance of the backfill mobilized by live load is taken into consideration in the analyses. Note that under live loads, since the movement of the abutment occurs away from the backfill above the superstructure centroid (Figure 5 (a)), no spring is introduced between the superstructure top and the superstructure centroid in the model. Above the superstructure centroid, the active backfill pressure will immediately develop behind the abutment at a negligibly small displacement; that is as soon as the bridge abutment slightly moves away from the backfill. At that instant, the active backfill pressure simply becomes a load (pressure) behind the abutment (i.e no stiffness to restrain the movement), which is already taken into consideration (either as active or as at-rest backfill pressure depending on the flexibility of the abutment) regardless of the presence of the live load to incorporate the effect of the backfill pressure at zero temperature condition in the design of the bridge. However, when the portion of the abutment underneath the superstructure centroid moves towards the backfill as a result of the rotation at the superstructure-abutment joint under live load effects, the restraining effect of the backfill creates a true abutment-backfill interaction condition affecting the lateral and rotational

stiffness of the abutment (i.e. it is not simply a load due to backfill pressure as in the case of active condition) and it is considered in the structural model. In fact, as stated earlier, the passive pressure modeling only includes the portion of the passive resistance (that is, the compression stiffness of the backfill) mobilized by the movement of the abutment under live load effects since the at-rest (or in some cases active) earth pressure condition is already there at zero temperature state. This modeling technique is valid at any temperature level for short to medium length SIBs since the model takes into consideration only the portion of the backfill resistance mobilized by the movement of the abutment due to live load.

Generally, the soil-pile interaction for a particular point along the pile is defined by a nonlinear load (P)-deformation (Y) curve or P-Y curve, where P is the lateral soil resistance per unit length of pile and Y is the lateral deflection. A typical P-Y curve for soil subjected to lateral movement of a pile is shown with a solid line in Figure 6 (a). This highly non-linear behavior is simplified using an elasto-plastic curve displayed on the same figure with a dashed line. The elastic portion is defined with a slope equal to the secant soil modulus,  $E_s$  ( $\text{kN/m}^2$ ), and the plastic portion is defined as the ultimate soil resistance per unit length of pile,  $Q_u$ . In this study, only the elastic portion ( $E_s$ ) of this elasto-plastic model is used to simulate the force-deformation response of the soil due to small lateral displacement of the piles under live load effects (soil response is practically linear). The calculation of the initial soil modulus  $E_s$  for clay requires the calculation of the ultimate soil resistance  $Q_u$  and the pile deflection,  $\Delta_{50}$ , at 50% of the ultimate soil resistance as described below.



(a)



(b)

Figure 6. (a) Idealization of a typical  $P$ - $Y$  curve for soil modeling (Dicleli and Erhan 2008a), (b)  $c_u$  versus  $\epsilon_{50}$  plot (Evans 1982)

Two types of soil behavior are generally considered in estimating  $Q_u$  for laterally moving piles in clay. The first type of behavior occurs near the surface, where the pile may push up a soil wedge by lateral movement resulting in so-called wedge action (Dicleli and Erhan 2008b). The second type of behavior occurs at some depth below the ground surface, where the soil attempts to flow around the pile. In the case of SIBs, the backfill and the

embankment soil exert surcharge pressures on the foundation soil and may prevent the wedge action. Accordingly, the ultimate soil resistance per unit length of pile,  $Q_u$ , is expressed considering only the second type of behavior. Thus,

$$Q_u = 9 \cdot C_u \cdot d_p \quad (4)$$

where  $C_u$  is the undrained shear strength of the clay and  $d_p$  is the pile width (Diciceli and Erhan 2008b).

Skempton (1951) proposed a method based on laboratory test data, correlated with field test to calculate the elastic soil modulus,  $E_s$ . Skempton found that about one-half of the ultimate soil resistance for a beam resting on soil (or pile pushing on soil) is developed at a structure deflection,  $\Delta_{50}$ , as follows;

$$\Delta_{50} = 2.5 \varepsilon_{50} d_p \quad (5)$$

where  $\varepsilon_{50}$  is the soil strain at 50% of ultimate soil resistance. For  $C_u = 20, 40, 80$  and  $120$  kPa used in the analyses, corresponding  $\varepsilon_{50}$  values of  $0.02, 0.01, 0.0065$  and  $0.0050$  are obtained using the range of suggested values (Evans 1982) shown in Figure 6 (b). If the ultimate soil resistance,  $Q_u$ , is determined, and the deflection,  $\Delta_{50}$ , at half resistance is computed, then the soil modulus for clay can be calculated using the following expression;

$$E_s = \frac{Q_u / 2}{\Delta_{50}} = \frac{9C_u}{5\varepsilon_{50}} \quad (6)$$

The estimated values for  $Q_u$ ,  $\varepsilon_{50}$  and the pile width,  $d_p$  are substituted in Eq. (4) to calculate the soil modulus. The elastic stiffness,  $k$ , of the springs along the pile is then calculated by multiplying the initial soil modulus,  $E_s$ , by the tributary length,  $h$ , between the nodes along the pile. Thus:

$$k = \frac{Q_u \cdot h}{5 \cdot \varepsilon_{50} \cdot d_p} \quad (7)$$

### 2.2.4 Two Dimensional Structural Model

For each 3-D structural model of the SIBs considered, a corresponding 2-D frame version is also built to enable the calculation of LLDFs. The 2-D structural model of a typical IB used in the analyses is shown in Figure 3. The model is built using 2-D elastic beam elements considering a single interior girder. In the structural models, the tributary width of the slab and abutments is set equal to the spacing of the girders (Figure 7). For the superstructure, full composite action between the slab and the girders is assumed. The stiffness properties of the composite slab-on-girder deck are expressed in terms of the properties of the slab using the transformed section method. The stiffness properties of the pile elements in the 2-D model are calculated as the stiffness properties of a single pile multiplied by the number of piles per girder. The deck-abutment joint is modeled using a horizontal and a vertical rigid linear elastic beam element (an elastic beam element with large modulus of elasticity). The soil-structure interaction modeling for the 2-D model is similar to that for the 3-D model except the spring constants are calculated using a tributary area equal to the girder spacing times the vertical spacing between the nodes.

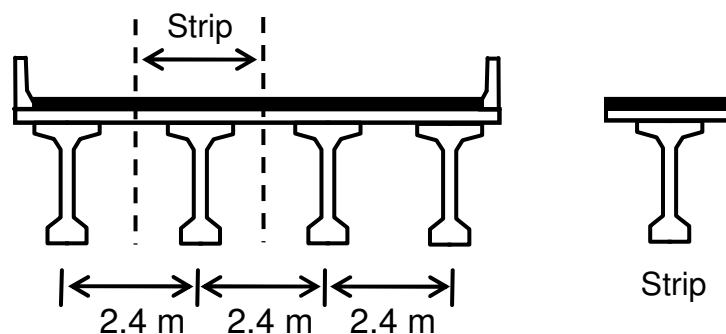


Figure 7. Cross section of a four girder bridge and a strip used in 2-D modeling

## **CHAPTER 3**

### **LOADING**

#### **3.1 Live Load Model**

The FEAs are performed using the AASHTO LRFD (2007) design live load designated as HL-93. The AASHTO LRFD design live load includes a design truck or a tandem and a lane load. The design lane load is not included in this research, as it was not considered in the development of LLDFs in AASHTO LRFD (Patrick et al. 2006). In addition, influence line analyses conducted in earlier studies (Dicleli and Erhan 2008b) have revealed that the tandem load does not govern the design for the bridges under consideration. Consequently, the analyses are performed using the design truck alone.

#### **3.2 Estimation of Most Critical Live Load Effects**

The maximum load effect on a bridge is based on the position of the truck both in the longitudinal and transverse directions, the number of loaded design lanes and the probability of the presence of multiple loaded design lanes. To calculate the maximum live load effects in the bridges under consideration, the position of the truck in the longitudinal direction as well as both the position and the numbers of trucks in the transverse direction are considered. The AASHTO LRFD spacing limitations, used in the analyses for the transversely positioned trucks, is shown in Figure 8 (a).

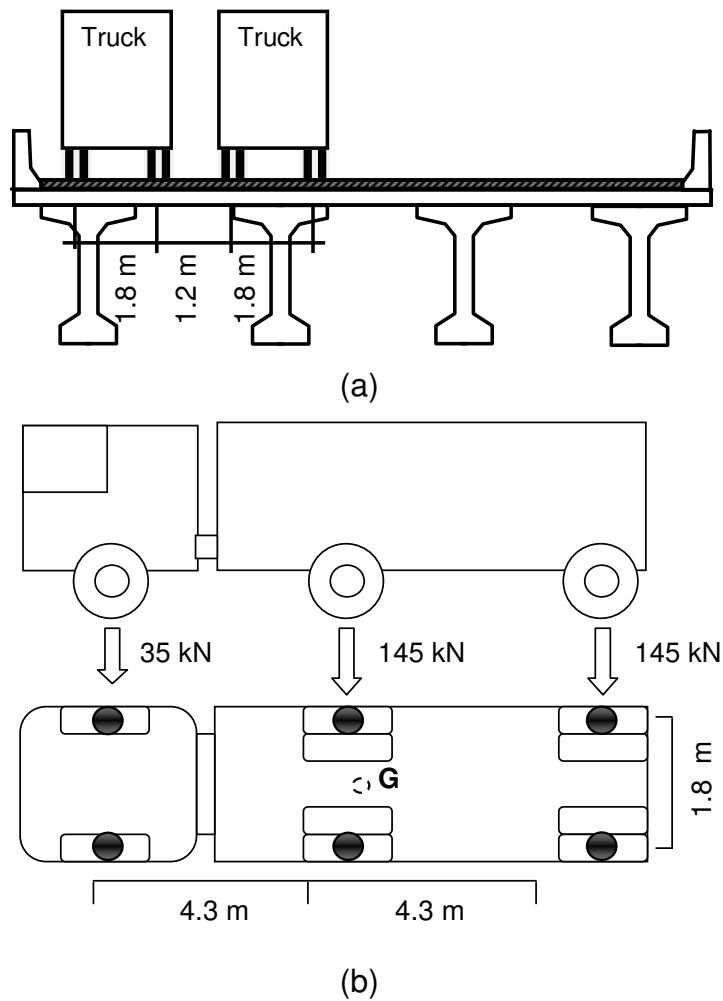


Figure 8. (a) Minimum clearances for design truck loading for a typical slab-on-girder bridge cross-section (Dicleli and Erhan 2008a), (b) Truck loading considered in analyses

First, the design truck longitudinal position is obtained by influence line analyses. The analyses results are found to be in good agreement with the findings of a recent research study conducted by Dicleli and Erhan (2008a) which revealed that a truck longitudinal position for maximum girder moment ( $M_g$ ) for an IB is nearly equal to that of a simply supported bridge (Figure 9 (a)). To obtain the maximum shear force in the girder ( $V_g$ ), the design truck is positioned such that the 145 kN rear axle of the truck is placed at the deck

abutment interface for the SIB as illustrated in Figure 9 (a). Then, the design trucks are moved transversely along the bridge width to obtain the maximum live load effects (moment and shear) in the girders. This procedure is repeated for the estimation of critical truck transverse positions for the maximum abutment moment ( $M_a$ ), abutment shear ( $V_a$ ), pile moment ( $M_p$ ) and pile shear ( $V_p$ ) due to live load. In the estimation of live load effects, the probability of the presence of multiple loaded design lanes is taken into consideration by using the multiple-presence factors defined in AASHTO LRFD (2007).

A sample of two and three lane truck loadings is shown in Figure 9 (b) where the hatched girder represents the girder where the maximum live load moment is calculated for an IB with zero skew. Note that the number of trucks and the arrangement of the transverse truck positions to produce the maximum live load effect changes based on the number of girders and girder spacing as shown in Figure 9 (b). The arrangement of transverse truck position does not change with the remaining parameters considered in this research study. Accordingly, for all the bridge models considered in this research study, only the cases where the bridges have various number of girders (4, 6, 8, 10) and girder spacings (1.2, 2.4, 3.6, 4.8) are loaded with different transverse truck configurations. This resulted in eight different transverse truck loading configurations.

In this research, the main live load effects considered are girder moment ( $M_g$ ), girder shear ( $V_g$ ), abutment moment ( $M_a$ ), abutment shear ( $V_a$ ), pile moment ( $M_p$ ) and pile shear ( $V_p$ ). Preliminary analysis revealed that, maximum values of these live load effects may occur with different truck configurations and positions. Truck configurations and positions which are used in this research are determined by influence line analyses to produce

the maximum live load effects for the considered output parameters. The number of trucks ( $N_T$ ) and the transverse position of first truck from the slab edge ( $x$  (m)) is given in Table 5 for various geometric configurations of the bridges considered (the table is presented for the most critical loading pattern as described in the following subsections).

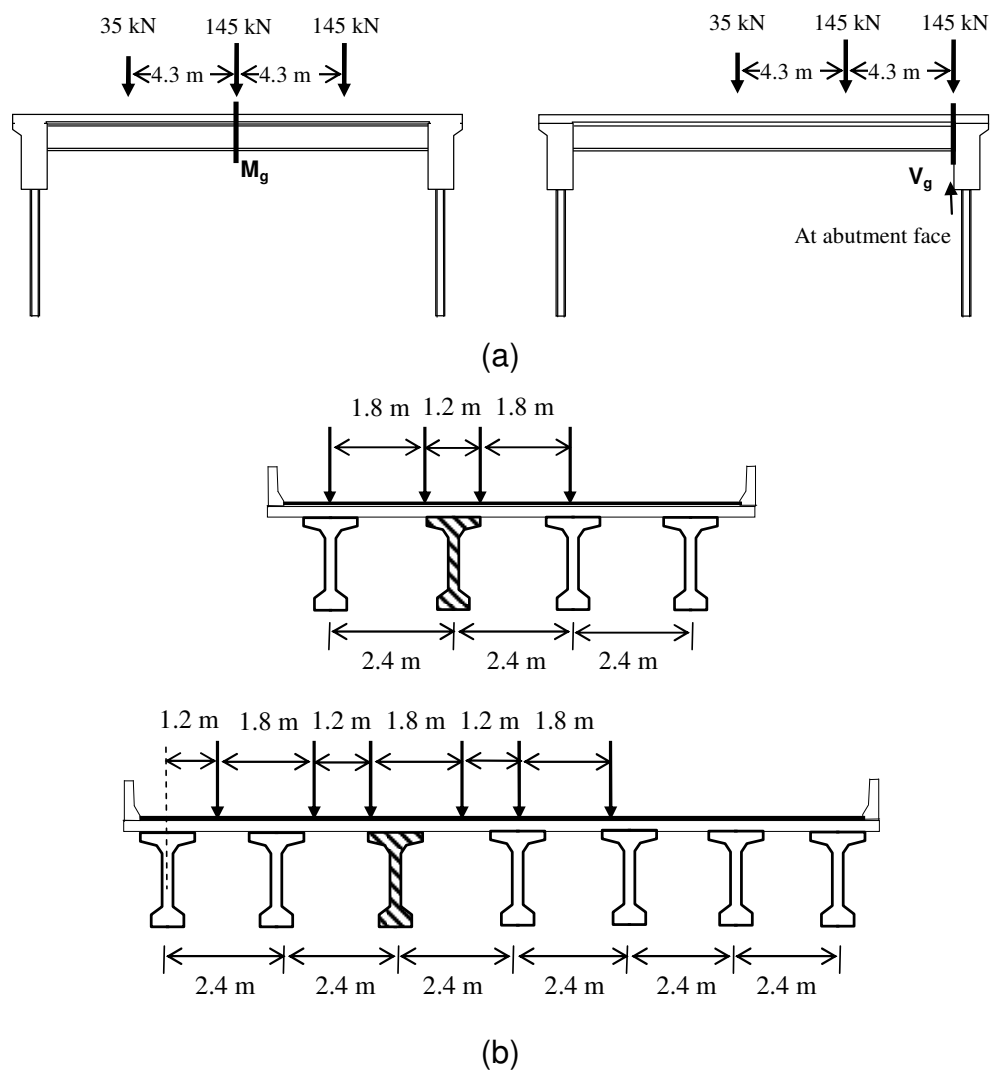


Figure 9. (a) Location of calculated maximum girder shear ( $V_g$ ) and moment ( $M_g$ ) for IB (Dicleli and Erhan 2008a), (b) A sample of transverse position of design trucks to produce maximum moment in the hatched girders for the cases where two- and three-lanes are loaded (Dicleli and Erhan 2008a)

Table 5: Sample of transverse positions and number of trucks for the maximum live load effects of bridge with 50° skew where two or more design lanes are loaded

Parameters		M <sub>g</sub>		M <sub>a</sub>		V <sub>a</sub>		M <sub>p</sub>		V <sub>p</sub>	
		N <sub>T</sub>	x(m)	N <sub>T</sub>	x(m)	N <sub>T</sub>	x(m)	N <sub>T</sub>	x(m)	N <sub>T</sub>	x(m)
Cons.		2	3	2	4.2	2	4.2	2	4.2	2	4.2
c <sub>u</sub>	20	2	3	2	4.2	2	4.2	2	4.2	2	4.2
c <sub>u</sub>	80	2	3	2	4.2	2	4.2	2	4.2	2	4.2
c <sub>u</sub>	120	2	3	2	4.2	2	4.2	2	4.2	2	4.2
Pile Size	310x125	2	3	2	4.2	2	4.2	2	4.2	2	4.2
S <sub>p</sub>	1.2	2	3	2	4.2	2	4.2	2	4.2	2	4.2
S <sub>p</sub>	1.8	2	3	2	4.2	2	4.2	2	4.2	2	4.2
S <sub>p</sub>	3	2	3	2	4.2	2	4.2	2	4.2	2	4.2
w	1.5	2	3	2	4.2	2	4.2	2	4.2	2	4.2
γ	18	2	3	2	4.2	2	4.2	2	4.2	2	4.2
γ	22	2	3	2	4.2	2	4.2	2	4.2	2	4.2
L	10	2	3	2	4.2	2	4.2	2	4.2	2	4.2
L	15	2	3	2	4.2	2	4.2	2	4.2	2	4.2
L	20	2	3	2	4.2	2	4.2	2	4.2	2	4.2
L	25	2	3	2	4.2	2	4.2	2	4.2	2	4.2
L	35	2	3	2	4.2	2	4.2	2	4.2	2	4.2
L	40	2	3	2	4.2	2	4.2	2	4.2	2	4.2
L	45	2	3	2	4.2	2	4.2	2	4.2	2	4.2
GT	Type II	2	3	2	4.2	2	4.2	2	4.2	2	4.2
GT	Type VI	2	3	2	4.2	2	4.2	2	4.2	2	4.2
t	15	2	3	2	4.2	2	4.2	2	4.2	2	4.2
t	25	2	3	2	4.2	2	4.2	2	4.2	2	4.2
t	30	2	3	2	4.2	2	4.2	2	4.2	2	4.2
H <sub>a</sub>	2.5	2	3	2	4.2	2	4.2	2	4.2	2	4.2
H <sub>a</sub>	4	2	3	2	4.2	2	4.2	2	4.2	2	4.2
H <sub>a</sub>	5	2	3	2	4.2	2	4.2	2	4.2	2	4.2
N <sub>b</sub>	6	3	0.6	2	0.6	4	3	4	3	4	3
N <sub>b</sub>	8	3	0.6	2	0.6	3	0.6	4	0.6	4	0.6
N <sub>b</sub>	10	3	0.6	2	0.6	3	15.6	4	0.6	3	0.6
S	1.2	2	2.4	2	3	2	3	2	3	2	3
S	2.4	1	2.4	1	1.8	1	2.4	1	2.4	1	2.4
S	3.6	3	1.2	2	6.6	4	0.6	4	0.6	4	0.6
S	4.8	3	1.8	3	2.4	4	0.6	4	4.2	4	0.6

N<sub>T</sub>: number of trucks

x: transverse position of the first truck from the slab edge

In the case of straight bridges, the truck loading position along the length of the bridge in a 3-D model completely coincides with that of the 2-D frame model (Figure 10 (a)). However, in the case of skewed bridges this is not the case (Figure 10 (b)). The truck longitudinal position in a 3-D model may be determined by taking as a reference either the lower (bottom) or upper (top) boundaries of the bridge in the transverse direction or the centerline of the bridge. Accordingly, in the case of skewed bridges, different loading patterns arise due to the geometry of the bridge. These loading patterns are categorized with respect to the way they are aligned along the length of the bridge. Three of them are straight loading patterns, where all the trucks are placed on the same line perpendicular to the bridge length, with different longitudinal alignment points as bottom, center and top of the bridge as shown in Figure 11. In this type of an arrangement, the longitudinal position of each transversely positioned truck changes with respect to the abutment (Figure 11). There is also an additional loading pattern where the trucks are aligned with respect to the skew of the bridge as shown in Figure 11. In this type of an arrangement, the longitudinal position of each transversely positioned truck does not change with respect to the abutment (Figure 11). The effect of these loading patterns on the maximum live load moment and shear in SIB components is studied in detail in the following section. This is done to determine the most critical loading pattern for obtaining maximum live load effects. The most critical loading pattern is then used in the remainder of this research study.

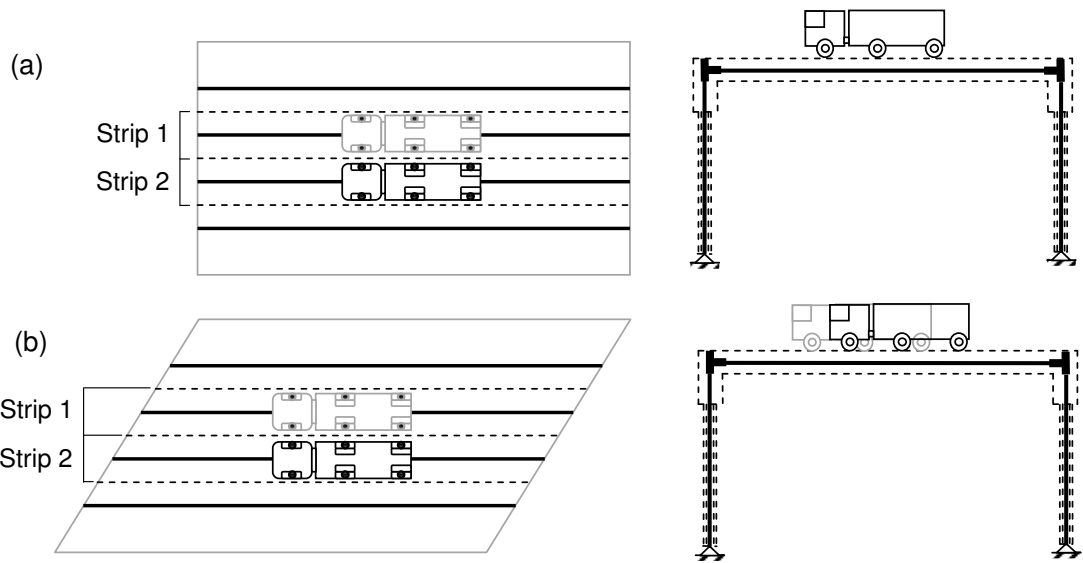


Figure 10. 3-D and 2-D models of bridges with truck loading (grey truck shows strip 1, black truck shows strip 2) (a) Straight (b) Skewed

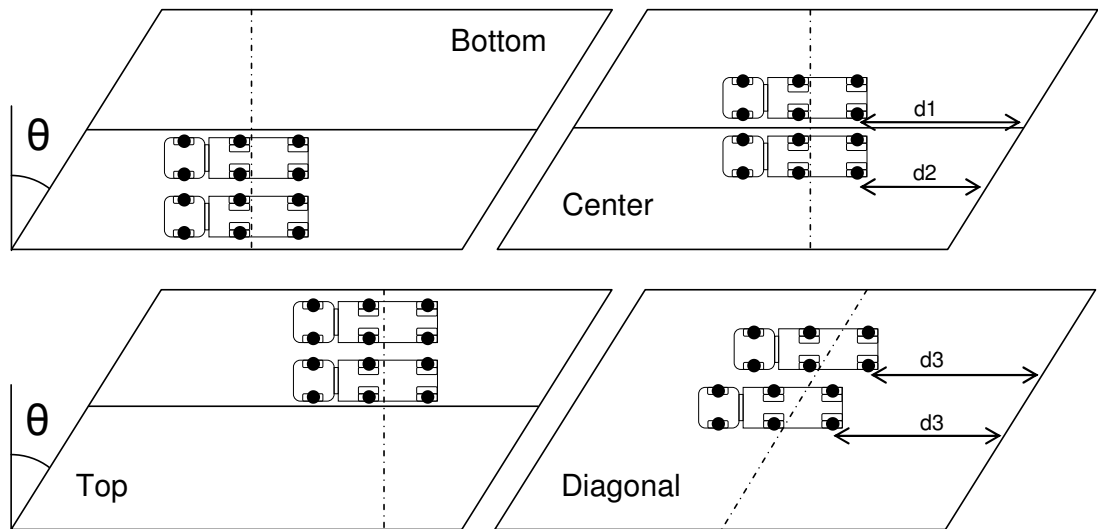


Figure 11. Sample of two lane truck loading pattern for bottom, center, top and diagonal loading patterns (distance of trucks to bridge abutment for straight and diagonal loading patterns shown with  $d_1$ ,  $d_2$  and  $d_3$ )

### **3.3 Determination of the Most Critical Loading Pattern**

In this section, more detailed information is given about the various loading patterns mentioned above in addition, the analyses results for the selection of the most critical loading pattern is outlined.

#### ***3.3.1 General Information about Loading Patterns***

For bridges with no skew the trucks are positioned at equal distances from the abutment (Figure 11). Therefore, each truck produces the same static live load moment per truck along the same line for each loaded strip along the bridge. This means that, there is only one loading pattern for straight bridges.

For skewed bridges however, three loading patterns arise depending on which part of the bridge is taken as a reference to coincide with the 2-D model as far as the truck positioning is concerned. These loading patterns are; bottom, center and top. In the case of the bottom loading pattern, the lower edge of the bridge (Figure 11) is taken as a reference to coincide with the 2-D model whereas, for the center and top loading patterns the centerline and the upper edge of the bridge (Figure 11) are respectively taken as reference to coincide with the 2-D model. There is an additional loading pattern for skewed bridges. This is called the diagonal loading pattern. In this loading pattern, all the trucks are positioned at equal distances from the abutment. Therefore, in such a loading case each loaded strip exactly coincides with the 2-D model as far as the truck positioning is concerned (Figure 11).

In the case of the straight loading patterns (bottom, center, top), the trucks are positioned along a line perpendicular to the centerline of the bridge. Such a positioning results in each truck being at a different distance from the

abutment for skewed bridges (Figure 11). This, in turn, produces different static live load moments per truck along the same line for each loaded strip. For instance, for the case where the bottom of the bridge is taken as a reference to coincide with the 2-D model (bottom loading pattern), when the trucks are placed to produce the maximum live load moment, only the truck positioned at the bottom produces the maximum live load effect, while the other trucks generate smaller live load effects (Figure 10 (b)). This may be the main reason for having smaller LLDFs for skewed bridges as evident from the cases considered in this research study and AASHTO. Consequently, loading pattern becomes an important parameter for determining the maximum live load effects for SIBs. In the case of straight loading patterns, some problems exist concerning the truck loading position to produce the maximum live load effect. For girder shear, the maximum live load effect is observed when the rear axle of the design truck is positioned at the deck abutment interface as observed from Figure 9 (a) (Dicleli 2009b). In the case of straight loading patterns however, this not possible, as the distance of the truck rear axle from the deck abutment interface increases as one moves away from the reference loading position (bottom, center or top) due to skew. Another problem with the straight loading patterns is that, for the case of short-to-medium length bridges with high skews some of the truck's wheels may remain outside the bridge boundaries (Figure 12). For instance, in the case of maximum girder shear loading of a 10 m long bridge with a skew of  $60^\circ$ , some of the trucks front axle wheels may remain outside the bridge boundaries.

For the diagonal loading pattern, as mentioned earlier, all the trucks are positioned at equal distances from the abutment (Figure 11). This, in turn, produces the same static live load moments per truck along the same line for each loaded strip. In the case of bridges with no skew, diagonal loading

becomes a straight loading pattern (Figure 12). Furthermore, compared to straight loading patterns, this loading pattern generally makes possible the placement of all trucks wheels within the bridge boundaries (Figure 12). Diagonal loading pattern is also a better option for girder shear loading as all the rear axles of the trucks are positioned closer to the abutment deck interface. However, there are some exceptions for the cases of 10 and 15 m bridges with high skews as far as the placement of the trucks wheels within the bridge boundaries is concerned. This is mainly due to one of the 1.8 m apart wheels not being accommodated within the boundaries of the bridge due to the effect of high skew (Figure 12).

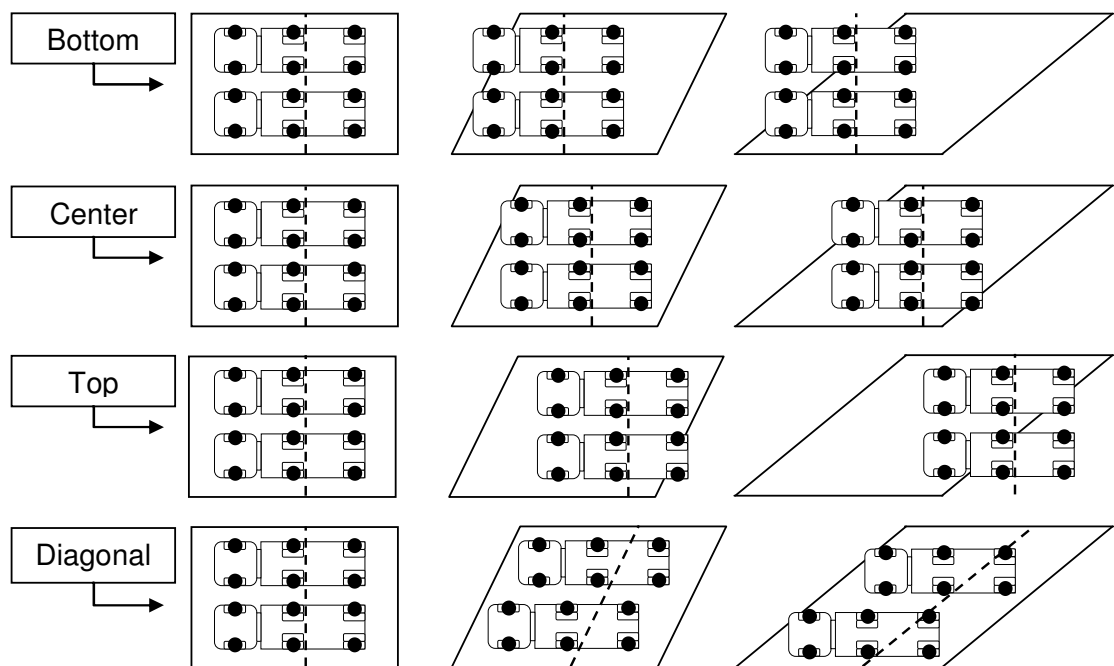


Figure 12. Effect of skew on truck loading patterns for a sample bridge model

### 3.3.2 Determination of Most Critical Loading Pattern

In this section, the most critical loading pattern producing the maximum live load effect is determined. For this purpose, eight 30 m long SIBs with 30°

skew and eight 30 m long SIBs with 50° skew are considered. Four of the 30° and 50° skew bridges have 4, 6, 8 and 10 girders with 2.4 m spacings, while the other four have 4 girders with 1.2, 2.4, 3.6 and 4.8 m spacings. In addition, two sets of bridges with 30° and 50° skew and span lengths of 10, 15, 20, 25, 35, 40 and 45 m are considered. This is done to cover a wide range of bridge geometric properties including the span length to accurately choose the most critical loading pattern producing the maximum live load effect. The bridges considered in this part of this research study are analyzed under the aforementioned four loading patterns to obtain the maximum girder live load moment as well as abutment and pile live load shear and moments. This resulted in 30 different SIB models and 4088 analyses cases. It is anticipated that, the diagonal loading will produce the maximum live load shear in the girders, as this is the only loading pattern where the truck wheel loads are placed closest to the deck abutment interface. Therefore, no analysis was conducted for the girder shear.

The analyses results are presented in Figures 13-21. Figures 13-17 display detailed analyses results for the 30 m long bridge with six girders and 30° skew. The results for the other cases are similar. In Figure 13-17 the horizontal axis represents the relative distance ( $x/W$  where,  $x$ : distance from the bottom end of the bridge,  $W$ : bridge width) of the first transversely placed truck across the bridge width while the vertical axis represents the maximum live load effect in a specific component. The figures are plotted for the cases of one, two, three and four transversely positioned trucks across the width of the bridge. The analyses results presented in these figures also includes the multiple presence factors to take into consideration the probability of presence of more than one truck across the width of the bridge. Figures 18-21 summarizes the analyses results for all the cases considered in a bar chart form. In the figures, the horizontal axis represents the model

considered in the analyses (For instance,  $N_b=4$ ,  $S=2.4$  represents a bridge with 4 girders spaced at 2.4 m) while the vertical axis represents the maximum live load effect in a specific component from all the truck loading cases considered.

The analyses results presented in Figures 13-17 reveal that the diagonal loading pattern produces similar or larger live load effects compared to the straight loading patterns (bottom, center or top). The live load effects in bridge components produced by the straight loading patterns become only more significant when the trucks are located closer to the reference point (bottom, center or top). For the case of short and / or highly-skewed bridges, the bottom and top loading patterns produce smaller live load effects in bridge components as one or more of the truck wheels generally remain outside the bridge boundaries. Center loading pattern on the other hand, produces larger live load effects in bridge components compared to those produced by bottom and top loading patterns. However, for highly skewed bridges (e.g. skew $>40$ ) even the center loading pattern cannot accommodate the placement of all truck wheels within the boundaries of the bridge when three or more trucks are placed across the bridge width.

The analyses results presented in Figures 18-21 reveal that the diagonal loading pattern produces the maximum live load effects in all the bridge components. Therefore, based on the analyses results from the 30 bridges considered, the diagonal loading pattern is selected to study the effect of skew on the distribution of live load effects among the components of SIBs for the remainder of this research study. However, to test the applicability of this important conclusion for bridges with substructure properties different than those used in the 30 base bridges considered as part of this research study further verification analyses are conducted. The analyses are

conducted for 30 m long bridges with 30° and 60° skew and four girders spaced at 2.4 m. For these bridges, two pile spacings of 1.8 and 3.0 m and two abutment heights of 2.5 and 5 m are considered. The bridges are then subjected to the diagonal truck loading pattern, the analyses results are compared in terms of the location where maximum live load effect occurs in various bridge components. The analyses results are presented in Table 6-Table 9. The results presented in these tables reveal that the maximum live load effects occur exactly at the same location (longitudinal and transverse) regardless of the substructure properties. Earlier, it was also found by Dicleli and Erhan (2010) that the pile and foundation soil stiffness does not alter the location of maximum live load effects. These further confirm the applicability of these finding to bridges with different substructure properties.

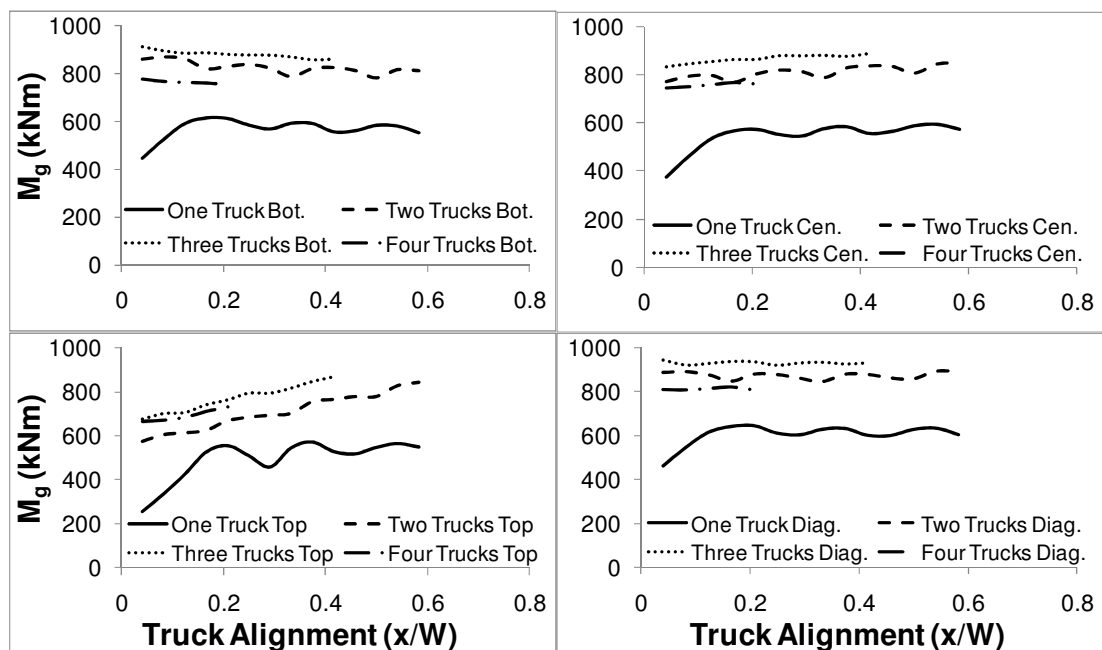


Figure 13. Girder moment comparison for 6 girder model with 30° skew and B-C-T-D loading patterns for different trucks

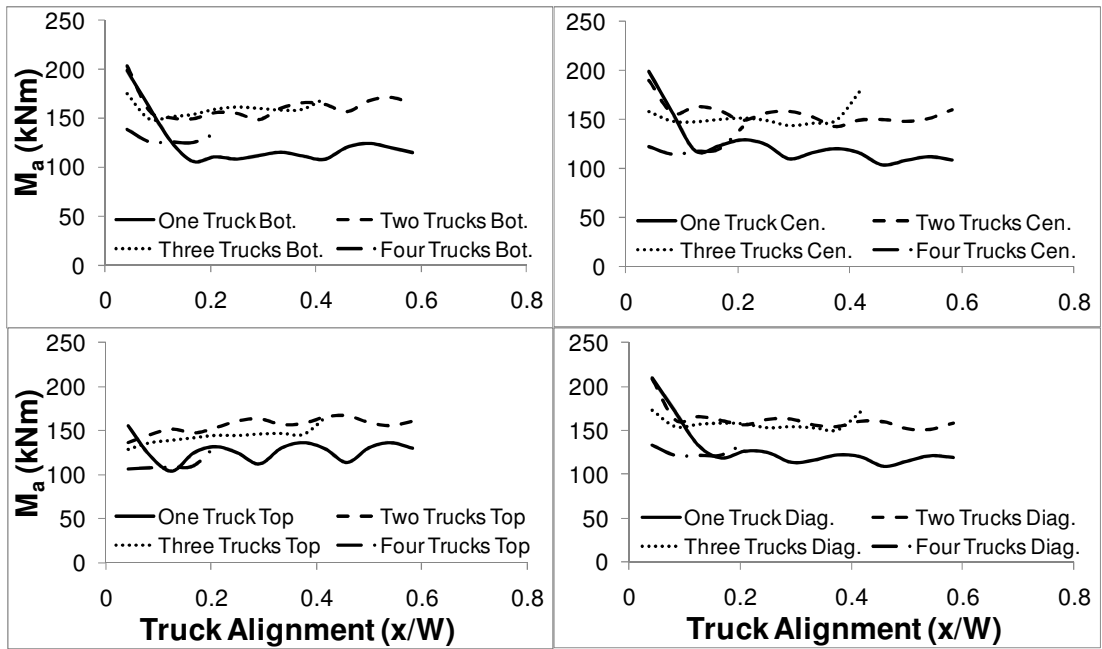


Figure 14. Abutment moment comparison for 6 girder model with 30° skew and B-C-T-D loading patterns for different trucks

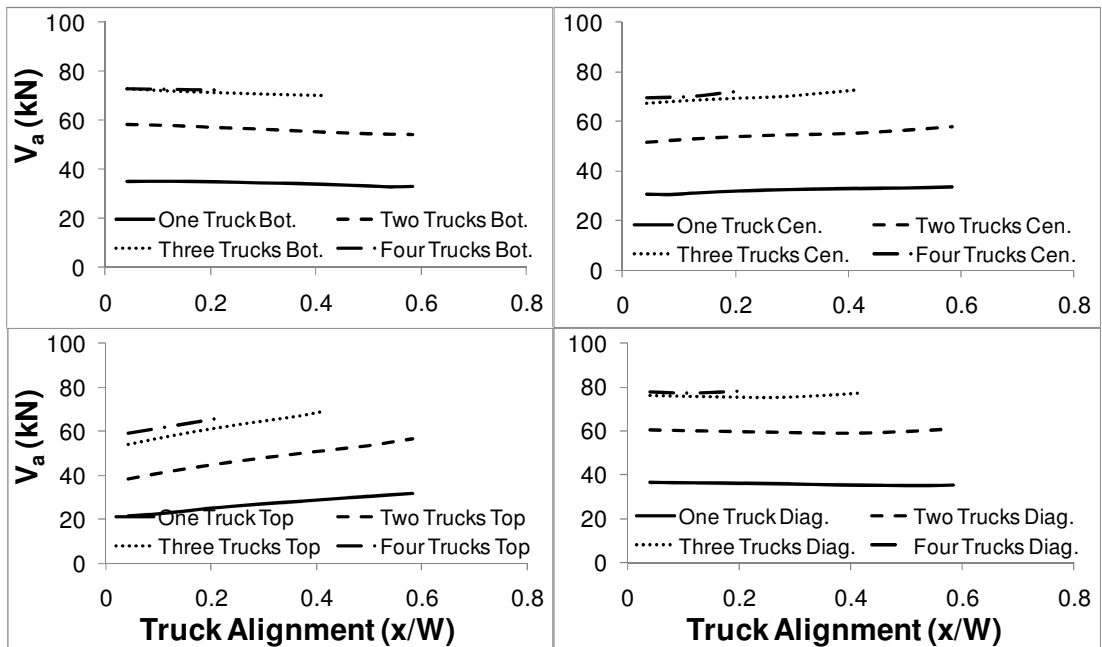


Fig 15. Abutment shear comparison for 6 girder model with 30° skew and B-C-T-D loading patterns for different trucks

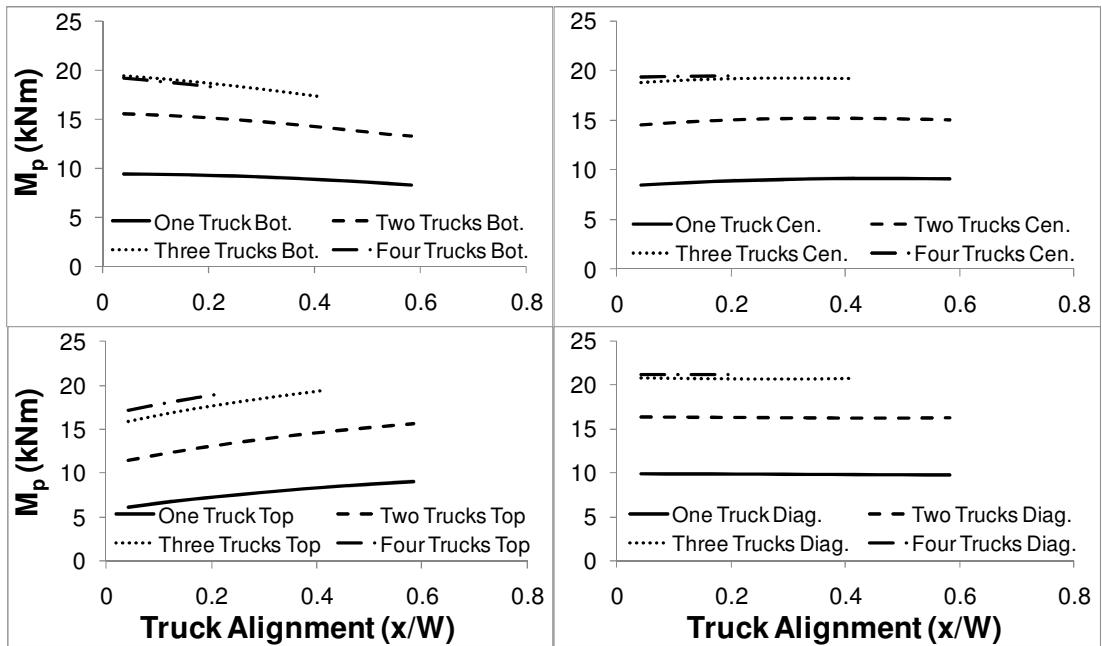


Figure 16. Pile moment comparison for 6 girder model with 30° skew and B-C-T-D loading patterns for different trucks

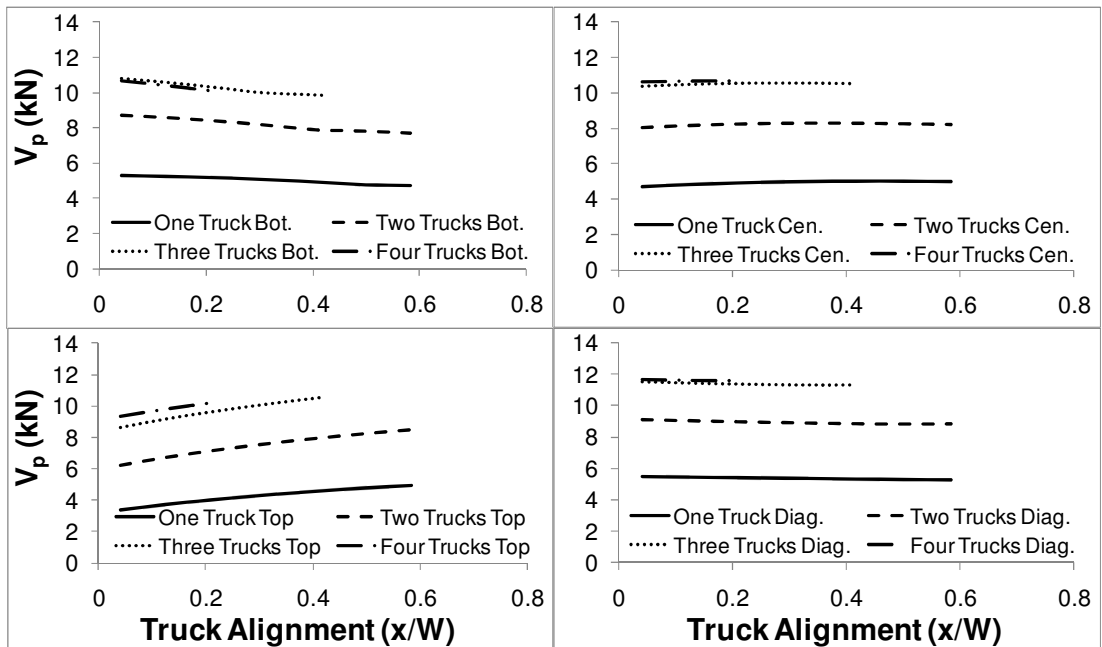


Figure 17. Pile shear comparison for 6 girder model with 30° skew and B-C-T-D loading patterns for different trucks

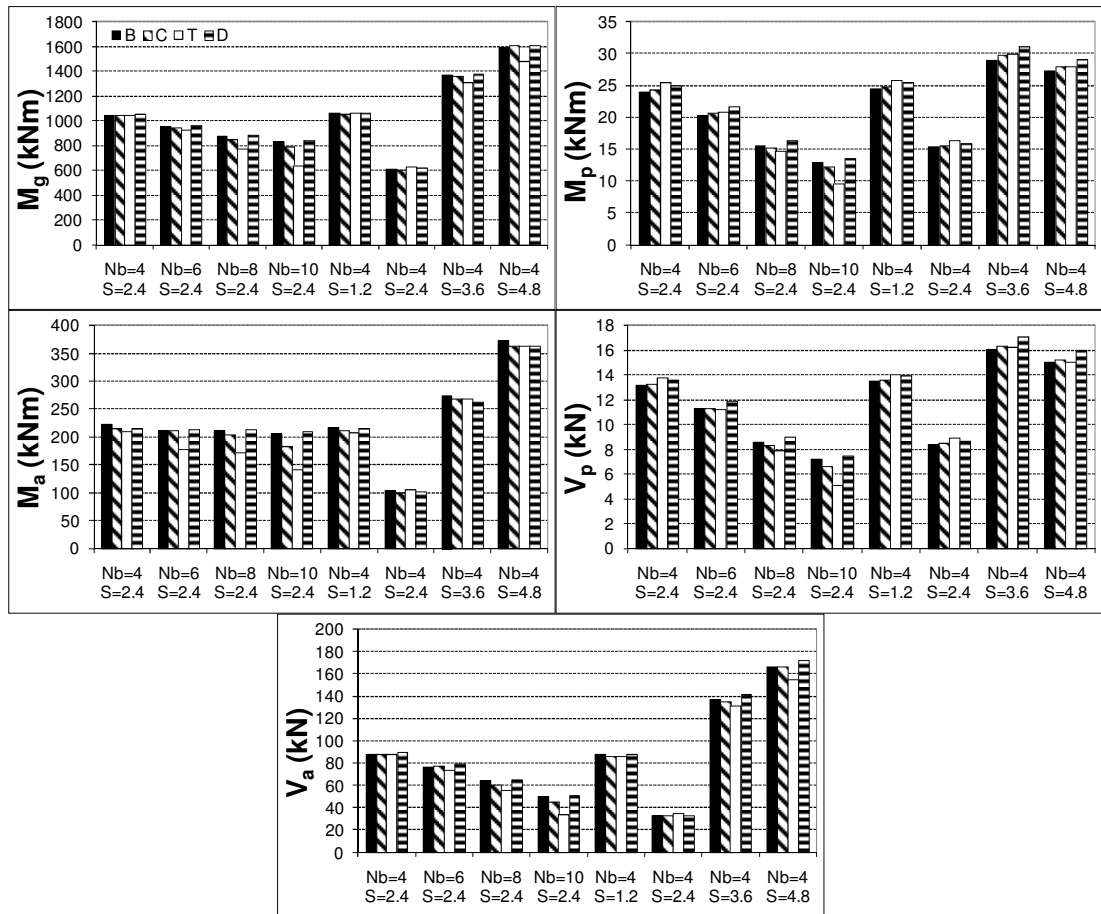


Figure 18. Maximum values of bottom, center, top and diagonal loading patterns for SIB with skew 30°

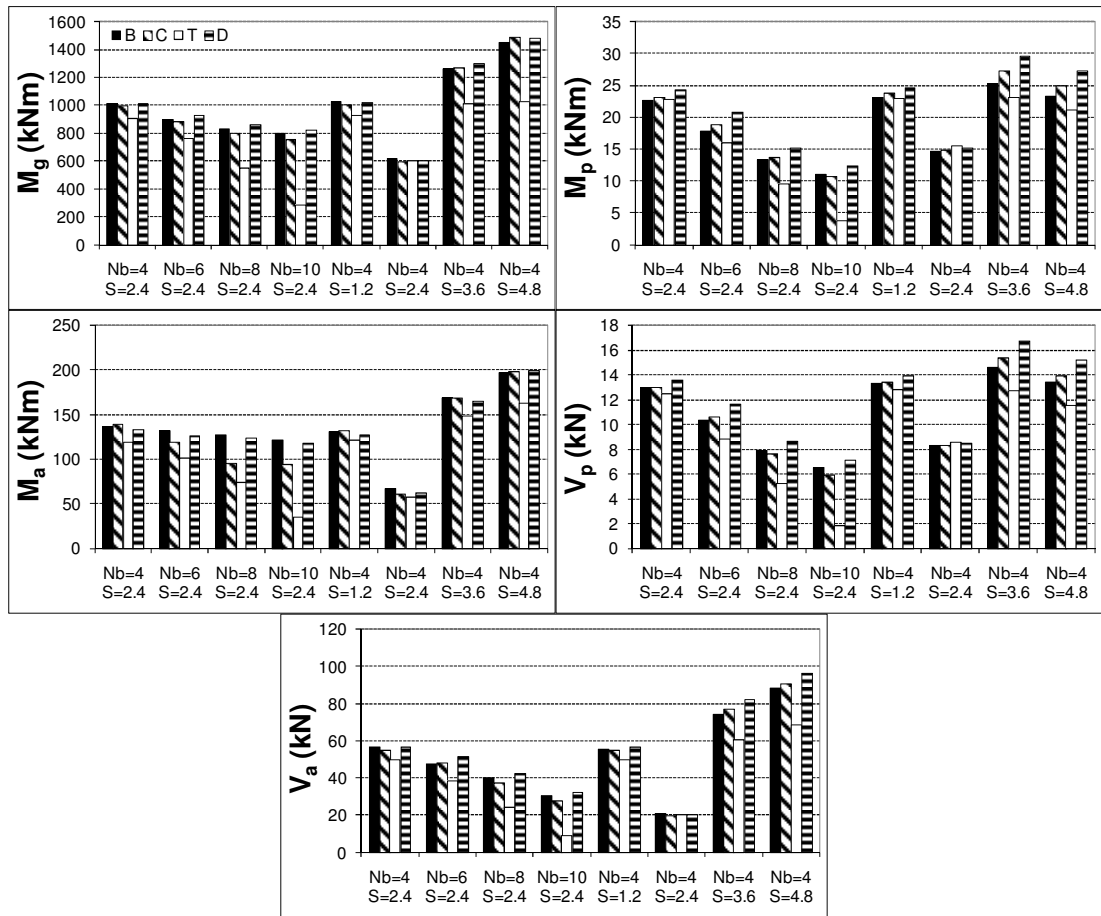


Figure 19. Maximum values of bottom, center, top and diagonal loading patterns for SIB with skew  $50^\circ$

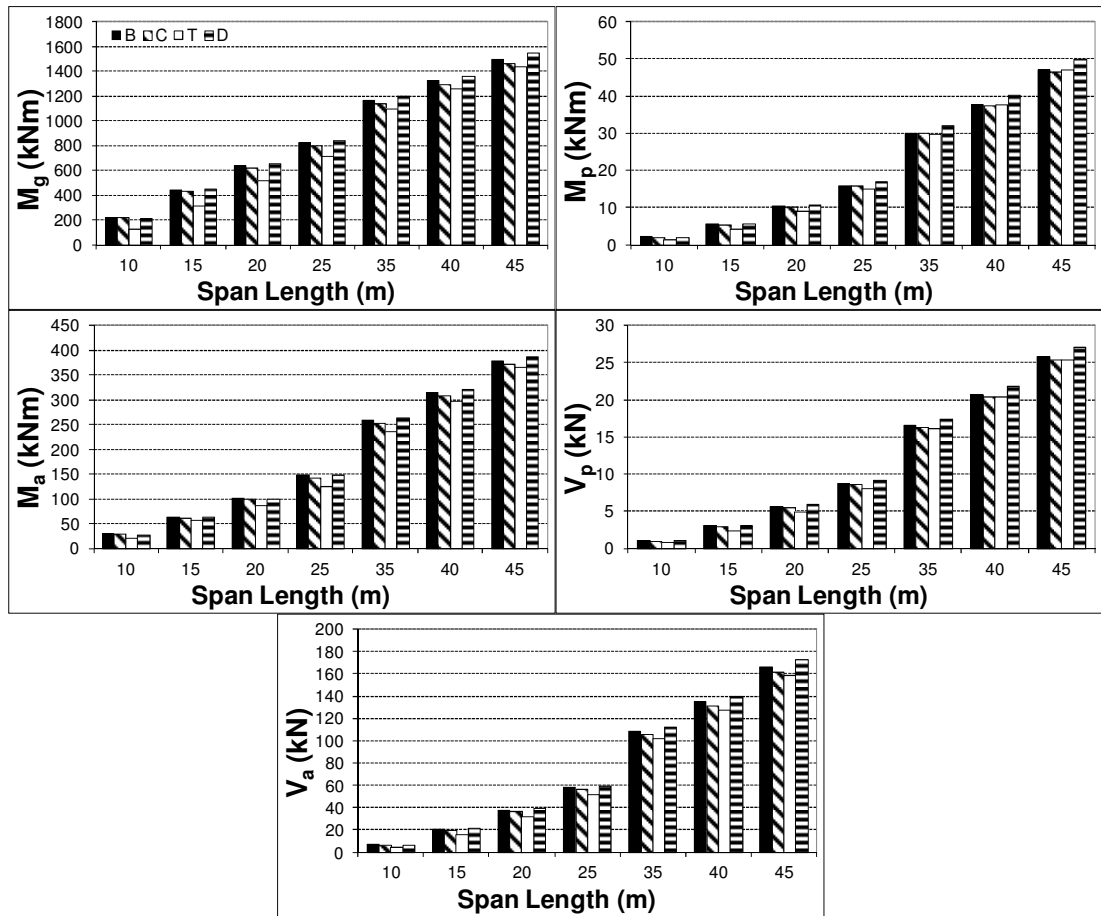


Figure 20. Maximum values of bottom, center, top and diagonal loading patterns for SIB where two or more design lanes are loaded 30° skew

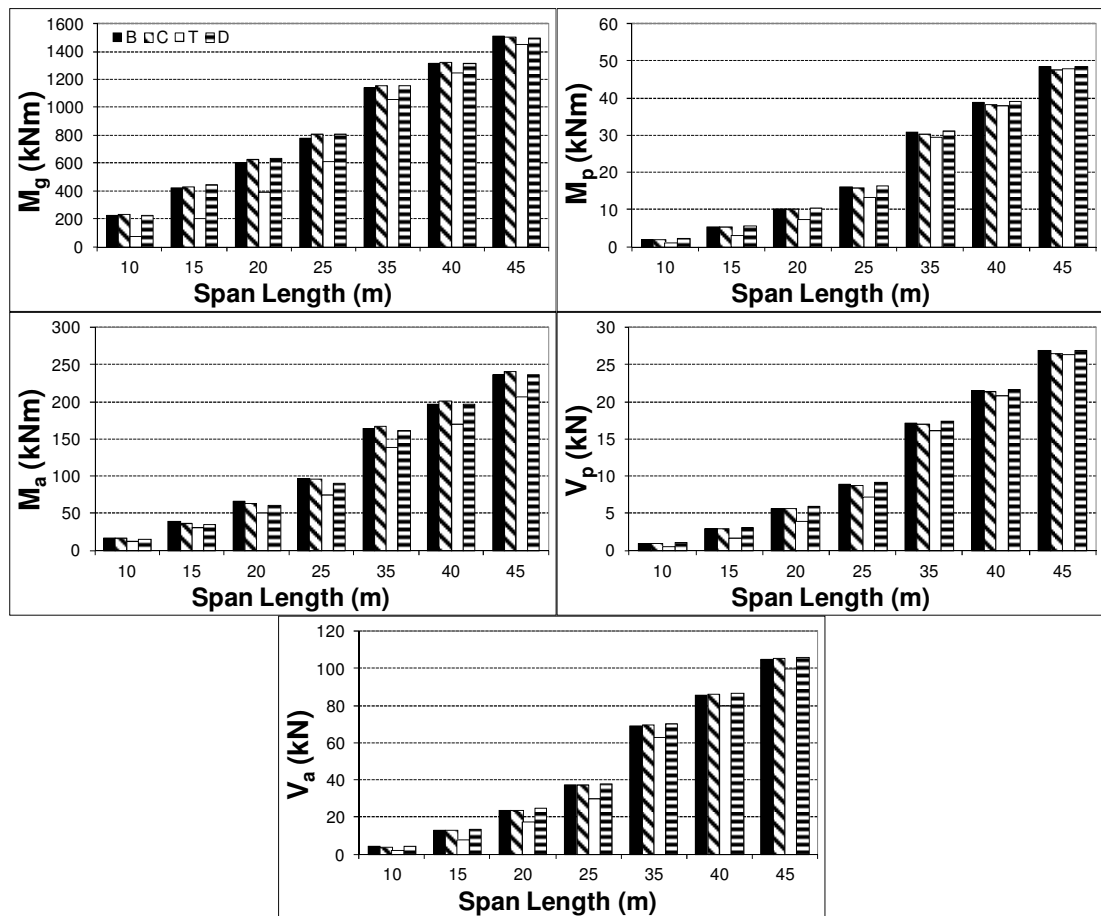


Figure 21. Maximum values of bottom, center, top and diagonal loading patterns for SIB where two or more design lanes are loaded 50° skew

Table 6: Comparison of applicability of maximum live load effects for skew 30 with respect to pile spacing

Skew 30	Pile Spacing 1.8m Two Trucks			Pile Spacing 3m Two Trucks		
	M <sub>g</sub>	M <sub>a</sub>	V <sub>a</sub>	M <sub>g</sub>	M <sub>a</sub>	V <sub>a</sub>
x/W						
0.143	1014.036	<b>217.638</b>	88.498	1035.242	<b>193.368</b>	82.040
0.286	1019.996	178.840	87.817	1041.162	154.594	82.057
0.429	1005.062	181.993	87.373	1026.081	157.802	82.143
0.571	984.443	176.112	87.173	1005.096	151.986	82.288
0.714	<b>1021.590</b>	174.170	87.300	<b>1042.120</b>	147.965	82.500
0.857	1020.327	175.457	87.975	1040.686	150.755	83.020
1.000	999.362	214.341	<b>88.835</b>	1019.616	190.207	<b>83.955</b>

Table 7: Comparison of applicability of maximum live load effects for skew 60 with respect to abutment height

Skew 30	Abutment Height 2.5m Two Trucks			Abutment Height 4m Two Trucks		
	x/W	M <sub>g</sub>	M <sub>a</sub>	V <sub>a</sub>	M <sub>g</sub>	M <sub>a</sub>
0.143	1070.401	<b>163.067</b>	63.485	926.988	<b>322.624</b>	117.978
0.286	1076.159	121.615	63.060	933.035	272.539	117.758
0.429	1061.119	124.902	63.059	918.222	275.108	117.649
0.571	1040.488	119.352	63.239	897.684	268.444	117.637
0.714	<b>1077.664</b>	114.900	63.591	<b>934.692</b>	257.455	117.734
0.857	1076.427	122.192	64.110	933.065	271.826	118.355
1.000	1055.568	159.775	<b>64.786</b>	911.835	313.164	<b>119.574</b>

Table 8: Comparison of applicability of maximum live load effects for skew 60 with respect to pile spacing

Skew 60	Pile Spacing 1.8m Two Trucks			Pile Spacing 3m Two Trucks		
	x/W	M <sub>g</sub>	M <sub>a</sub>	V <sub>a</sub>	M <sub>g</sub>	M <sub>a</sub>
0.143	901.253	90.741	37.744	926.156	79.816	35.711
0.286	888.750	77.253	37.087	913.880	66.240	35.220
0.429	891.033	66.652	36.863	916.275	53.508	35.013
0.571	863.647	68.602	36.877	888.258	53.917	35.037
0.714	900.840	70.521	37.119	925.054	58.212	35.293
0.857	894.307	82.383	37.582	918.073	70.241	35.775
1.000	<b>903.673</b>	<b>94.837</b>	<b>38.261</b>	<b>926.975</b>	<b>82.890</b>	<b>36.476</b>

Table 9: Comparison of applicability of maximum live load effects for skew 60 with respect to abutment height

Skew 60	Abutment Height 2.5m Two Trucks			Abutment Height 4m Two Trucks		
	x/W	M <sub>g</sub>	M <sub>a</sub>	V <sub>a</sub>	M <sub>g</sub>	M <sub>a</sub>
0.143	952.660	68.889	29.390	829.169	129.623	47.537
0.286	939.373	56.086	28.957	817.802	114.626	46.982
0.429	941.120	44.108	28.754	820.803	100.662	46.779
0.571	913.623	43.914	28.733	793.943	95.229	46.865
0.714	951.022	50.170	28.900	830.225	105.679	47.239
0.857	944.913	61.501	29.250	822.482	118.821	47.888
1.000	<b>954.926</b>	<b>73.331</b>	<b>29.775</b>	<b>830.227</b>	<b>132.747</b>	<b>48.810</b>

## **CHAPTER 4**

### **AUTOMATED ANALYSES PROCEDURE**

#### **4.1 General**

In this research, the effects of skew and several selected parameters on the distribution of live load effects among the components of SIBs are investigated. Due to the nature of the large parametric study conducted as part of this research, 231 SIB models were built and more than 25000 analyses were conducted under various AASHTO LRFD truck loading cases. The large number of bridge models and loading cases required an automated analysis procedure. For this purpose, a set of programs were coded using Visual Basic programming language and calculation tables (IO worksheet) were created with Microsoft Excel. The Visual Basic program and the Microsoft Excel tables were used to prepare the loading input data for the already created FEMs of SIBs in the structural analysis program SAP2000 v11 (Computers and Structures inc, 2007) and to extract the necessary data such as girder shear and bending moment from the output files generated by SAP2000.

#### **4.2 Properties of the IO Worksheet**

The IO worksheet requires as input data the length, width and the skew of the bridge, the coordinates used for building the FEMs in SAP2000,

dimensions of shell elements, distance between the axles of the truck and axle loads, the longitudinal position of the truck obtained by influence line analysis and the truck loading pattern (Bottom, Center, Top or Diagonal). Then, the IO worksheet calculates the values and the coordinates of the truck loading with built-in Microsoft Excel functions for each bridge model by using the assigned geometric properties (Figure 22). In the figure the term "row" represents the row of wheels of the trucks positioned on the bridge and the grey hatched cells show the required input data. For instance, if there are two trucks positioned on the bridge there will be four rows of wheels. Details of these calculations and assumptions are explained below.

Bridge Length	30	First Coord.	-15	Shell Dim.	0.6	Run and take results of analysis	
Shells along width	26	Bridge Width	15.6	Skew Effect	0.715		
Skew	50	Longitudinal position of first axle to reference point			3.572		
Transverse Position	1	Horizontal distance of first axle to bridge center			2.857		
Loading Type	D						
Axle Loads	17.5	72.5	72.5	Axle Distance	4.3		
X Coordinates of Truck Loading							
							Y Coordinates
8. Row	-8.151	-7.551	-12.551	-11.951	-16.951	-16.351	3.6
7. Row	-7.896	-7.296	-12.296	-11.696	-16.696	-16.096	1.8
6. Row	-4.576	-3.976	-8.976	-8.376	-13.376	-12.776	0.6
5. Row	-4.321	-3.721	-8.721	-8.121	-13.121	-12.521	-1.2
4. Row	-1.001	-0.401	-5.401	-4.801	-9.801	-9.201	-2.4
3. Row	-0.746	-0.146	-5.146	-4.546	-9.546	-8.946	-4.2
2. Row	2.575	3.175	-1.825	-1.225	-6.225	-5.625	-5.4
1. Row	2.830	3.430	-1.570	-0.970	-5.970	-5.370	-7.2
Values of Truck Loading							
8. Row	9.259	8.241	26.276	46.224	14.193	58.307	
7. Row	16.692	0.808	57.070	15.430	44.986	27.514	
6. Row	9.259	8.241	26.276	46.224	14.193	58.307	
5. Row	16.692	0.808	57.070	15.430	44.986	27.514	
4. Row	9.259	8.241	26.276	46.224	14.193	58.307	
3. Row	16.692	0.808	57.070	15.430	44.986	27.514	
2. Row	9.259	8.241	26.276	46.224	14.193	58.307	
1. Row	16.692	0.808	57.070	15.430	44.986	27.514	

Figure 22. The IO worksheet formed for the calculation of values and coordinates of truck load

#### 4.2.1 Parameters Used for Calculation

Presence of various span lengths and skews brings out the necessity of defining a reference point to define the position of the truck loading on the bridge. Variation of span length as well as the skew leads to a change in start-end coordinates of the bridges under consideration. Therefore, a reference point is defined as the bottom-left corner of the bridge deck for the ease of calculations (Figure 23). The reference point does not change as a function of skew. It is only dependent on the span length. The coordinates and values of truck loading are calculated with respect to the reference point.

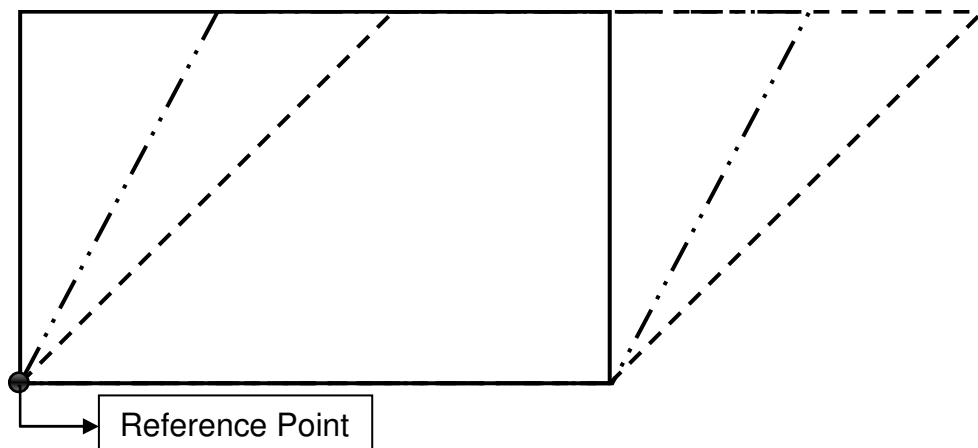


Figure 23. Reference point for different skews (dashed lines represents the skewed bridge deck for different skews)

Truck loading parameters, such as distance between the axles of the truck and axle loads, are also defined as input to broaden the application of the developed IO worksheet to various truck loading cases other than the AASHTO truck. In this research, AASHTO LRFD Specifications HL-93 design truck (Figure 8) is used to obtain the maximum live load effects. HL-93 design truck is composed of three 1.8 m wide axles spaced at 4.3 m. Loading

values and geometric properties of the design truck are added to the IO worksheet as an input parameter.

As discussed earlier, four types of truck loading patterns (bottom, center, top and diagonal) are considered in this research (Figure 11). These loading patterns are also added to the IO worksheet as input parameters and used for the calculation of the longitudinal position of the design trucks with respect to the corresponding reference position (bottom, center, top) across the width of the bridge. Moreover, a transverse position parameter is also used as an input parameter to determine the position of the first design truck across the width of the bridge (this is done to position the truck relative to an existing curb or barrier / railing on the bridge and for greater flexibility). Then, these parameters are used for the calculation of values and coordinates of the design truck loading. Detailed information about the calculation procedure is explained in the following section.

#### ***4.2.2 Calculation Procedure***

First, the IO worksheet calculates the coordinates of the reference point with respect to its span length. Then, the skew angle and the length of the bridge are used to calculate the coordinates of each shell. The skew angle, the length of the bridge and the longitudinal position of the design truck obtained from influence line analyses are also used to calculate the coordinates of the longitudinal position of the truck wheels with respect to the reference point. The transverse position of the design trucks as well as the type of the loading pattern (bottom, center, top and diagonal) under consideration are taken into account when calculating the longitudinal coordinates of the truck wheels. SAP2000 requires the wheel loads to be assigned to the shell nodes only. However, the calculated wheel positions may not coincide with the exact

positions of the shell nodes. Therefore, in such cases, an inverse ratio procedure is used to distribute the wheel loads to the shell nodes. According to this procedure, the wheel load is distributed inversely proportional to the distance between the wheel load and the neighboring shell nodes (similar to the calculation of support reactions in a simply supported beam due to a point load applied on the beam). This procedure is carried out for each loading point which is not coinciding with the existing shell nodes. For the SIB models considered in the analyses, the wheel loads needed to be distributed to the shell nodes in the majority of the cases.

The IO worksheet, which is formed for the calculation of the design truck loading values and coordinates, normally works with manual input. For analyzing numerous models and analyses cases, an automated procedure is required. A Visual Basic program is coded for this purpose. The Visual Basic program prepares the required input data for the IO worksheet, automatically assigns the design truck loads to FEMs in SAP2000, conducts the analyses of the models and extracts the response values from the output files. Detailed information about the Visual Basic program is presented in the following section.

### **4.3 Visual Basic Program**

Visual basic is a well known programming language for its ability to work in combination with various programs. Most of the Microsoft software supports this programming language, which is embedded within the Microsoft modules such as Excel. The finite element based program SAP2000 v11 also supports the visual basic commands via a specific feature named OAPI (Open Application Interface). This feature of the program makes possible the automation of tedious and time consuming repetitive modeling and analysis

procedures as well as output reading in SAP2000. For example, the loading values and coordinates are calculated by the IO worksheet and are assigned to SAP2000 by the visual basic program utilizing the OAPI feature of SAP2000. A flowchart demonstrating the way the Visual Basic program and the IO worksheet works is presented in Figure 24.

Although SAP2000 brings many time-saving innovations through its OAPI feature, it has some drawbacks. One of these drawbacks is that the stress values at a specific nodal point on a shell element may differ with the output reading method. Stress values of shell elements obtained from the Graphical User Interface (GUI) of the program are not similar to those of the output tables. This difference occur because the stress averaging method, which is the correct procedure for estimating shell stresses, is available for the GUI but not for the output tables (SAP2000 2007). The stress output for shell elements can only be taken from output tables via the OAPI feature. Therefore, some simplifications and extra calculations, which are described below, were performed in order to obtain accurate results.

For instance, assume that in a structural system there are four shell elements; A, B, C and D as shown in Figure 25. Joint 5 shown in the figure is common to all these shell elements. Each of these shell elements has different internal stresses at joint 5 (for instance, for a beam sectioned at a specific point, the shear forces in the beam segments to the left and to the right of the point are different). Stress averaging option combines these four different internal stresses and takes their average as the stress at joint 5. Finer meshes will result in smaller differences between neighboring shells' joints. Nevertheless, when finer meshing is not possible, stress averaging method minimizes the error of the finite element analyses results.

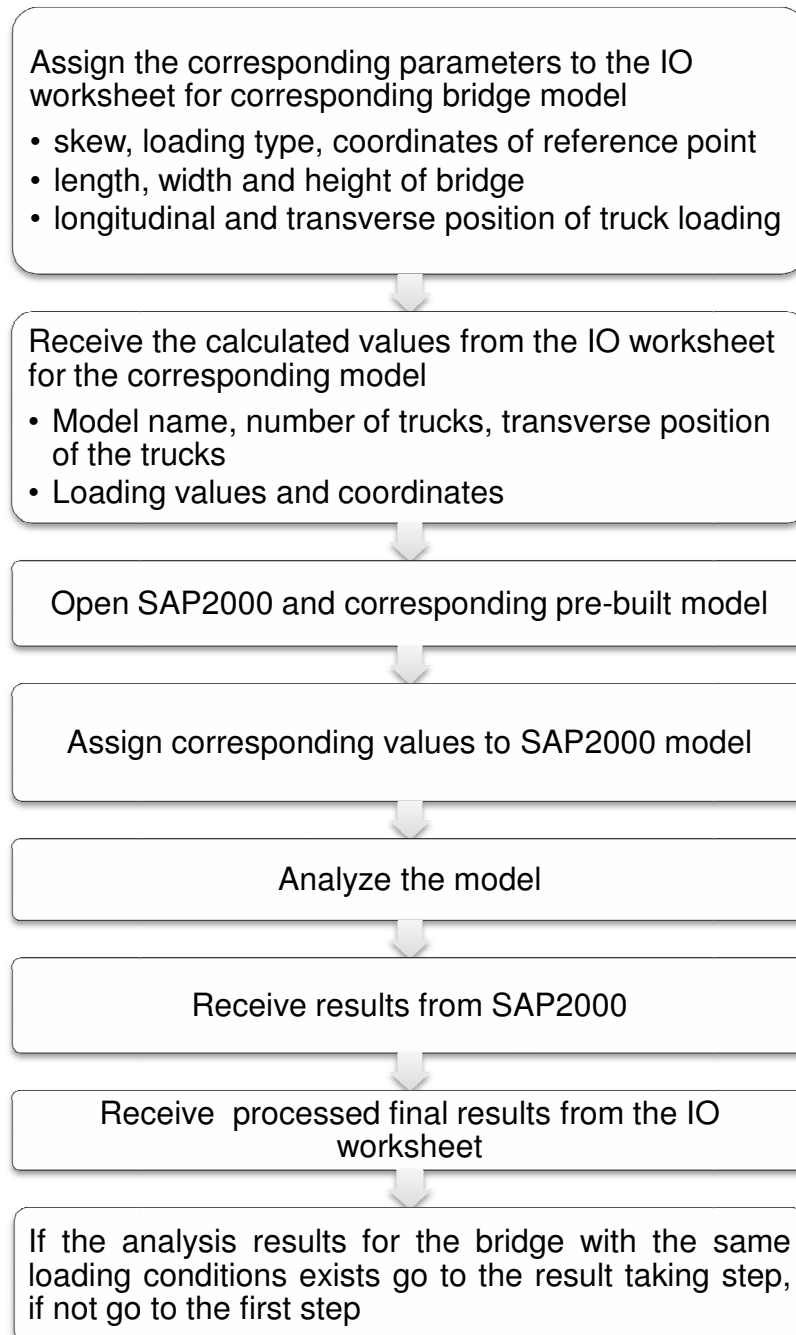
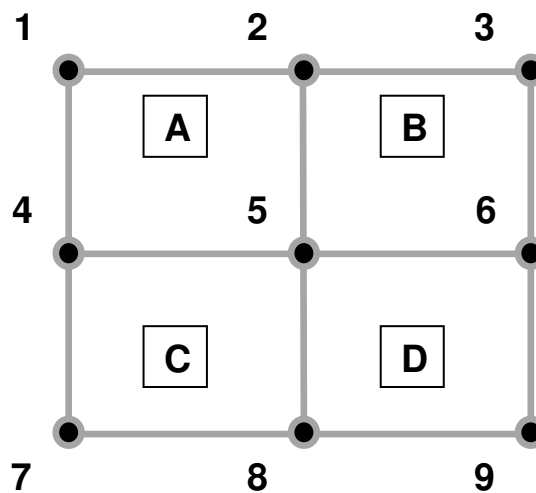


Figure 24. Flowchart of Visual Basic program used for each analysis

The absence of stress averaging method in the output tables renders the OAPI feature of SAP2000 ineffective for reading the correct shell stresses for the abutments. To use this useful feature of SAP2000, extra calculations are required to process the data extracted from the output tables. For this purpose, the stresses of each shell element at their intersection joint are taken and averaged by the IO worksheet created as part of this research.



*Figure 25. Sample for stress averaging method*

Girder moment and girder shear results are obtained from the summation of frame and shell results. This can be automatically done by using the section cut feature of SAP2000. Section cut in SAP2000 is a feature which combines the results along a selected line from GUI and obtains the total internal forces as a resultant force. Although, this feature includes stress averaging and gives more precise results, automation of this feature is harder because SAP2000 OAPI lacks the necessary command for creating a section cut. In SAP2000, results of frames, shells, asolids, planes and solids can be obtained with this feature. Stress averaging method for these elements is automatically performed at the location of the section cut. For instance, assume that in a bridge deck there are four shell elements; A, B, C and D

and a beam element FR1 as shown in Figure 26. A GUI section cut, which is shown with a grey double arrowed line, determines the resultant moment and the shear values from the beam element FR1 and shell elements B and C. Section cut determines this resultant effects at the center of the selected line with an angle measured counterclockwise from the positive global X-axis to the positive X-axis of the local coordinate system (SAP2000 2007). This angle is very important for receiving correct results of girder moments, especially when skewed section cuts are considered (the angle must be  $90^\circ$  to obtain the correct moment in the girders in a skewed bridge). On the contrary, angle of section cut does not affect girder shear values because the plane of girder shear force remains unaffected with the change in skew.

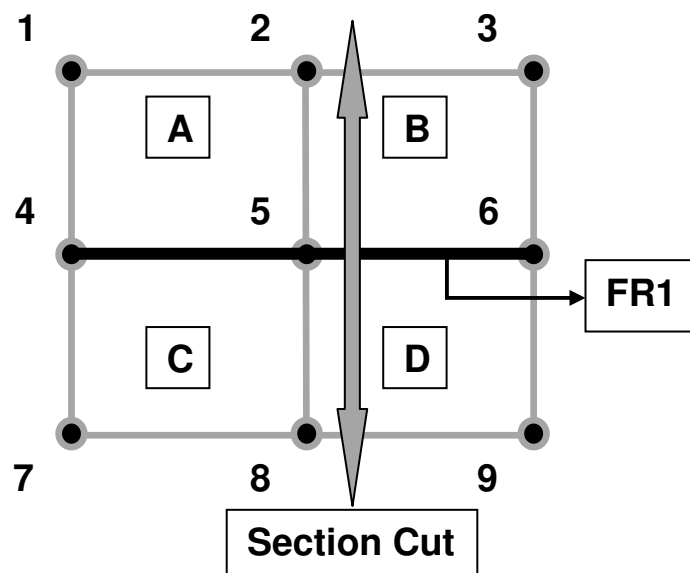


Figure 26. Section cut for frame and shell elements

## **CHAPTER 5**

### **PARAMETRIC STUDY AND EVALUATION OF RESULTS**

#### **5.1 General**

In this chapter, first general details about the calculation of LLDFs are given. Then, the effect of skew as well as other parameters considered in this research study on the distribution of live load effects among the interior and exterior girders, abutments and piles are presented.

#### **5.2 Calculation of Live Load Distribution Factors**

LLDFs are calculated for the composite interior and exterior girders, abutments and piles. For the composite interior and exterior girders, the maximum live load effects (moment and shear) from 3-D analyses are calculated as the summation of the maximum effects in the girder element and within the tributary width of the slab (equal to the girder spacing) at the same location along the bridge. For the abutments, the maximum live load effects from 3-D analyses are calculated as the summation of the forces within the tributary width of the abutment. The maximum live load effects for the piles from 3-D analyses are directly obtained as the related effect (shear or moment) at the top of the pile. The live load distribution factors are then calculated as the ratio of the maximum live load effects obtained from 3-D analyses to those obtained from 2-D analyses under a single truck load.

In this research study, LLDFs for interior and exterior girders are calculated for the cases where only one design lane and two or more design lanes are loaded. LLDFs for abutments and piles are calculated with the maximum values obtained along the bridge width for the cases where only one design lane and two or more design lanes are loaded.

### **5.3 Evaluation of Analyses Results with Respect to the Skew Angle**

The results of Analysis Set 1 where the number of girders is taken as a dominant parameter together with the skew angle are depicted in Figure 28. The figure presents the analyses results for the case where two or more design lanes are loaded. In the figure, the variations of LLDFs are plotted as a function of the skew angle. It is observed from the figure that the skew angle has a significant effect on LLDFs for interior and exterior girder shears and abutment moment. The main reason for this is that in the case of the girder shear, the presence of the skew results in one of the truck wheels being further away from the support. In addition, the distribution of live load shear to the most critical girder from the second and other trucks becomes less effective due to the effect of skew. These produce, smaller girder live load shear for larger skew angles. In the case of the abutment moment, the presence of the skew results in smaller bending moments ( $M_{s1}$ ) about an axis parallel to the width of the abutment, which is shown in Figure 27. Consequently, the abutment live load bending moment and hence, the LLDF decreases with increasing skew angle. The effect of skew angle on the LLDFs for the interior and exterior girder moments, abutment shear as well as pile moment and shear is less significant.

It observed that LLDFs for the interior and exterior girder shears decrease nearly linearly as the skew angle increases. Nonetheless, LLDFs for the

interior and exterior girder moments as well as pile moment and shear are practically constant up to a skew angle of  $50^\circ$ . For skew angles larger than  $50^\circ$  a slight reduction in LLDF is observed. In the case of the abutment moment however, the LLDFs are observed to decrease slightly up to a skew angle of  $20^\circ$  and for skew angles larger than  $20^\circ$  a significant reduction in LLDFs is noted. A less pronounced, but similar variation as a function of skew angle is also observed for the LLDFs of abutment shear.

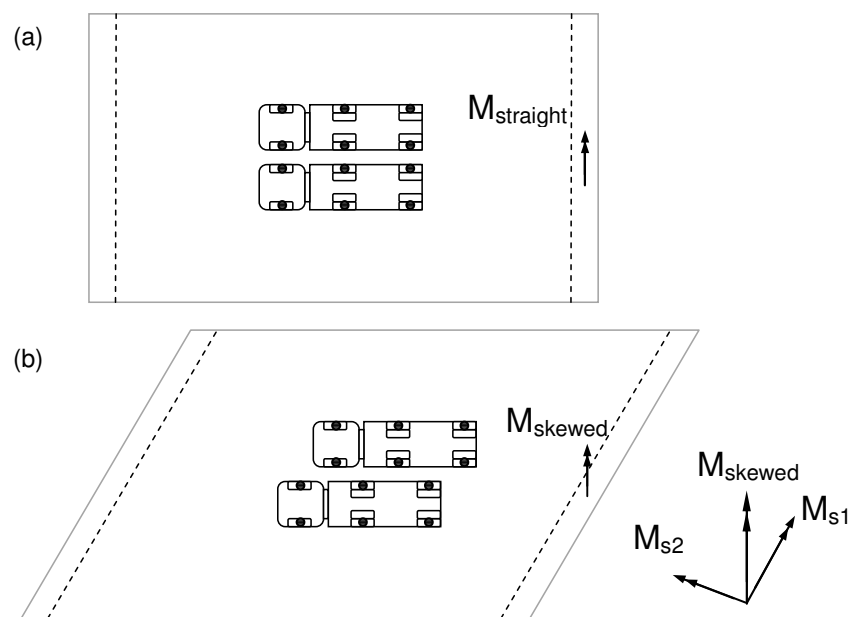


Figure 27. Abutment moment for IBs (a) for straight IB (b) for SIB

The results of Analysis Set 1 where the number of girders is taken as a dominant parameter together with the skew angle are depicted in Figure 29 for the case where one design lane is loaded. The variation of the LLDFs as a function of the skew angle is similar to that of the case where two or more design lanes are loaded except for the interior girder shear. The LLDFs for the interior girder shear are nearly constant regardless of the skew angle. This is mainly due to the lack of additional number of trucks (compared to the

two or more design lanes loaded case) where their load distribution to the critical girder is more affected by the presence of skew.

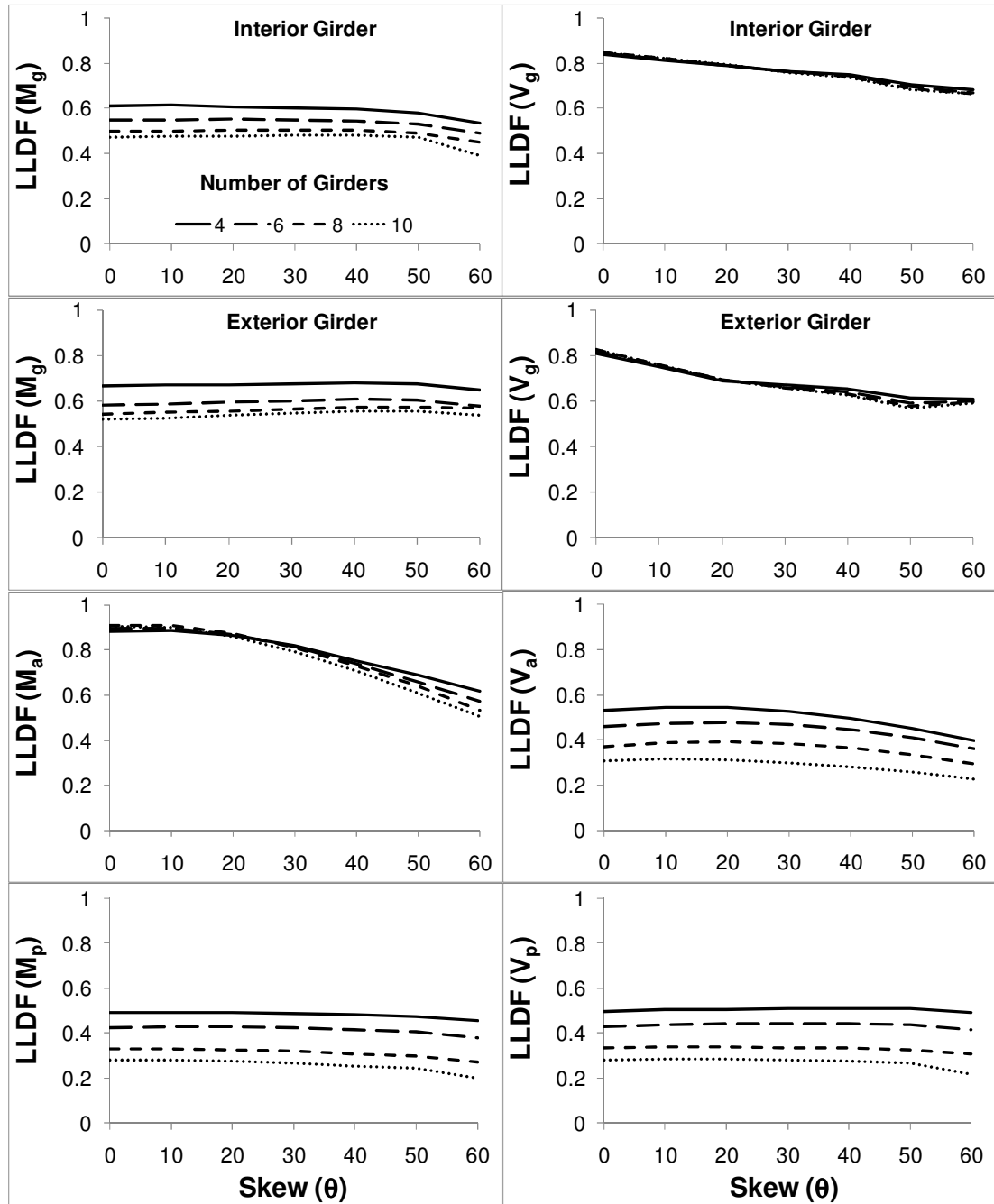


Figure 28. Effect of skew on LLDFs of SIBs for Analysis Set 1 where two or more design lanes are loaded

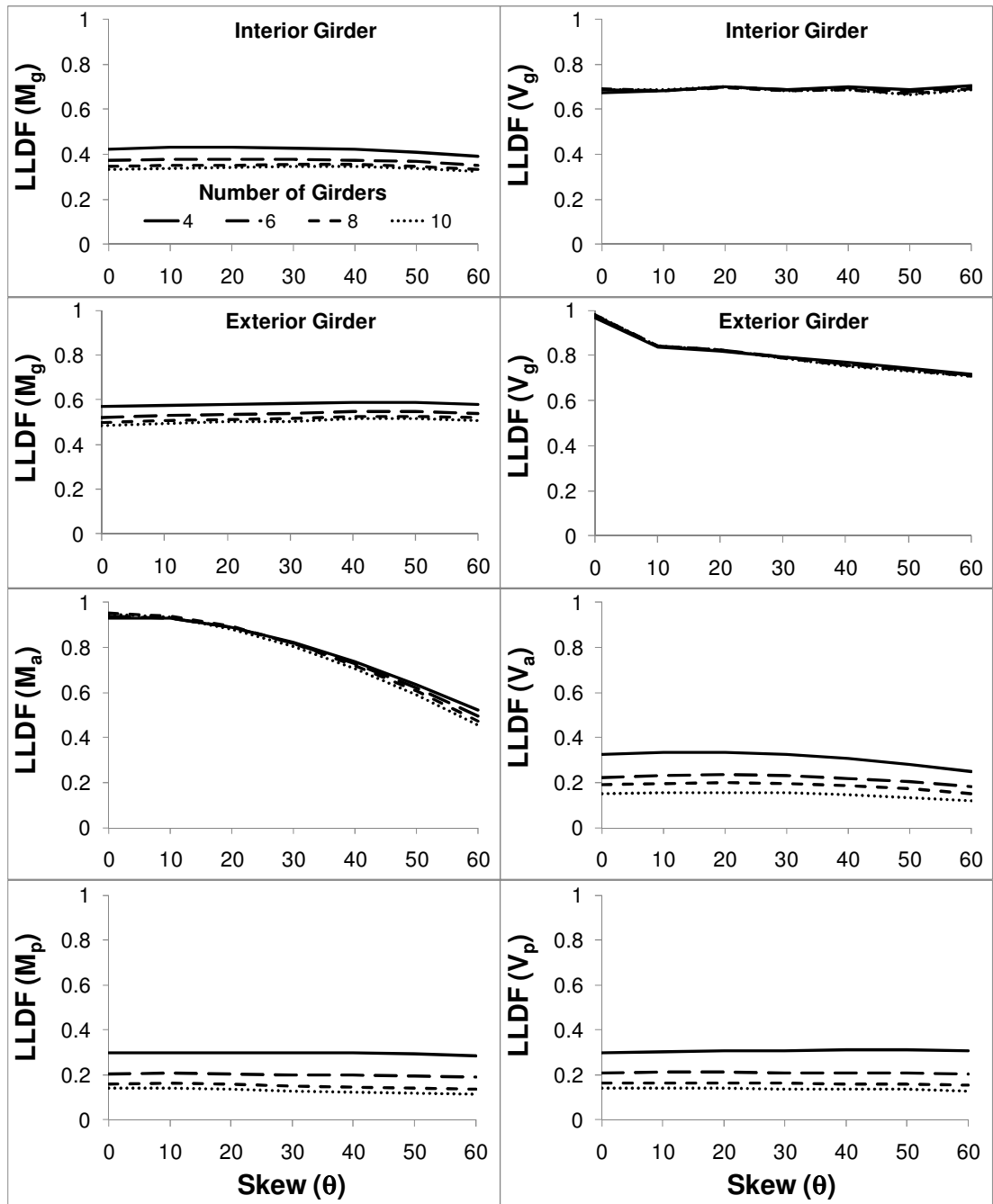


Figure 29. Effect of skew on LLDFs of SIBs for Analysis Set 1 where one design lane is loaded

For the cases where the remaining parameters other than the girder spacing are taken as dominant parameters together with the skew angle similar variations in LLDFs as a function of the skew angle is observed. The figures related to these parameters are presented in the Figures 32-49.

For the case where the girder spacing is taken as a dominant parameter together with the skew angle, the variation in LLDFs as a function of the skew angle is different. The analyses results in the form of LLDFs vs. skew angle are presented in Figures 30-31 for the cases where two or more design lanes are loaded and one design lane is loaded respectively. In the analyses, the number of girders was kept same for all girder spacings considered. This resulted in very narrow bridges for smaller girder spacings. As observed from the figures the effect of skew on LLDFs becomes less significant as the girder spacing and hence the bridge width decreases. This is mainly due to the smaller width of the bridge and the number of trucks that can be accommodated within this small width.

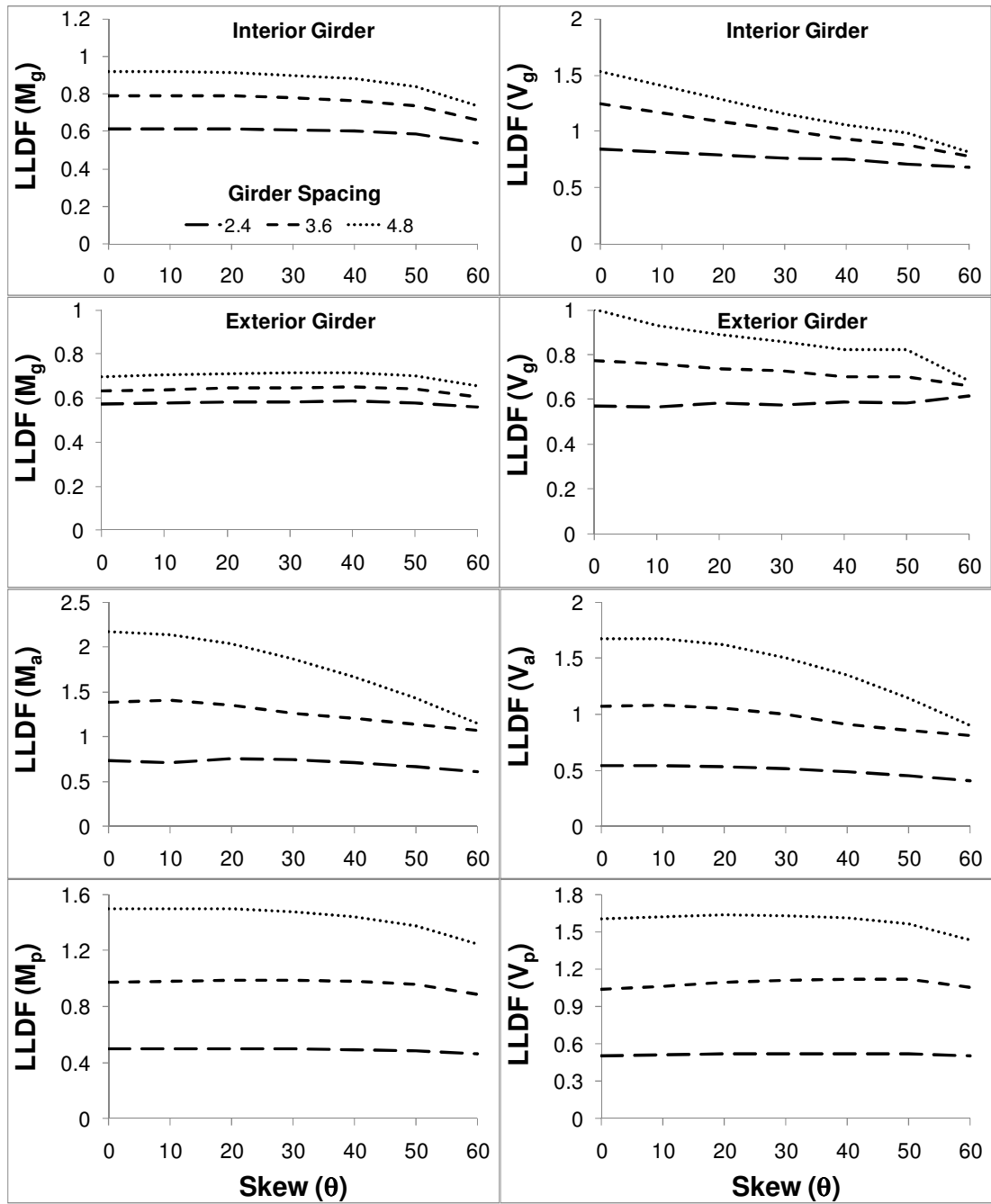


Figure 30. Effect of skew on LLDFs of SIBs for Analysis Set 9 where two or more design lanes are loaded

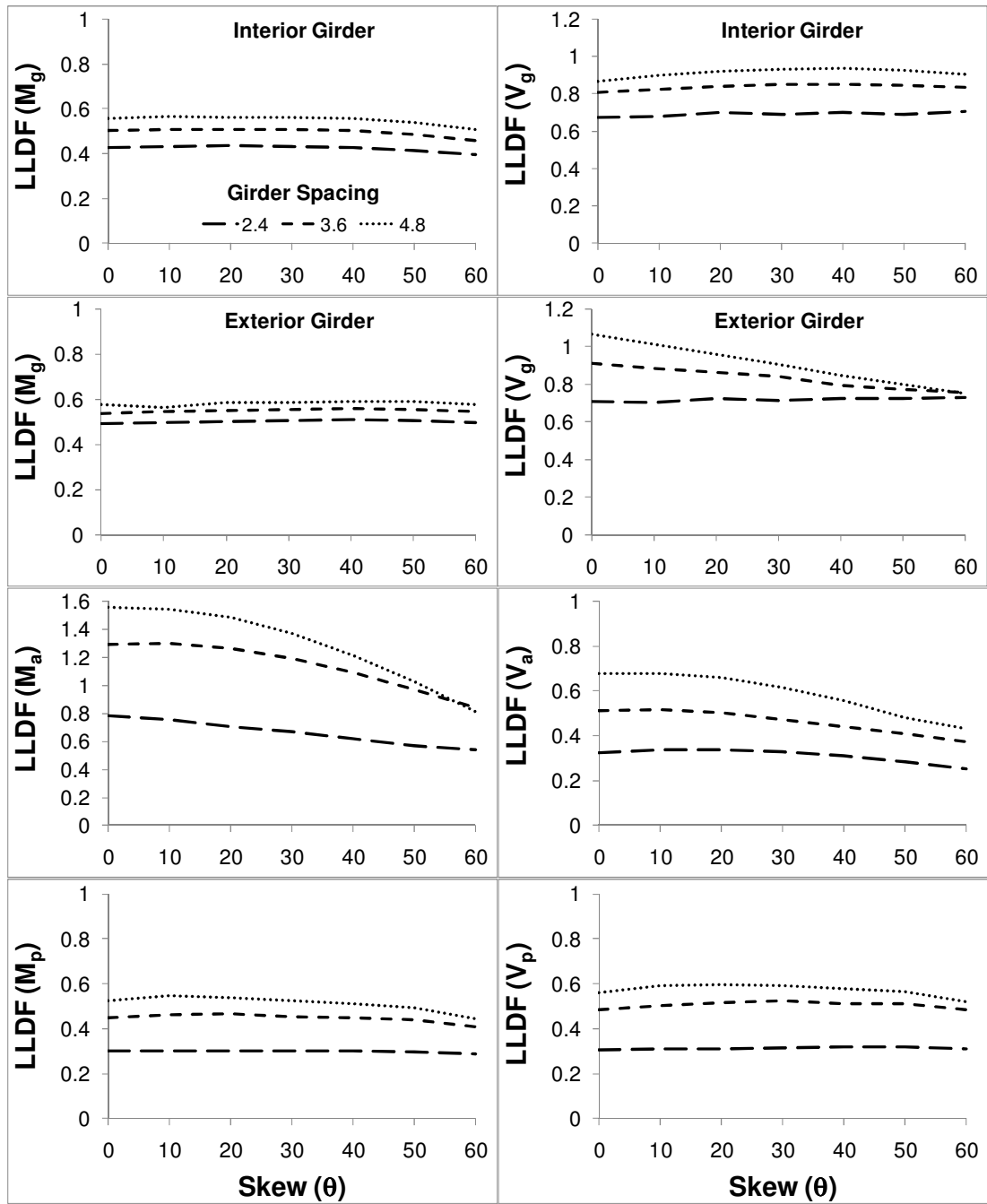


Figure 31. Effect of skew on LLDFs of SIBs for Analysis Set 9 where one design lane is loaded

#### **5.4 Evaluation of Analyses Results with Respect to the Other Parameters**

In this section, the effect of the parameters other than the skew angle on the distribution of live load effects among the components of SIBs is discussed.

Figures 28-29 display the LLDFs for the SIB components as a function of skew angle for various number of girders (4, 6, 8, 10) for the cases where two or more design lanes are loaded and one design lane is loaded respectively. As observed from the figure, for the cases of interior and exterior girder shears as well as abutment moment, the plots for SIBs with various number of girders overlap. This clearly shows that the effect of number of girders on the LLDFs for the interior and exterior girder shears as well as abutment moment is negligible. For the remainder of the LLDFs, the number of girders is observed to have noticeable effect. This effect is more pronounced for LLDFs for abutment shear as well as pile moment and shear as the dispersion of the plots becomes larger in these cases. Similar findings were also reported by Yalçın and Dicleli (2009).

Figures 30-31 display the LLDFs for the SIB components as a function of skew angle for various girder spacings (2.4, 3.6, 4.8 m) for the cases where two or more design lanes are loaded and one design lane is loaded respectively. As observed from the figure, for the cases of interior and exterior girder moment and shears, abutment moment and shear as well as pile moment and shear, girder spacing is observed to have significant effect. This effect is less pronounced for LLDFs for exterior girder moment as the dispersion of the plot becomes smaller in this case. Similar findings were also reported by Dicleli and Erhan (2009a).

Figures 32-36 display the LLDFs for the SIB components as a function of skew angle respectively for various foundation soil stiffnesses (20, 40, 80, 120 kPa), pile sizes (250x85, 310x125), pile spacings (1.2, 2.4, 3.6, 4.8 m), abutment thickness's (1, 1.5m) and backfill compaction levels (18, 20, 22 kN/m<sup>3</sup>) for the case where two or more design lanes are loaded Figures 37-41 display similar information but for the case where only one design lane is loaded. As observed from the figures, for the cases of interior and exterior girder moment and shears, abutment shear as well as pile moment and shear, the plots overlap in each figure. This clearly shows that the effect of foundation soil stiffness, pile size, pile spacing, abutment thickness and backfill compaction level on the LLDFs for the interior and exterior girder moment and shears, abutment shear as well as pile moment and shear is negligible. For the abutment moment however, the above mentioned parameters are observed to have noticeable effect. This effect is less pronounced for backfill compaction level as the dispersion of the plot becomes smaller in this case (Figure 36 and Figure 41). Similar findings were also reported by Dicleli and Erhan (2009b).

Figures 42-43 display the LLDFs for the SIB components as a function of skew angle for abutment heights (2.5, 3, 4, 5 m) for the cases where two or more design lanes are loaded and one design lane is loaded respectively. As observed from the figure, for the cases of interior and exterior girder shears as well as pile moment and shear, the plots for SIBs with various abutment heights overlap. This clearly shows that the effect of abutment height on the LLDFs for the interior and exterior girder shears as well as pile moment and shear is negligible. For the remainder of the LLDFs, the abutment height is observed to have noticeable effect. This effect is more pronounced for LLDFs for abutment moment and shear as the dispersion of the plots becomes

larger in these cases. Similar findings were also reported by Dicleli and Erhan (2009b)

Figures 44-45 display the LLDFs for the SIB components as a function of skew angle for various span lengths (15, 20, 25, 30, 35, 40, 45 m) for the cases where two or more design lanes are loaded and one design lane is loaded respectively. As observed from the figure, for the cases of interior girder moment and shear, exterior girder moment as well as pile moment and shear, the plots for SIBs with various span lengths overlap. This clearly shows that the effect of span length on the LLDFs for the interior girder moment and shear, exterior girder moment as well as pile shear and moment is negligible. For the remainder of the LLDFs, the span length is observed to have noticeable effect. This effect is more pronounced for LLDFs for exterior girder shear as well as abutment moment as the dispersion of the plots becomes larger in these cases. Similar findings were also reported by Dicleli and Erhan (2009a).

Figures 46-47 display the LLDFs for the SIB components as a function of skew angle for girder types (AASHTO II, AASHTO IV, AASHTO VI) for the cases where two or more design lanes are loaded and one design lane is loaded respectively. As observed from the figure, for the cases of interior girder moment, exterior girder shear as well as pile moment and shear, the plots for SIBs with various girder types overlap. This clearly shows that the effect of girder type on the LLDFs for the interior girder moment, exterior girder shear as well as pile moment and shear is negligible. For the remainder of the LLDFs, the girder type is observed to have noticeable effect. This effect is more pronounced for LLDFs for abutment moment as the dispersion of the plot becomes larger in this case. Similar findings were also reported by Dicleli and Erhan (2009a).

Figures 48-49 display the LLDFs for the SIB components as a function of skew angle for various slab thicknesses (15, 20, 25, 30 cm) for the cases where two or more design lanes are loaded and one design lane is loaded respectively. As observed from the figure, for the cases of interior girder moment, abutment shear as well as pile moment and shear, the plots for SIBs with various slab thicknesses overlap. This clearly shows that the effect of slab thickness on the LLDFs for the interior girder moment, abutment shear as well as pile moment and shear is negligible. For the remainder of the LLDFs, the slab thickness is observed to have noticeable effect. This effect is more pronounced for LLDFs for abutment moment as the dispersion of the plot becomes larger in this case. Similar findings were also reported by Dicleli and Erhan (2009a).

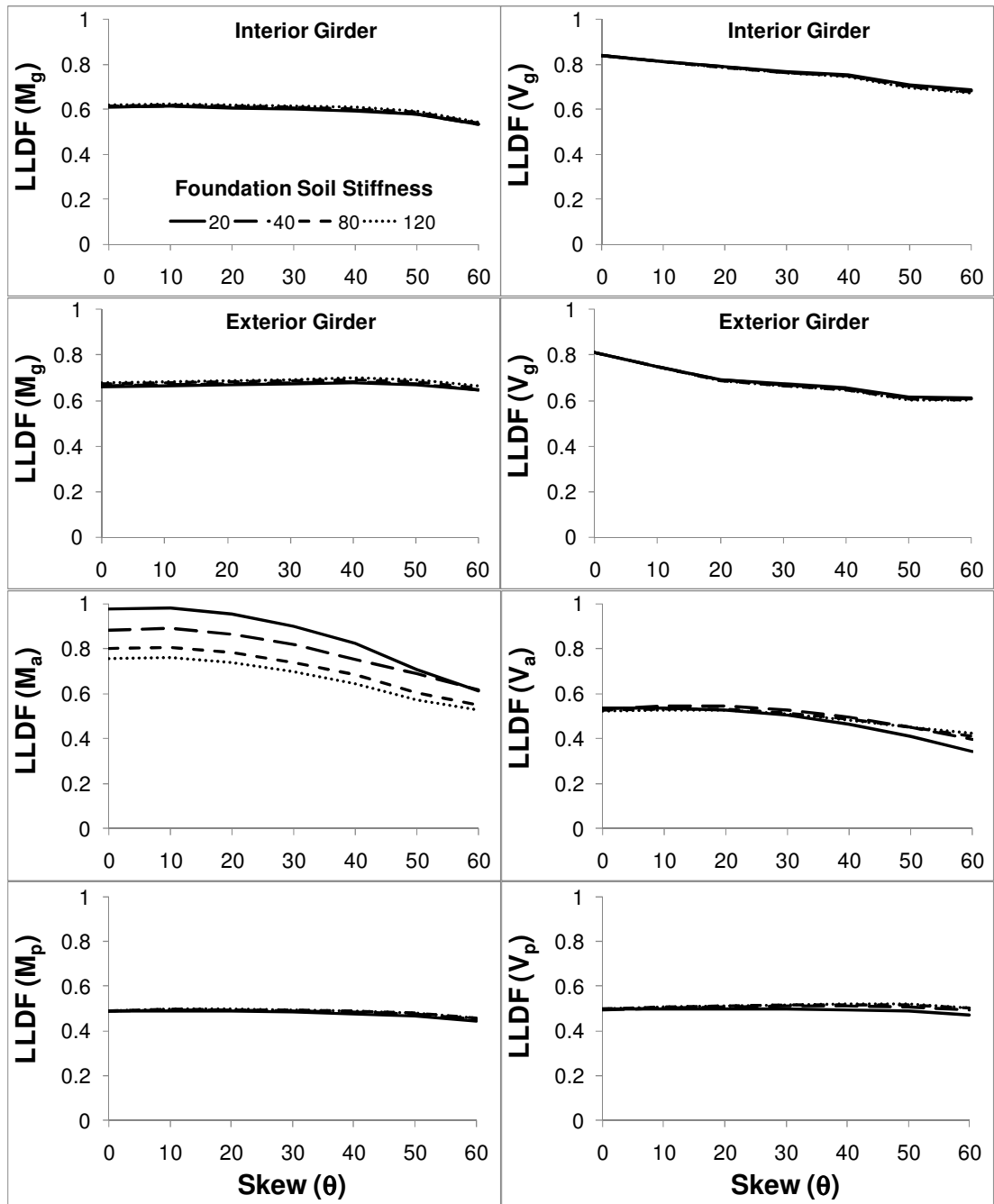


Figure 32. Effect of skew on LLDFs of SIBs for Analysis Set 2 where two or more design lanes are loaded

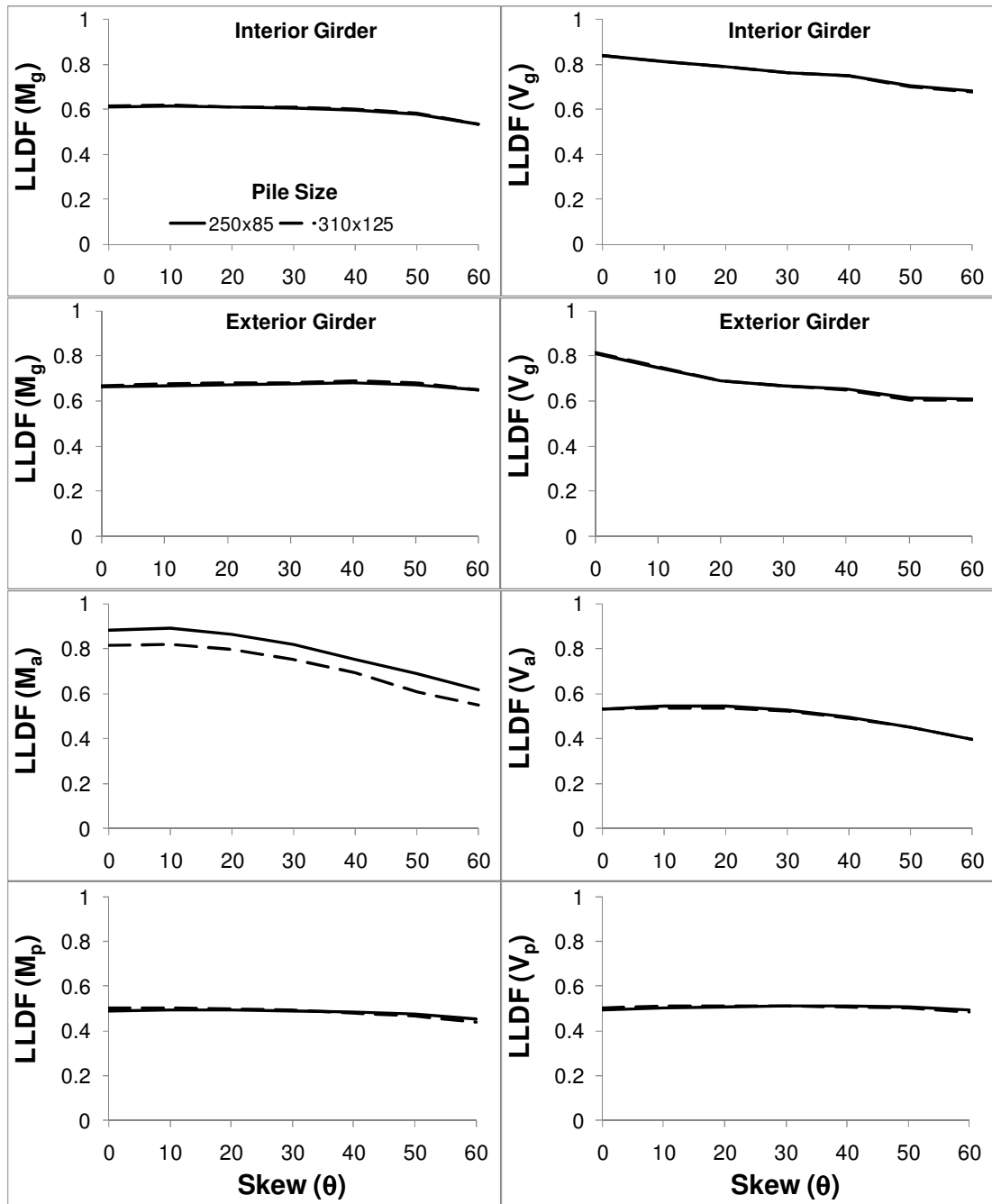


Figure 33. Effect of skew on LLDFs of SIBs for Analysis Set 3 where two or more design lanes are loaded

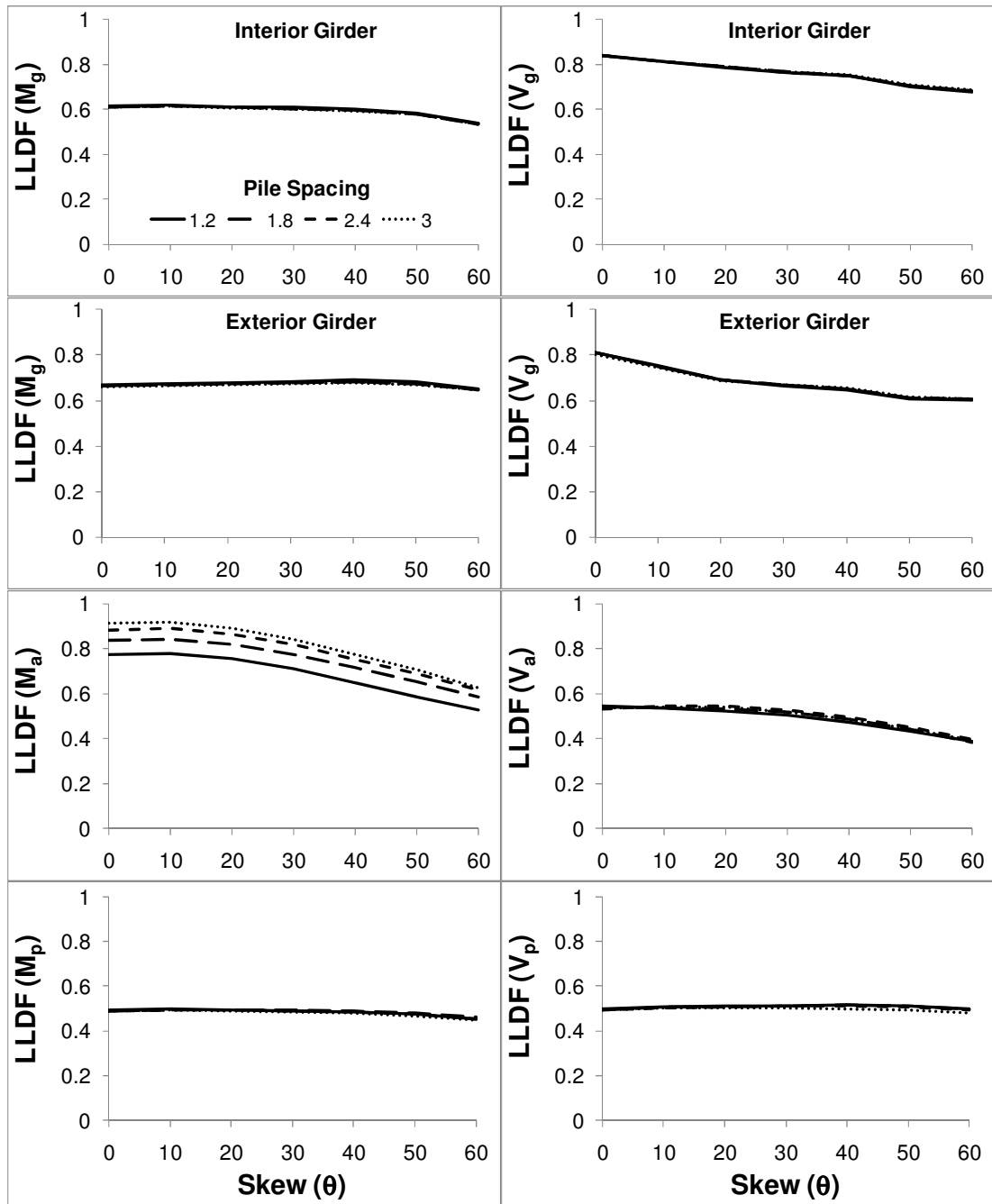


Figure 34. Effect of skew on LLDFs of SIBs for Analysis Set 4 where two or more design lanes are loaded

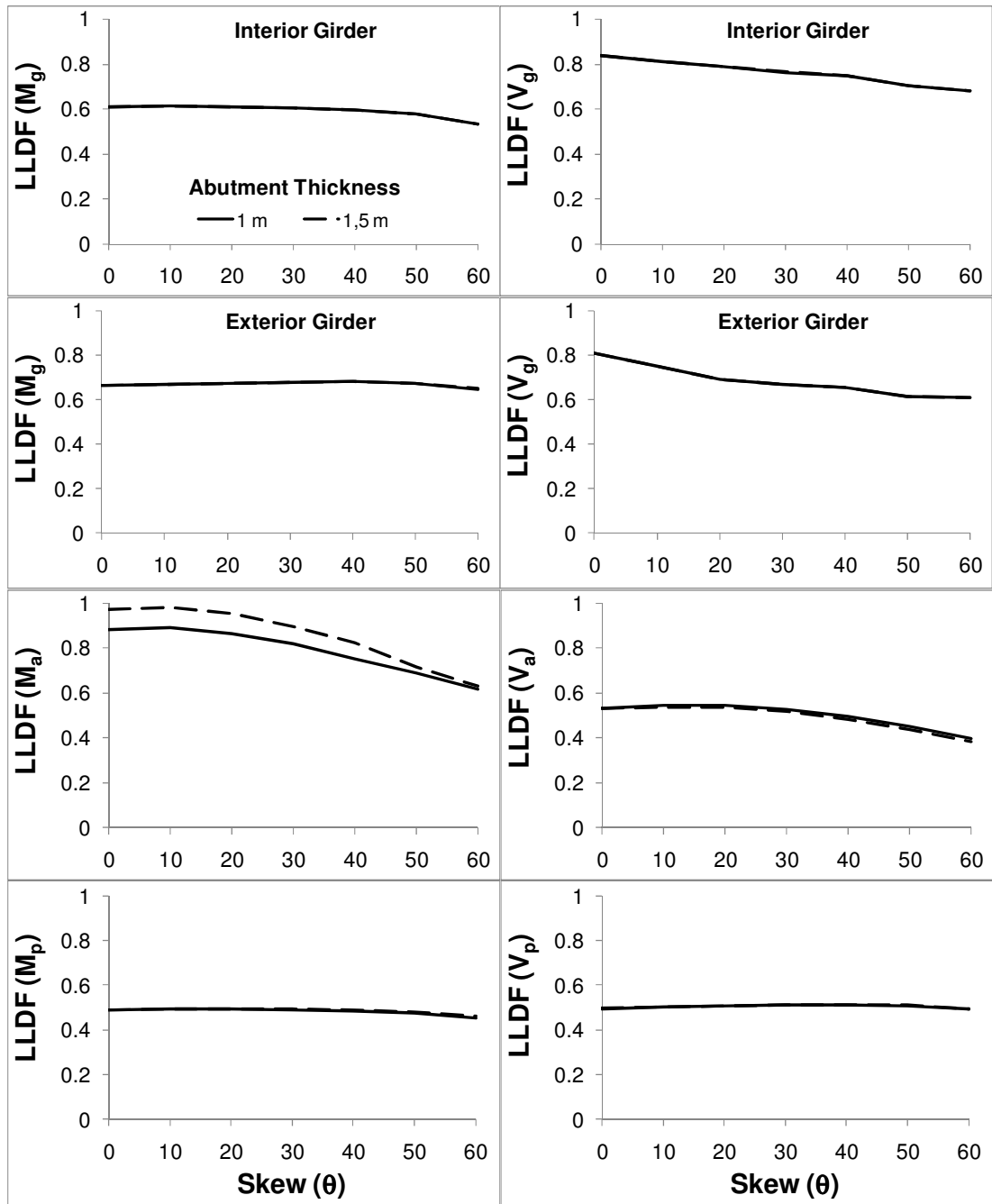


Figure 35. Effect of skew on LLDFs of SIBs for Analysis Set 6 where two or more design lanes are loaded

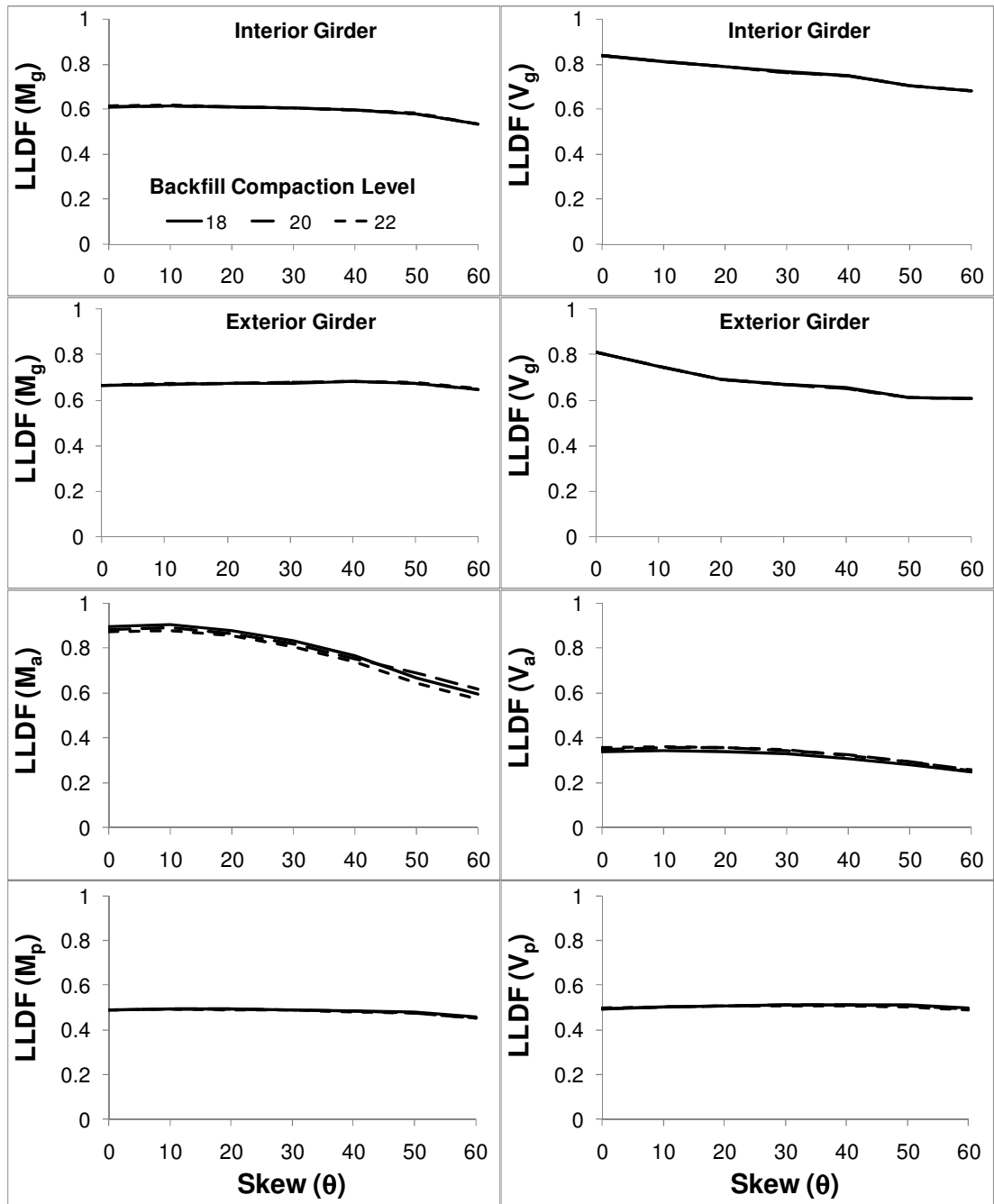


Figure 36. Effect of skew on LLDFs of SIBs for Analysis Set 7 where two or more design lanes are loaded

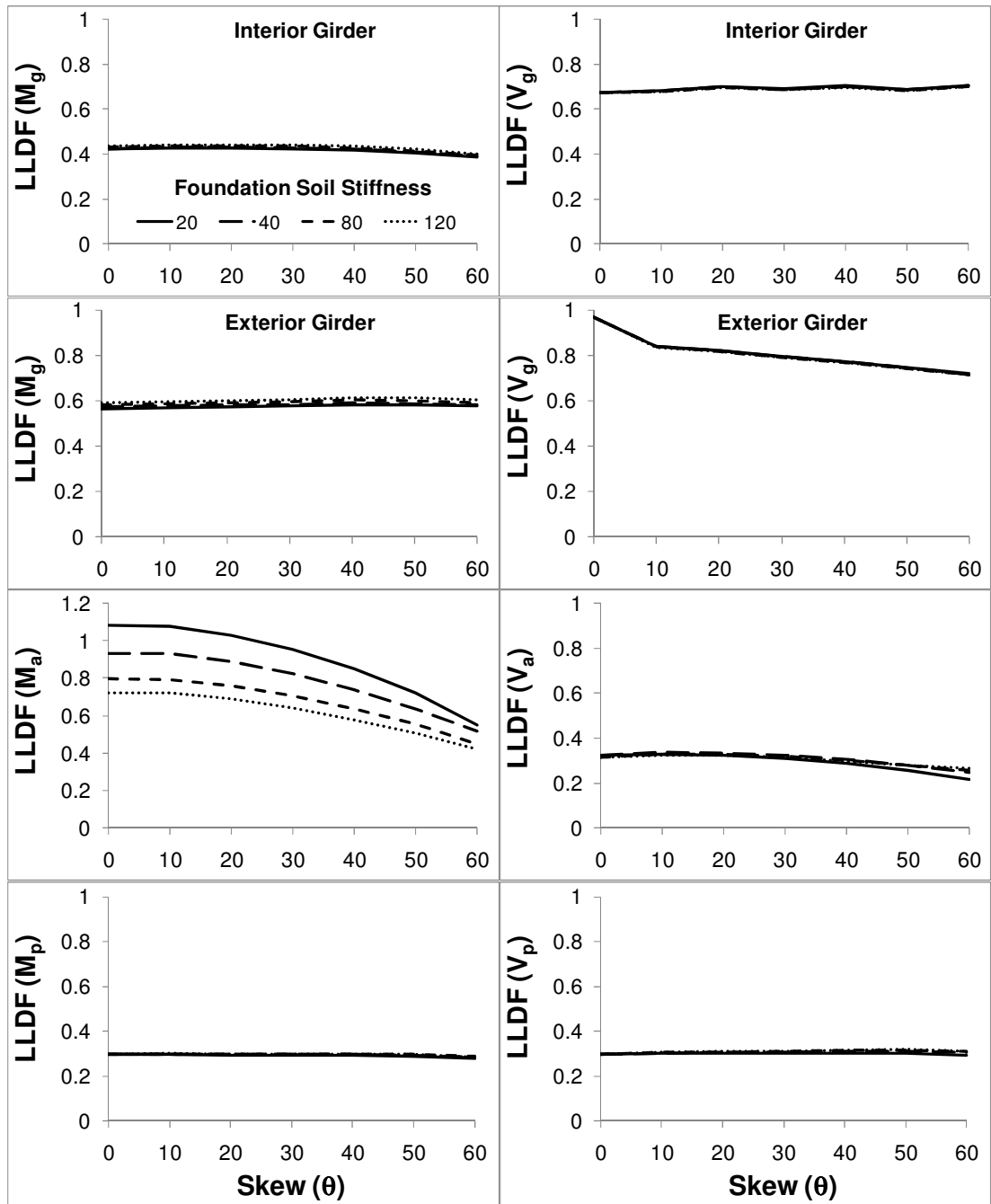


Figure 37. Effect of skew on LLDFs of SIBs for Analysis Set 2 where one design lane is loaded

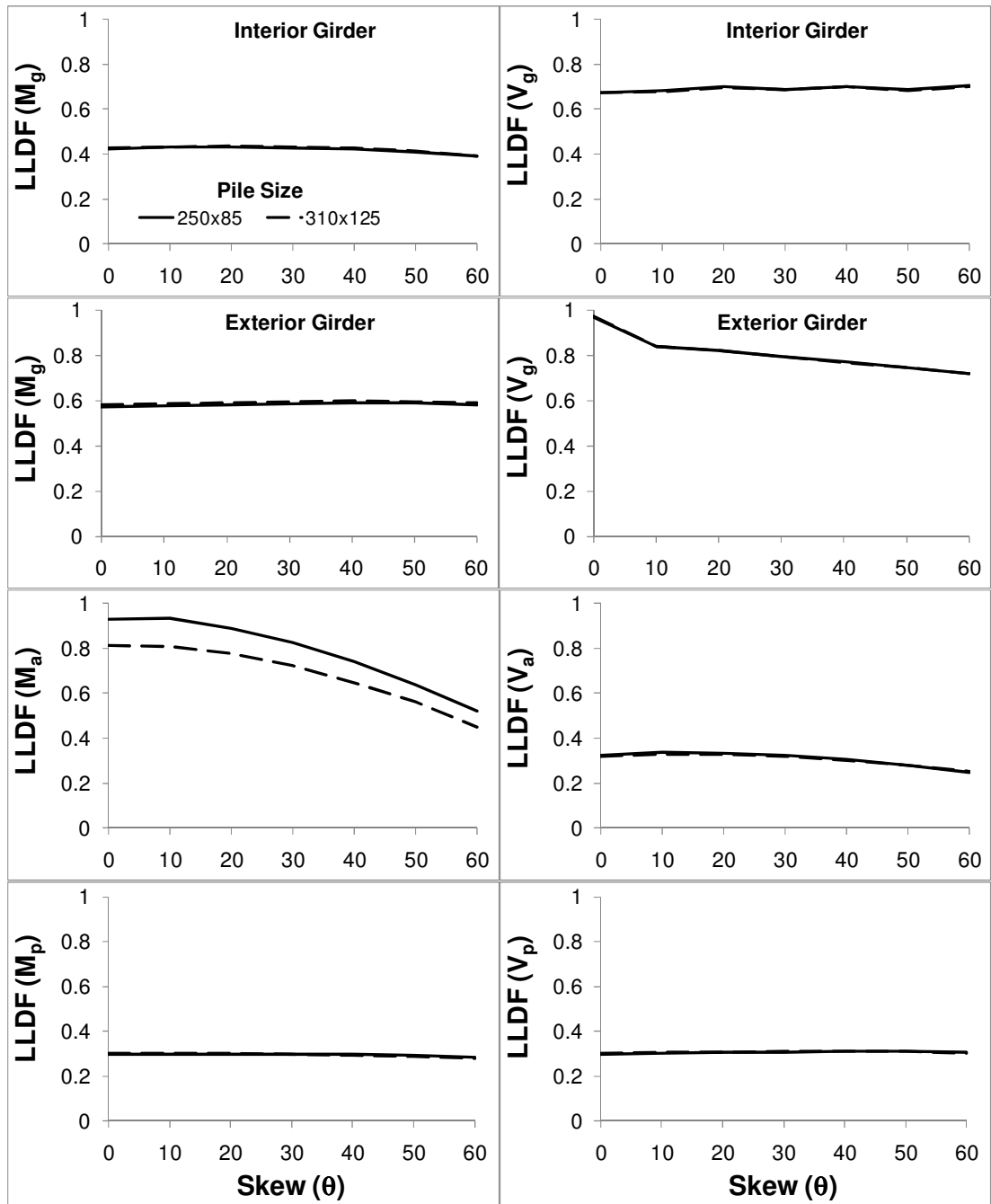


Figure 38. Effect of skew on LLDFs of SIBs for Analysis Set 3 where one design lane is loaded

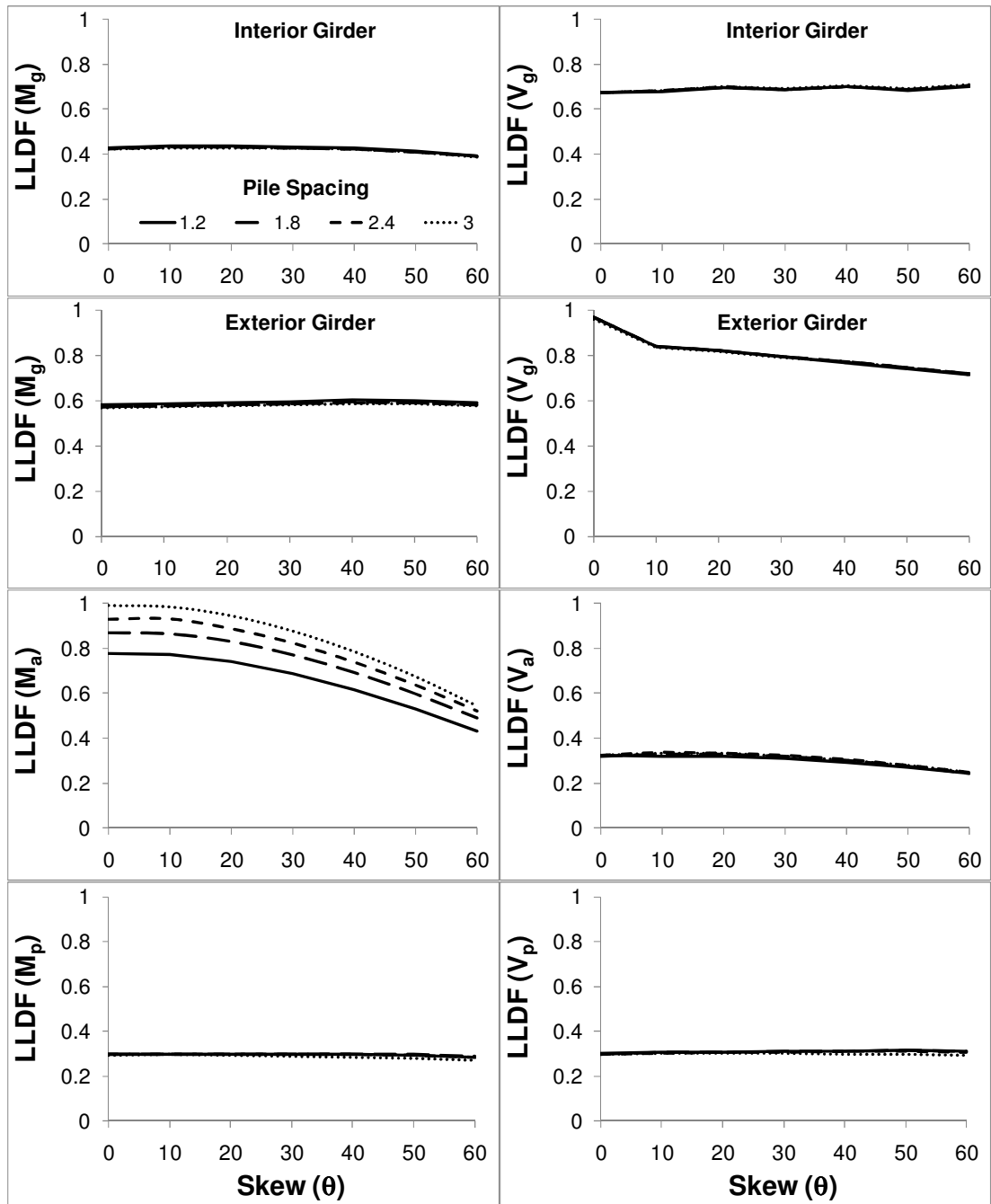


Figure 39. Effect of skew on LLDFs of SIBs for Analysis Set 4 where one design lane is loaded

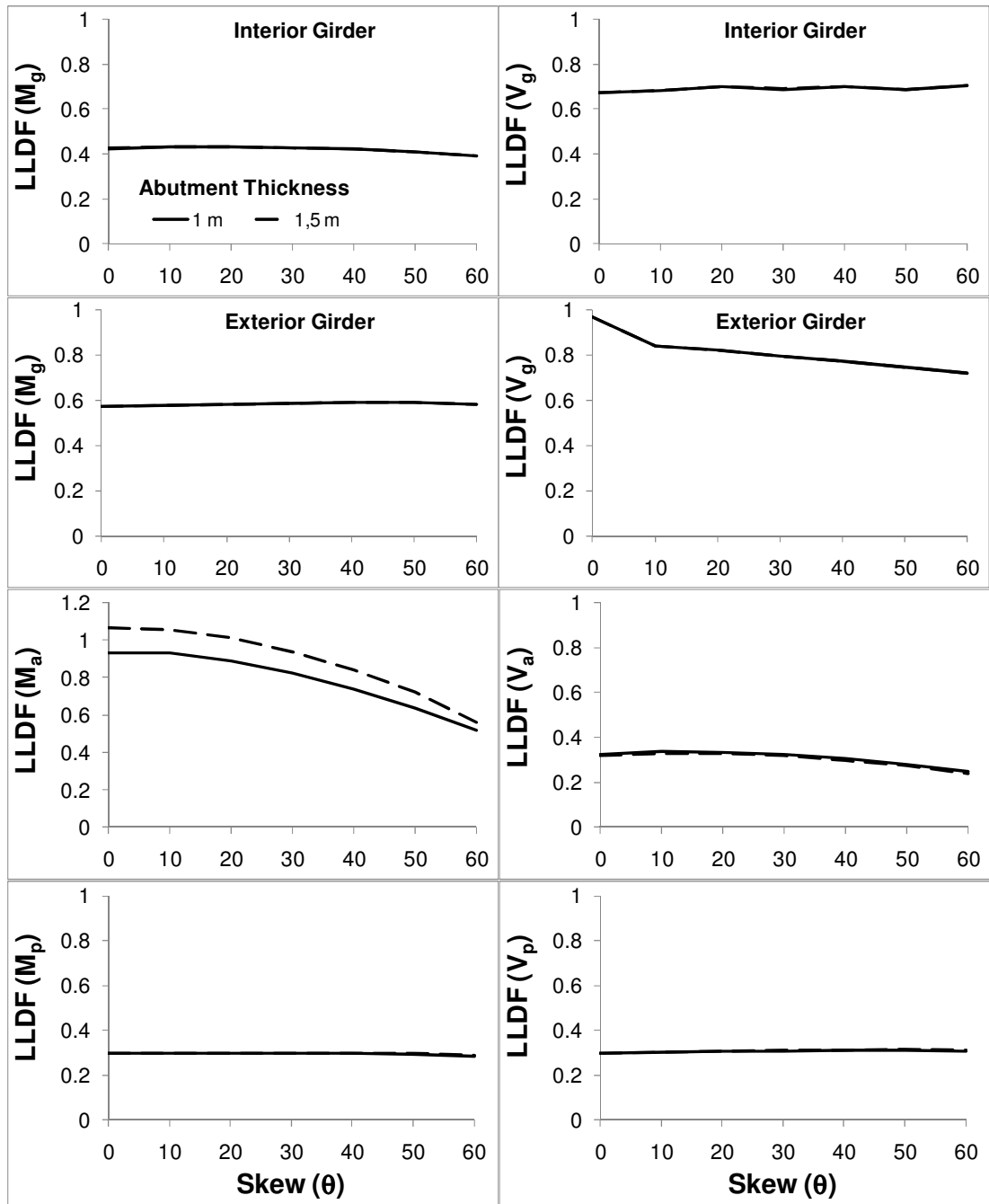


Figure 40. Effect of skew on LLDFs of SIBs for Analysis Set 6 where one design lane is loaded

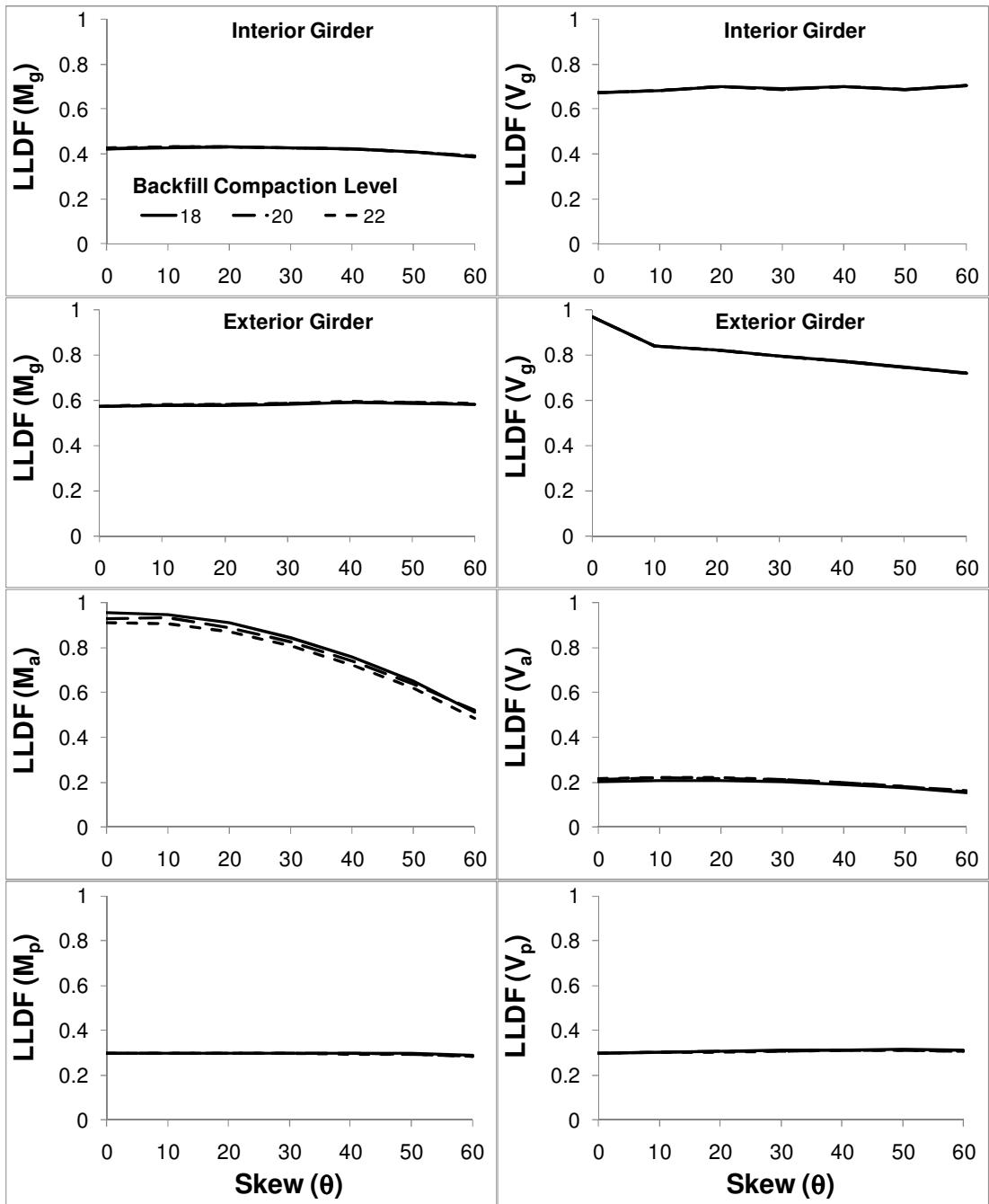


Figure 41. Effect of skew on LLDFs of SIBs for Analysis Set 7 where one design lane is loaded

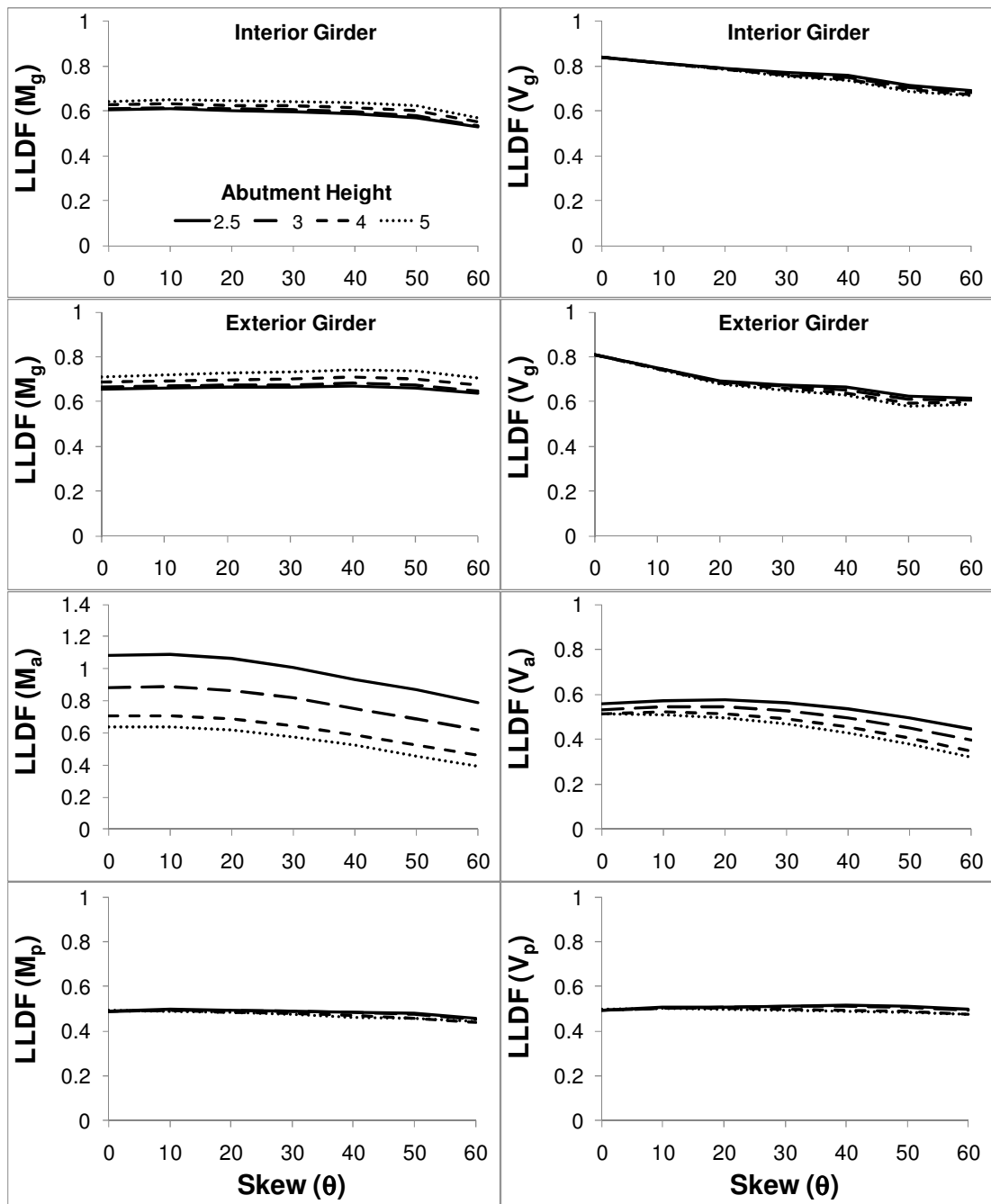


Figure 42. Effect of skew on LLDFs of SIBs for Analysis Set 5 where two or more design lanes are loaded

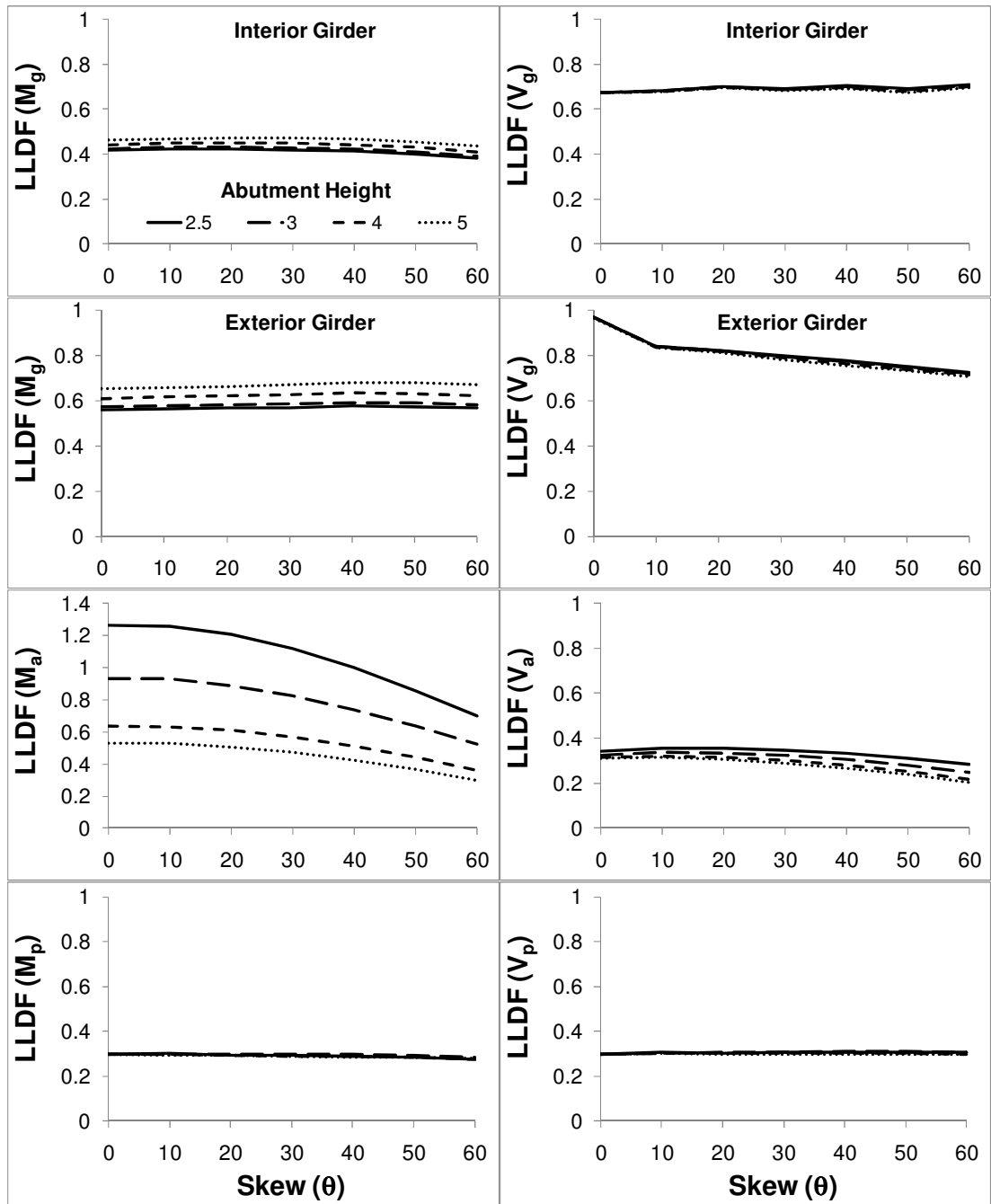


Figure 43. Effect of skew on LLDFs of SIBs for Analysis Set 5 where one design lane is loaded

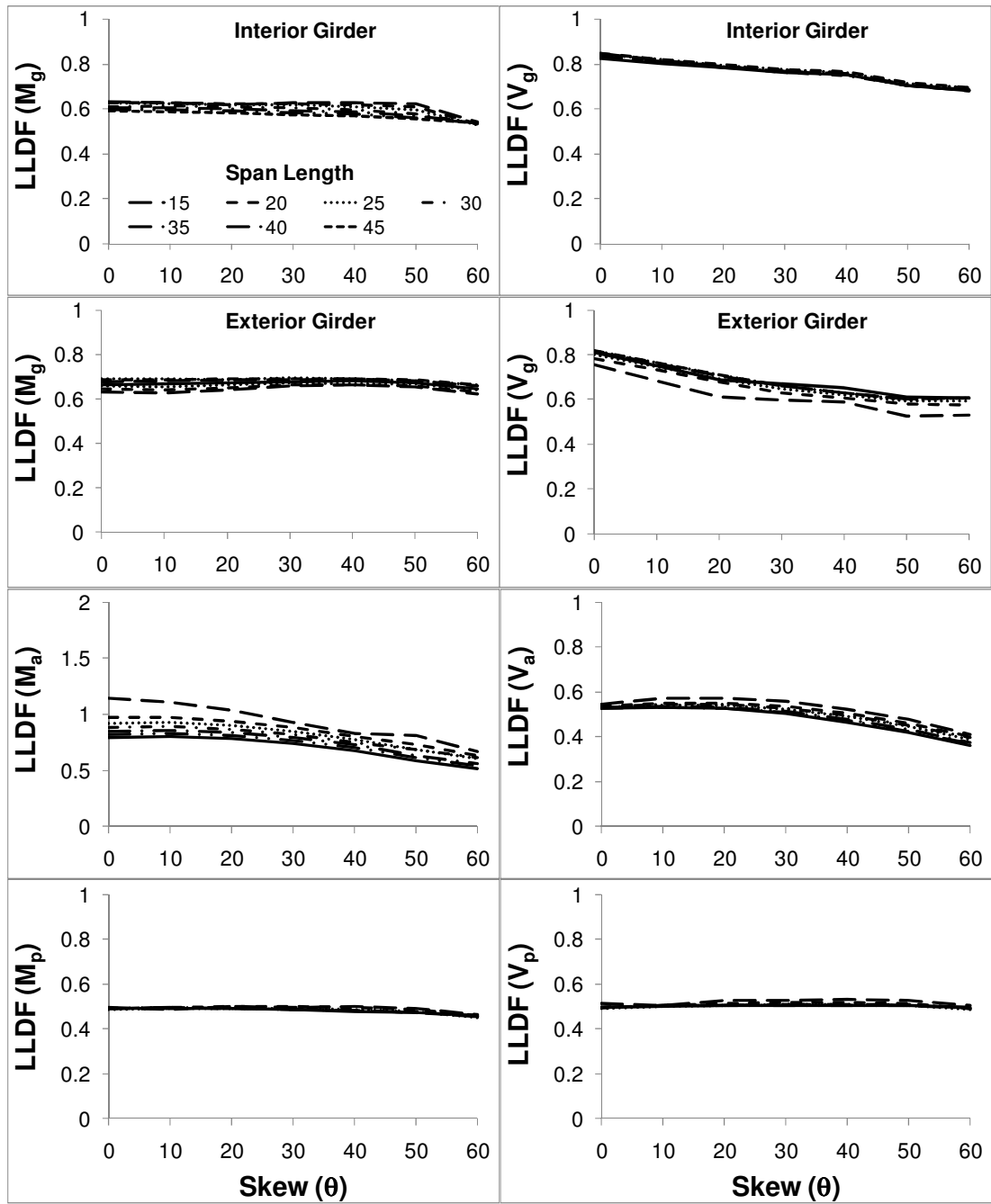


Figure 44. Effect of skew on LLDFs of SIBs for Analysis Set 8 where two or more design lanes are loaded

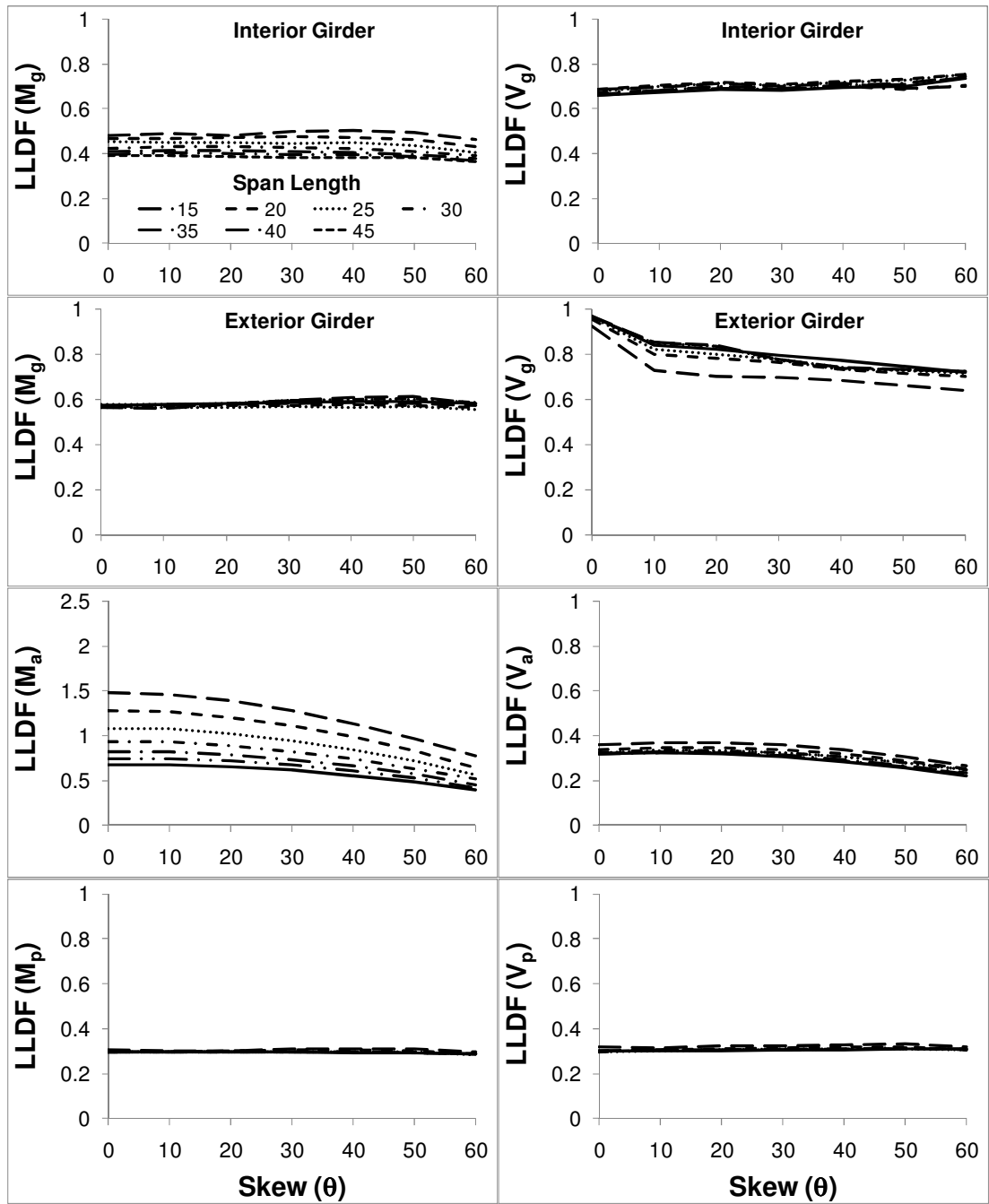


Figure 45. Effect of skew on LLDFs of SIBs for Analysis Set 8 where one design lane is loaded

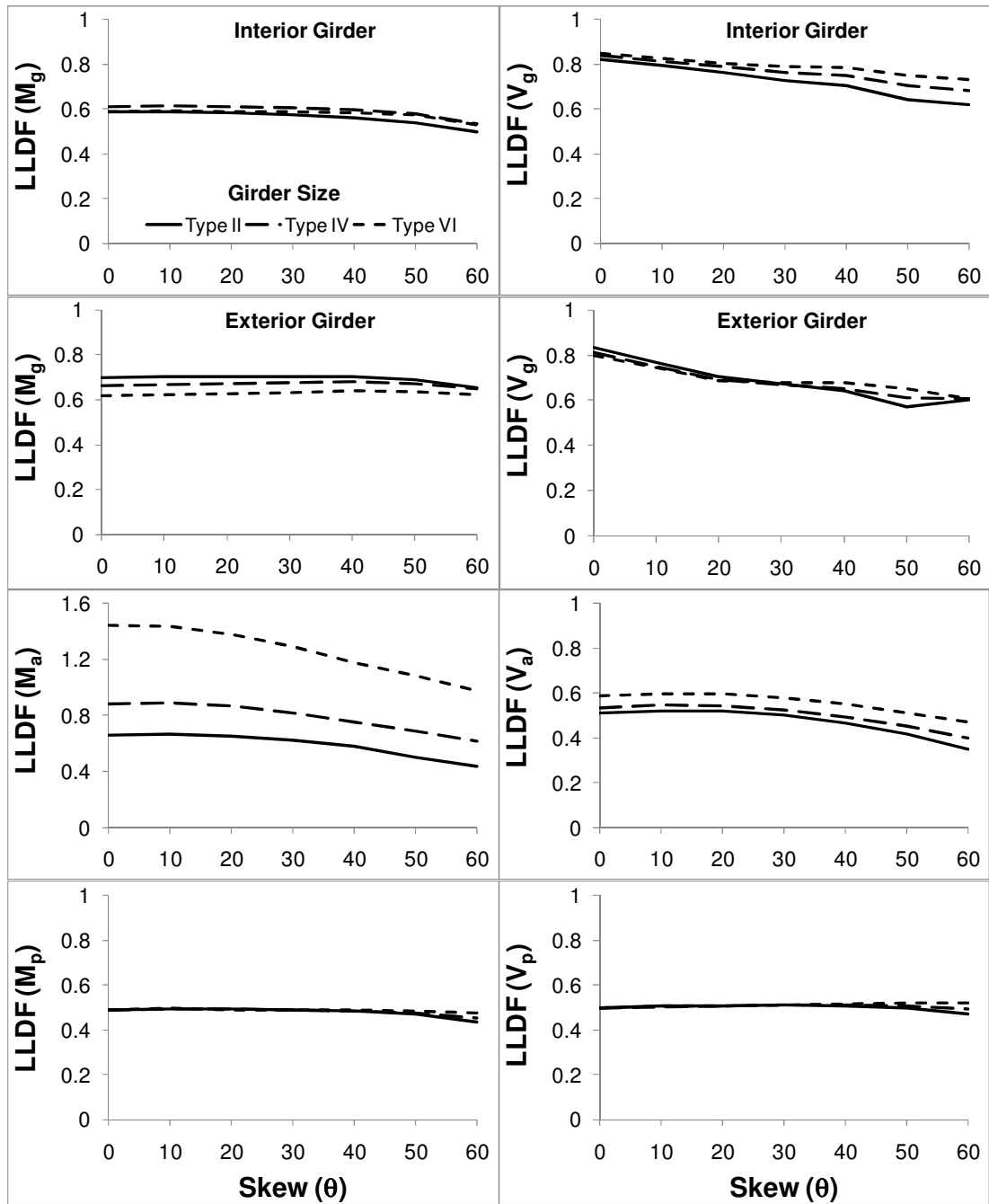


Figure 46. Effect of skew on LLDFs of SIBs for Analysis Set 10 where two or more design lanes are loaded

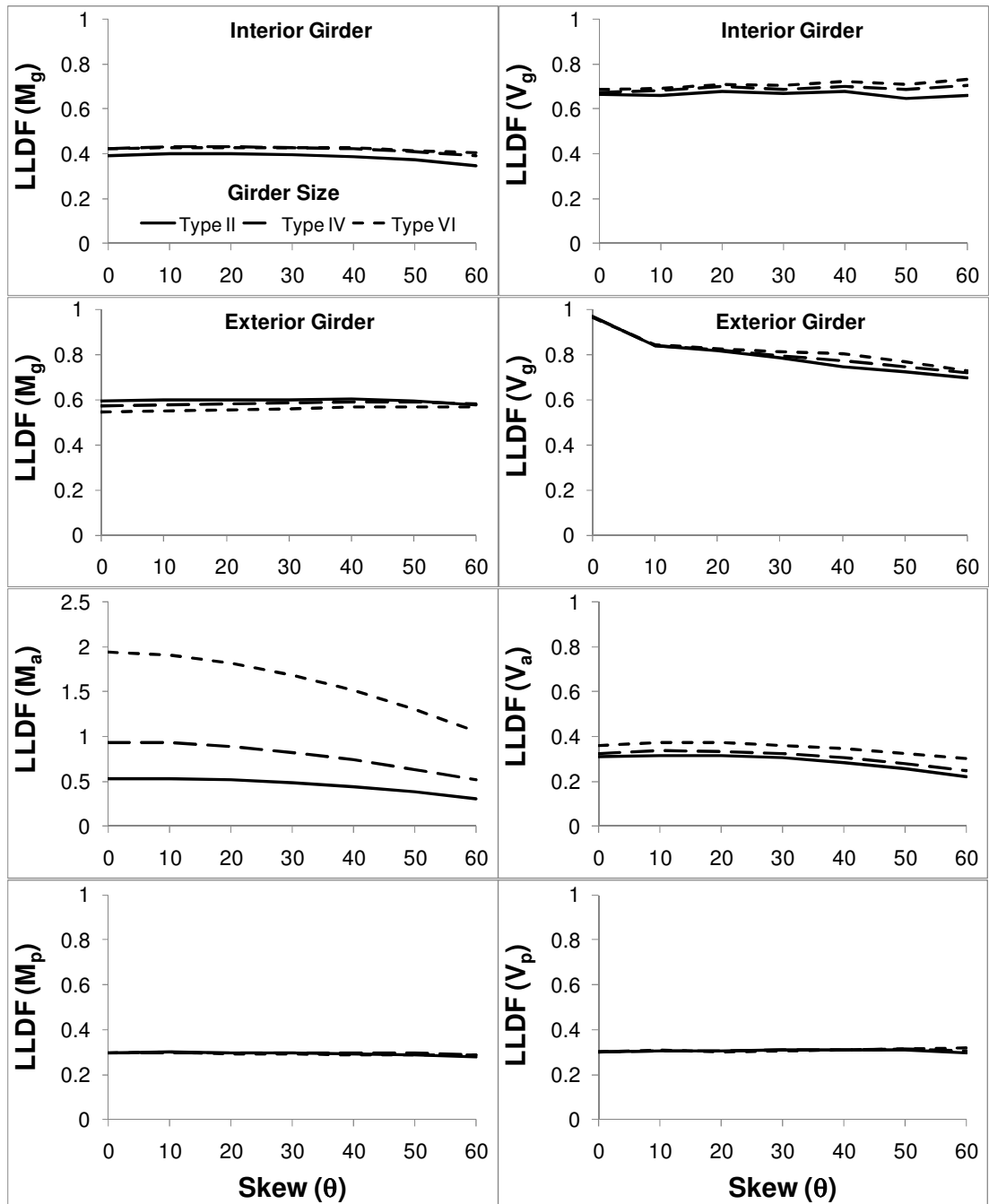


Figure 47. Effect of skew on LLDFs of SIBs for Analysis Set 10 where one design lane is loaded

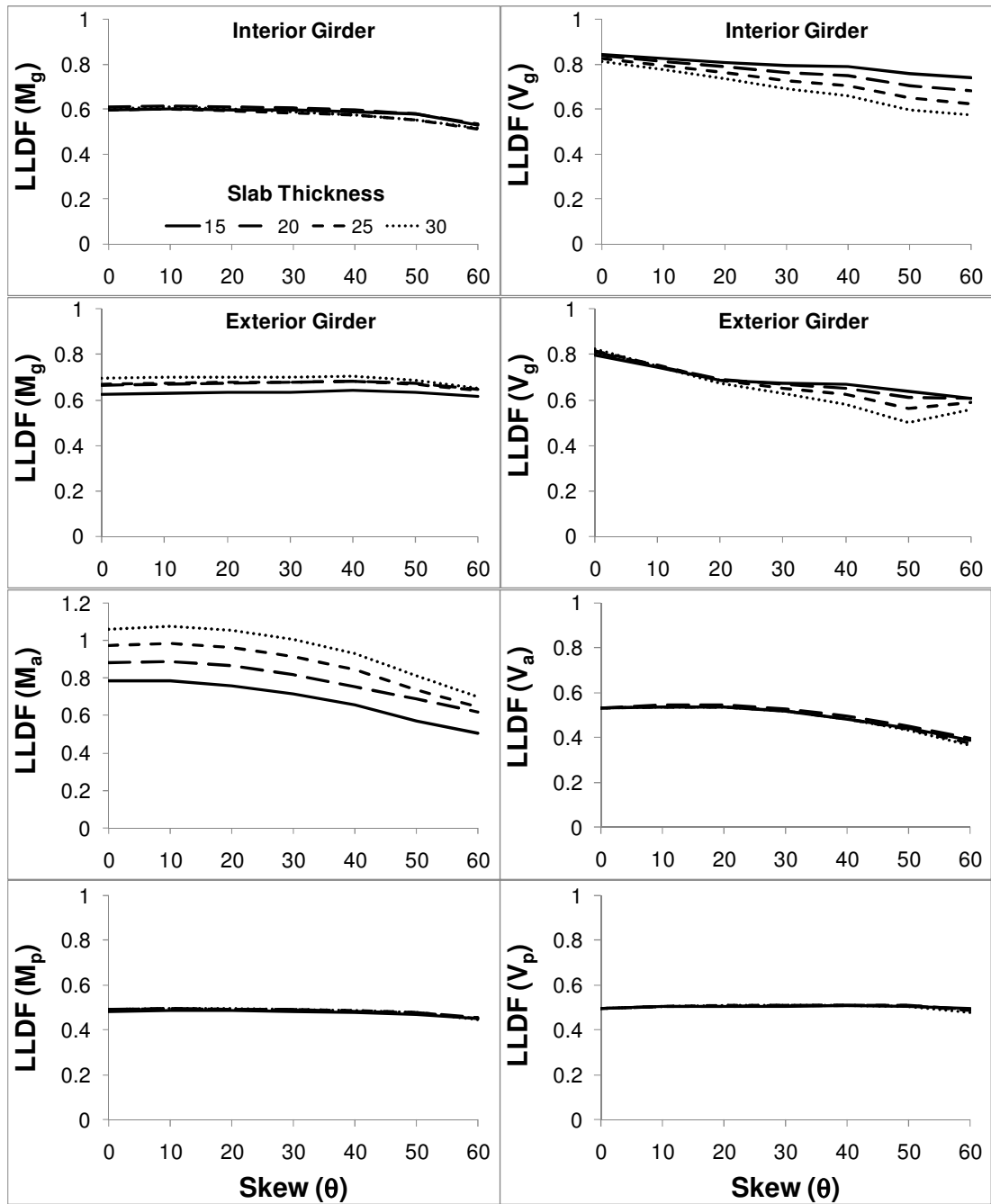


Figure 48. Effect of skew on LLDFs of SIBs for Analysis Set 11 where two or more design lanes are loaded

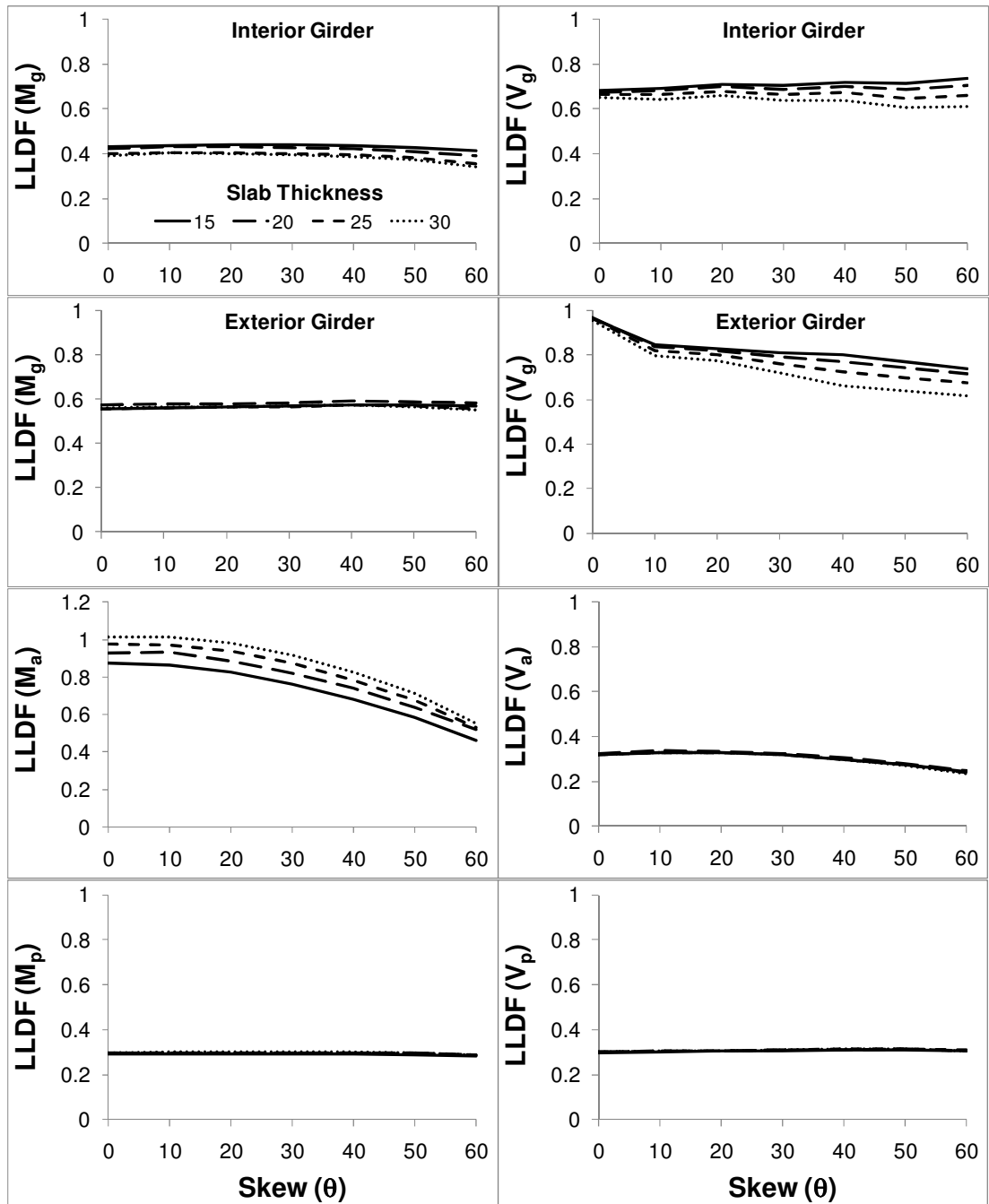


Figure 49. Effect of skew on LLDFs of SIBs for Analysis Set 11 where one design lane is loaded

## CHAPTER 6

### SKEW CORRECTION FACTORS FOR SIBs

#### 6.1 Determination of the Dominant Parameters for the Derivation of SCFs

The ratio of the LLDFs for various skews to that for zero skew angle,  $R_s$ , is used to determine the parameters which will be included in the skew correction factor that will be developed as part of this research study. For this purpose, for each sets of dominant parameters (analyses sets) considered the ratio of the LLDFs obtained from the analyses to that for zero skew angle is plotted as a function of the skew angle. Figure 60 shows the plot of this ratio as a function of the skew angle for the case where the slab thickness is taken as a dominant parameter. In the figure, the thick solid line is a reference line representing a 1.0 ratio where the skew has no effect. The comparison of the plots in the figure with this reference line determines whether skew affects the LLDF associated with a particular component response. Similar figures are also obtained for other dominant parameters (analyses sets) considered in the analyses and presented in Figures 50-60. As observed from Figure 60, the skew has no effect on the LLDFs for the exterior girder moment as well as pile shear, since all the plots overlap the reference line. From the same figure, it is also observed that slab thickness has a noticeable effect on the effect of skew on LLDFs for the interior and exterior girder shears, since the plots for various slab thicknesses are largely dispersed. Furthermore, it is also observed that in some cases the effect of skew becomes noticeable only beyond a certain skew angle. For instance,

for the interior girder moment the effect of skew becomes more noticeable only beyond a skew angle of 30°. These facts are all considered in the development of SCFs. Similar observations are made from the other plots presented in Figures 50-60. The observations are summarized in Table 10 for the case where two or more design lanes are loaded. In the table, the effect of a particular dominant parameter on the effect of skew on LLDFs is reported as either negligible (N) or significant (S). For instance, if the plots for the various values of the parameters are dispersed (e.g. Figure 60, slab thickness for interior girder shear), then this parameter need to be included in the development of the SCF. The parameters which are reported as N in the table are not included in the development of SCFs. Furthermore, the effect skew angle is also reported in the same table (SA) either negligible (N) or skew angle (0, 10, 20, 30, 40, 50, 60) beyond which the effect of skew becomes noticeable. For instance, for the exterior girder moment, skew has negligible effect but for the abutment moment, the skew has significant effect which becomes noticeable beyond a skew angle of 10° as shown in Figure 60. The SCFs are only developed for angles greater than those reported in the table for a particular component response. As observed from the table skew has only a negligible effect on the LLDFs for the exterior girder moment and pile shear. For the case where only one design lane is loaded, the observations are similar except for the interior girder shear where skew has no effect on LLDFs. Therefore, for these components there is no need for SCFs.

As mentioned earlier, some of the bridge configurations considered in this research study are unrealistic (such as 10 m long, 9.6 m wide bridge with four girders spaced at 2.4 m and 30 m long, 4.8 m wide bridge with four girders spaced at 1.2 m). For instance, in the case of the 10 m long SIB, some of the truck wheels remain outside the boundaries of the bridge due to

the skew. This may not happen if the skew angle is zero. This results in smaller load effects obtained from the 3-D model in short SIBs although the live load effects obtained from the 2-D model remains unchanged. Since, LLDF is calculated as the ratio of the 3-D effect to the 2-D effect, this results in smaller LLDFs for such odd cases (10 m long bridge with high skew angles is very rare). This is obviously not directly due to the structural effect of skew. In addition, for the case where there are only four girders spaced at 1.2m (4.8 m wide bridge) it is only possible to place a single truck on the bridge. This results in a totally different trend in LLDFs for the case where two or more design lanes are loaded. Such a case is also very rare (There are not that many bridges which accommodate only a single lane of loading; for instance, a 30 m long bridge with 4.8 m width). Such odd cases will result in biased interpretation of the effect of skew on LLDFs. Consequently, in the development of the SCFs for SIBs such odd cases are excluded.

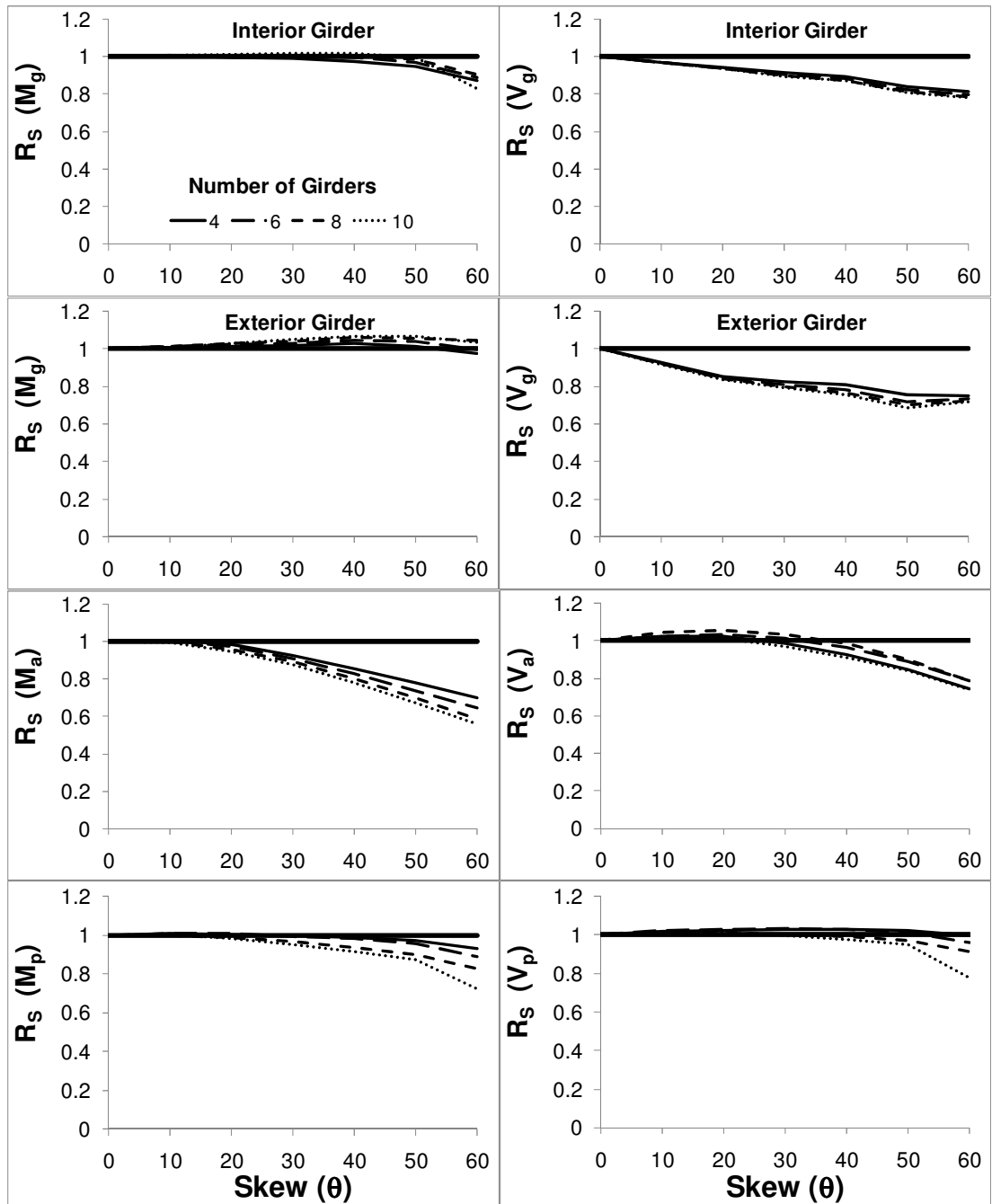


Figure 50. Effect of skew on  $R_s$  for Analysis Set 1 where two or more design lanes are loaded

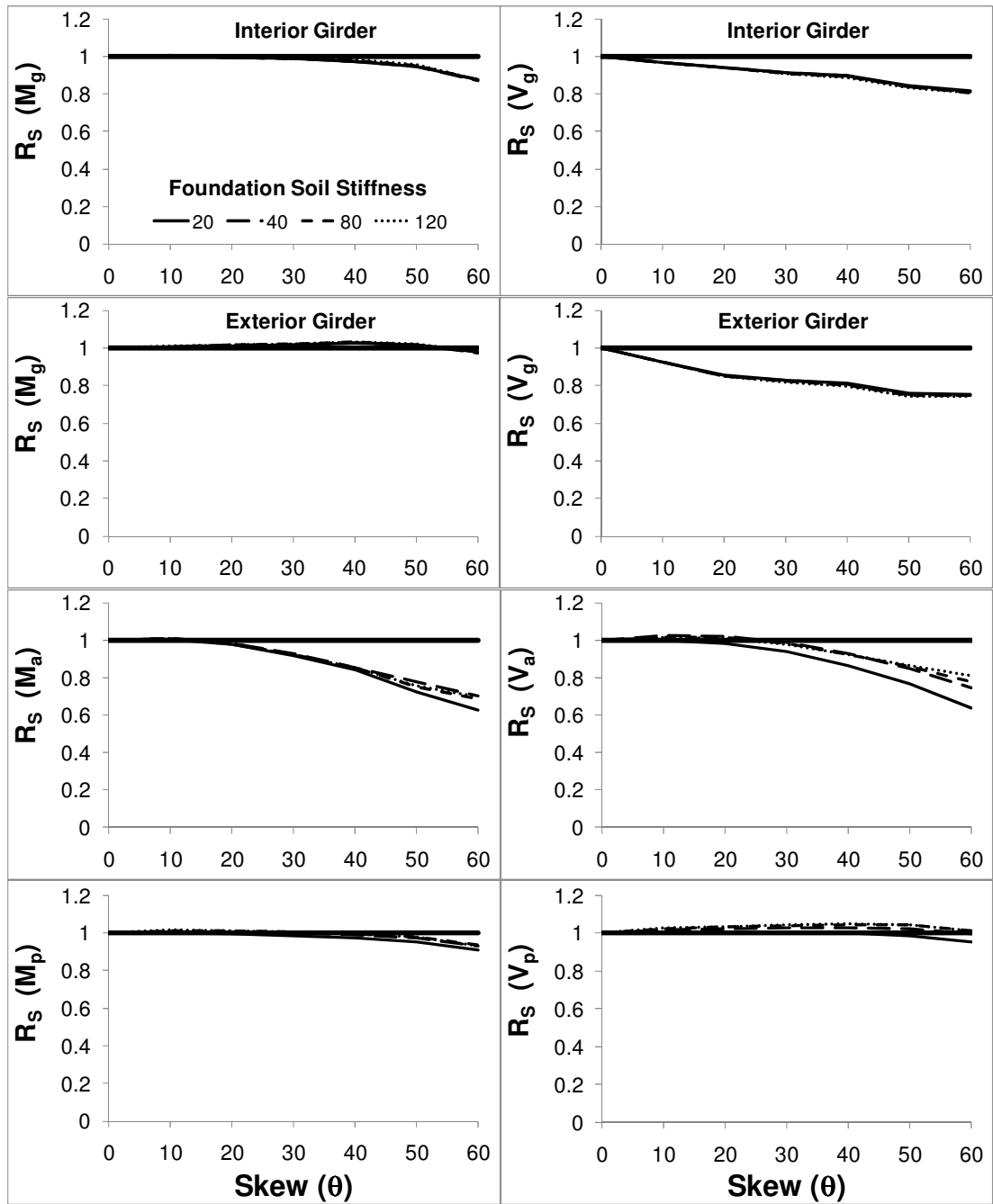


Figure 51. Effect of skew on  $R_s$  for Analysis Set 2 where two or more design lanes are loaded

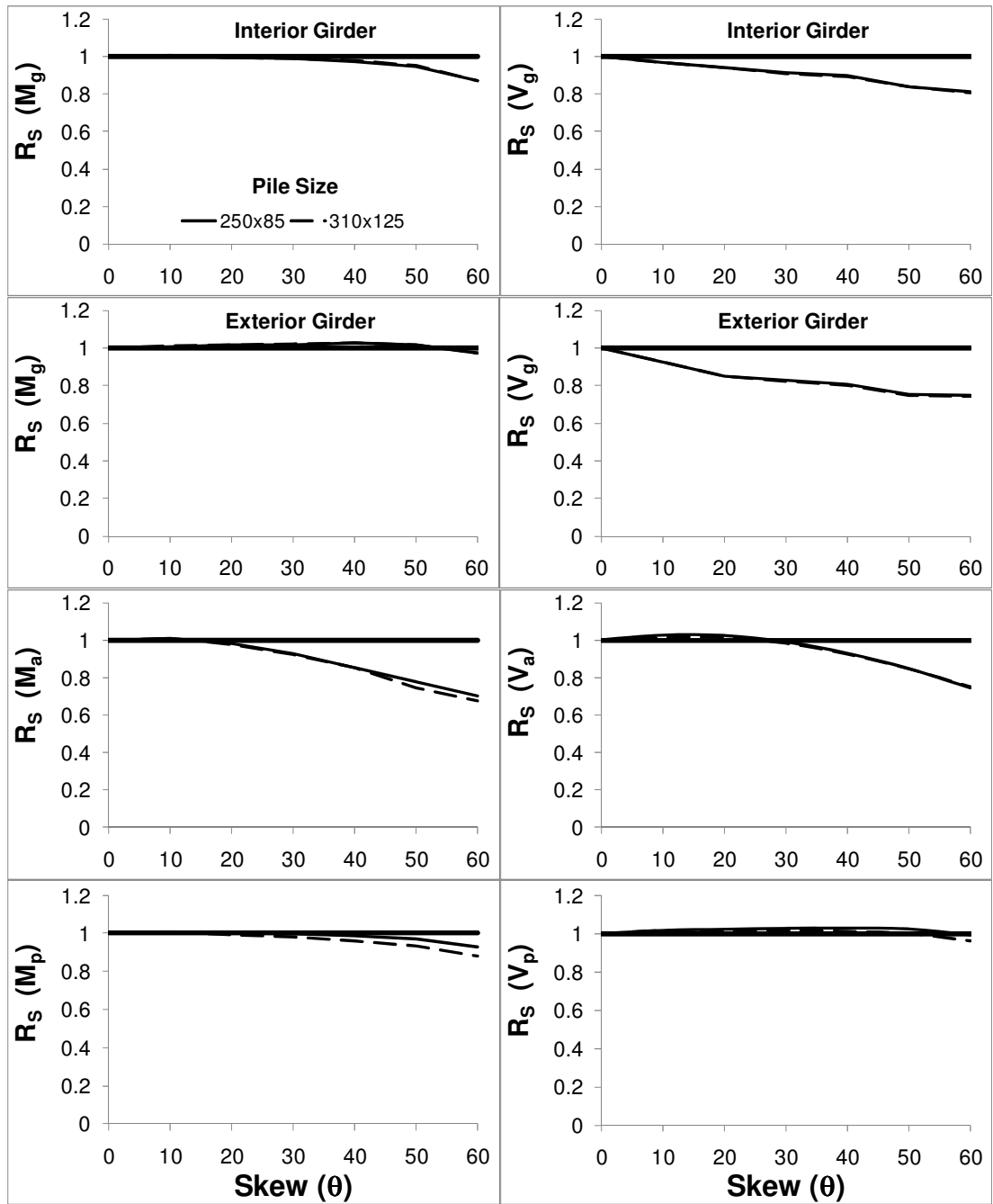


Figure 52. Effect of skew on  $R_s$  for Analysis Set 3 where two or more design lanes are loaded

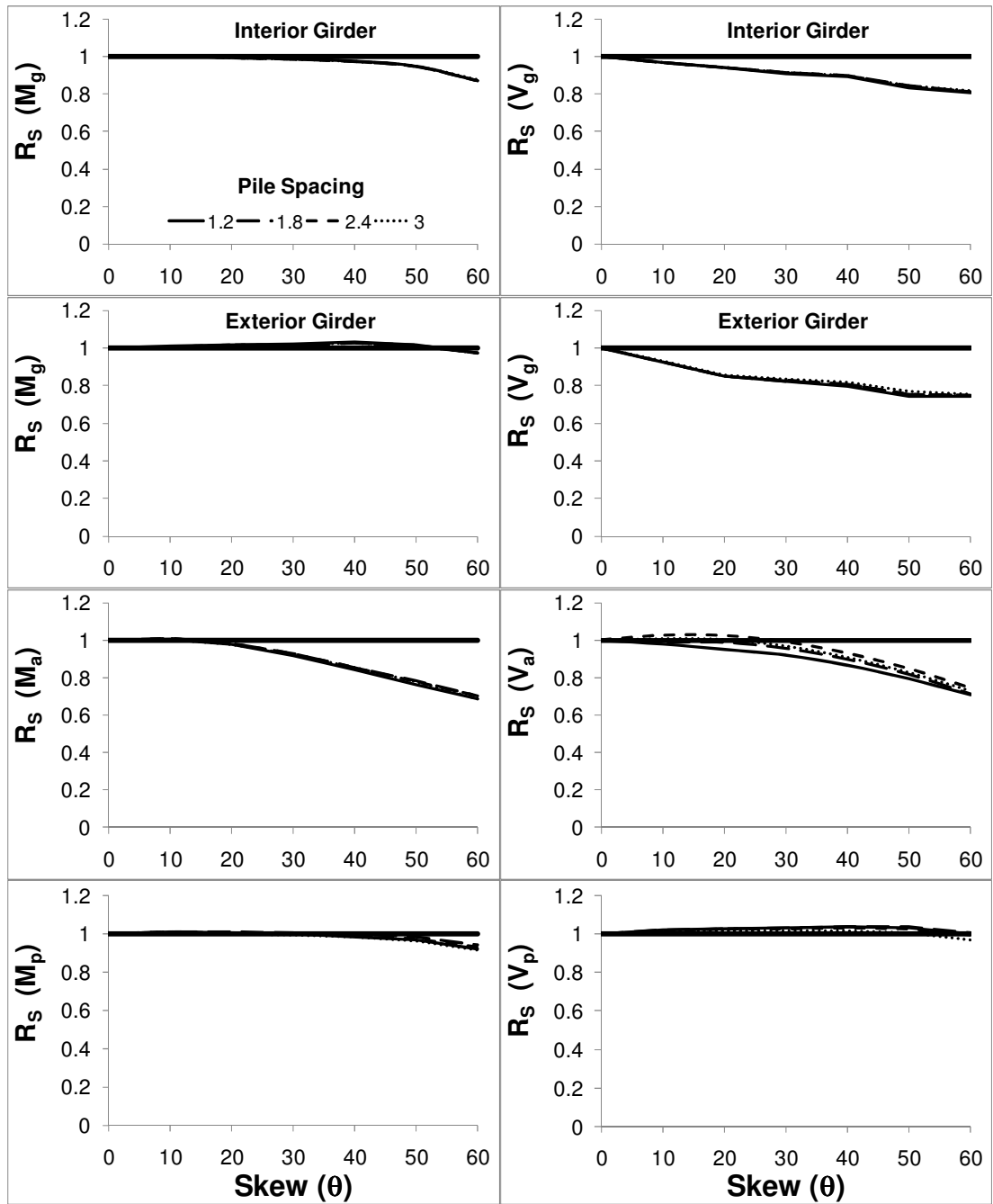


Figure 53. Effect of skew on  $R_s$  for Analysis Set 4 where two or more design lanes are loaded

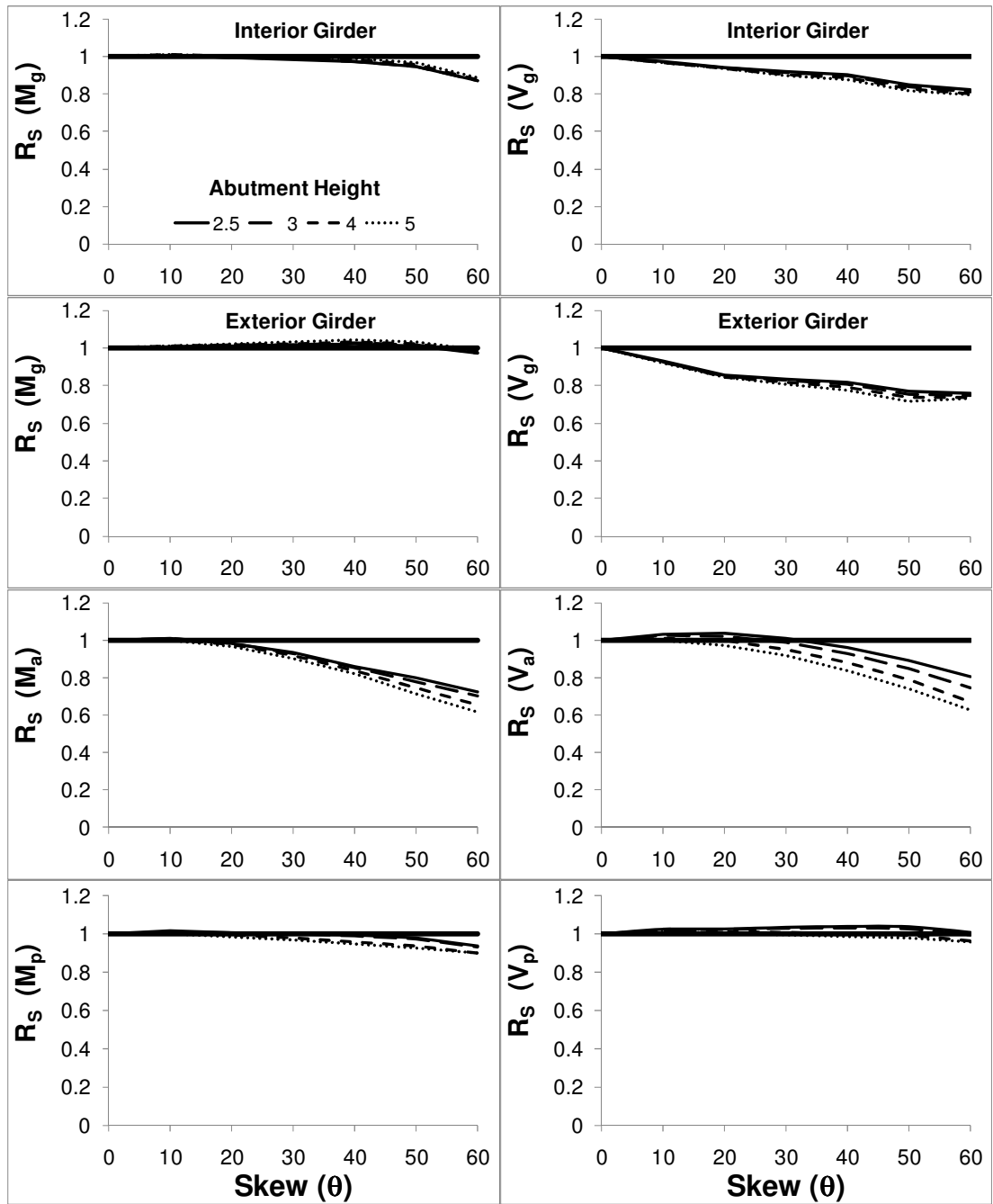


Figure 54. Effect of skew on  $R_s$  for Analysis Set 5 where two or more design lanes are loaded

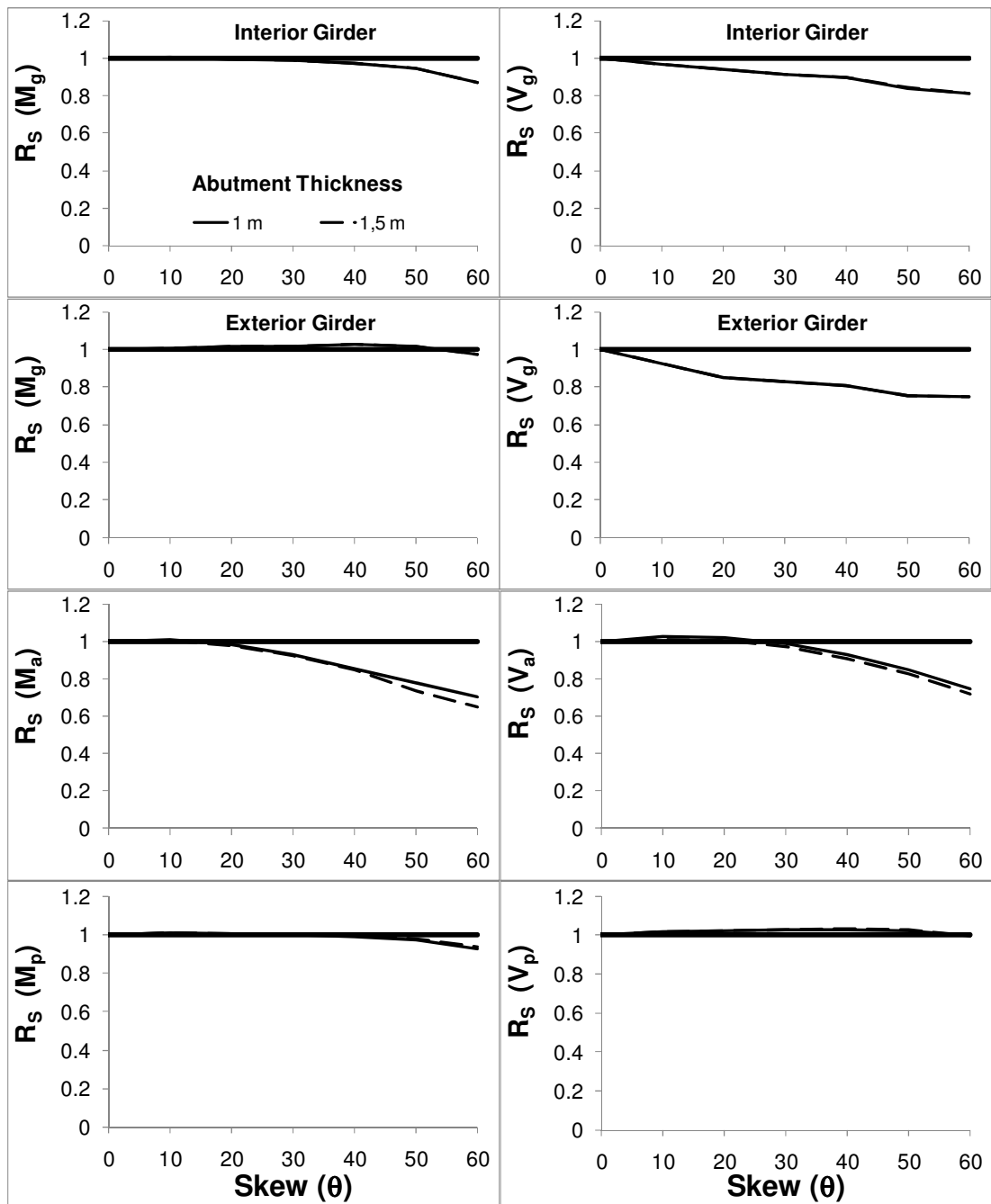


Figure 55. Effect of skew on  $R_s$  for Analysis Set 6 where two or more design lanes are loaded

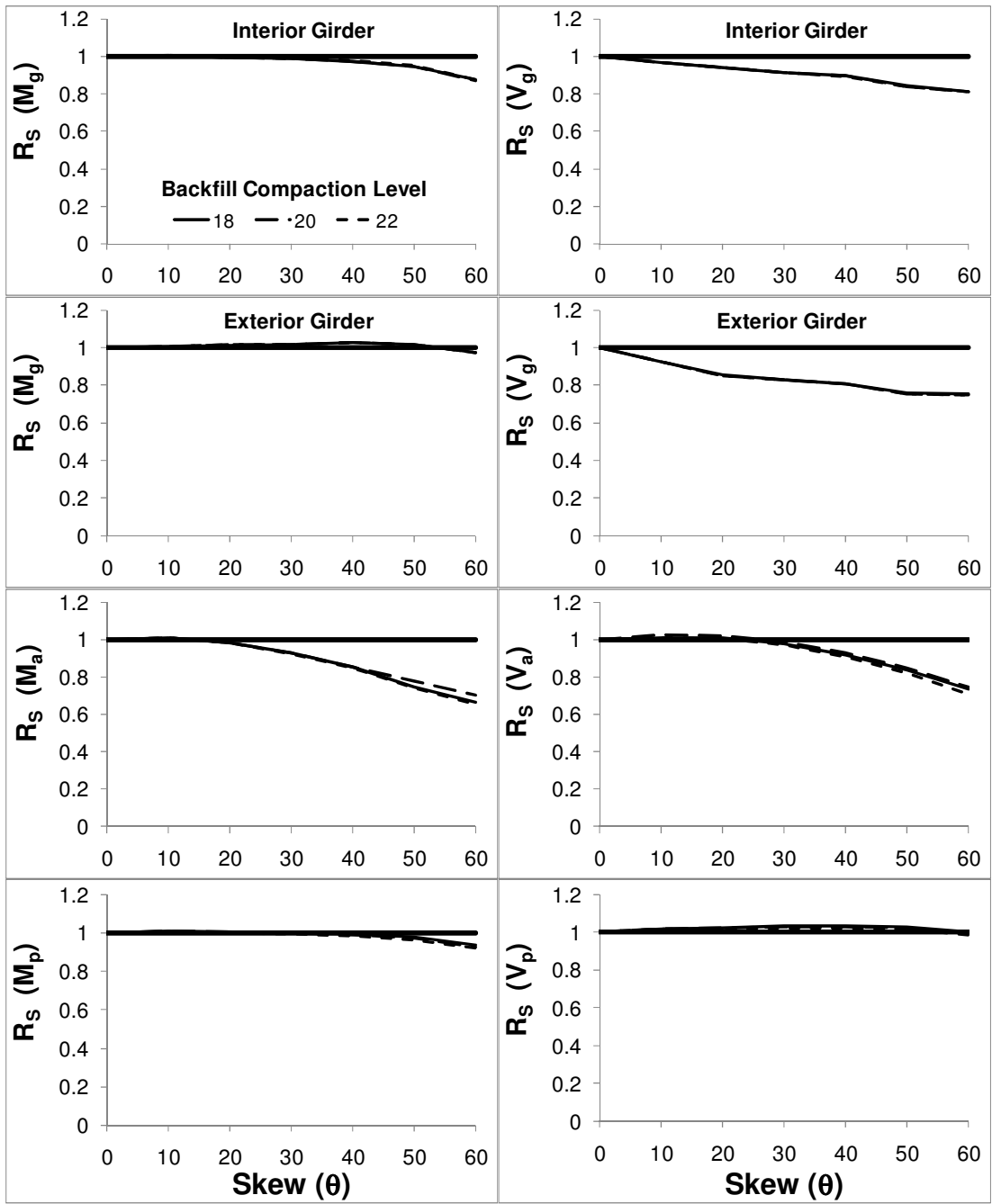


Figure 56. Effect of skew on  $R_s$  for Analysis Set 7 where two or more design lanes are loaded

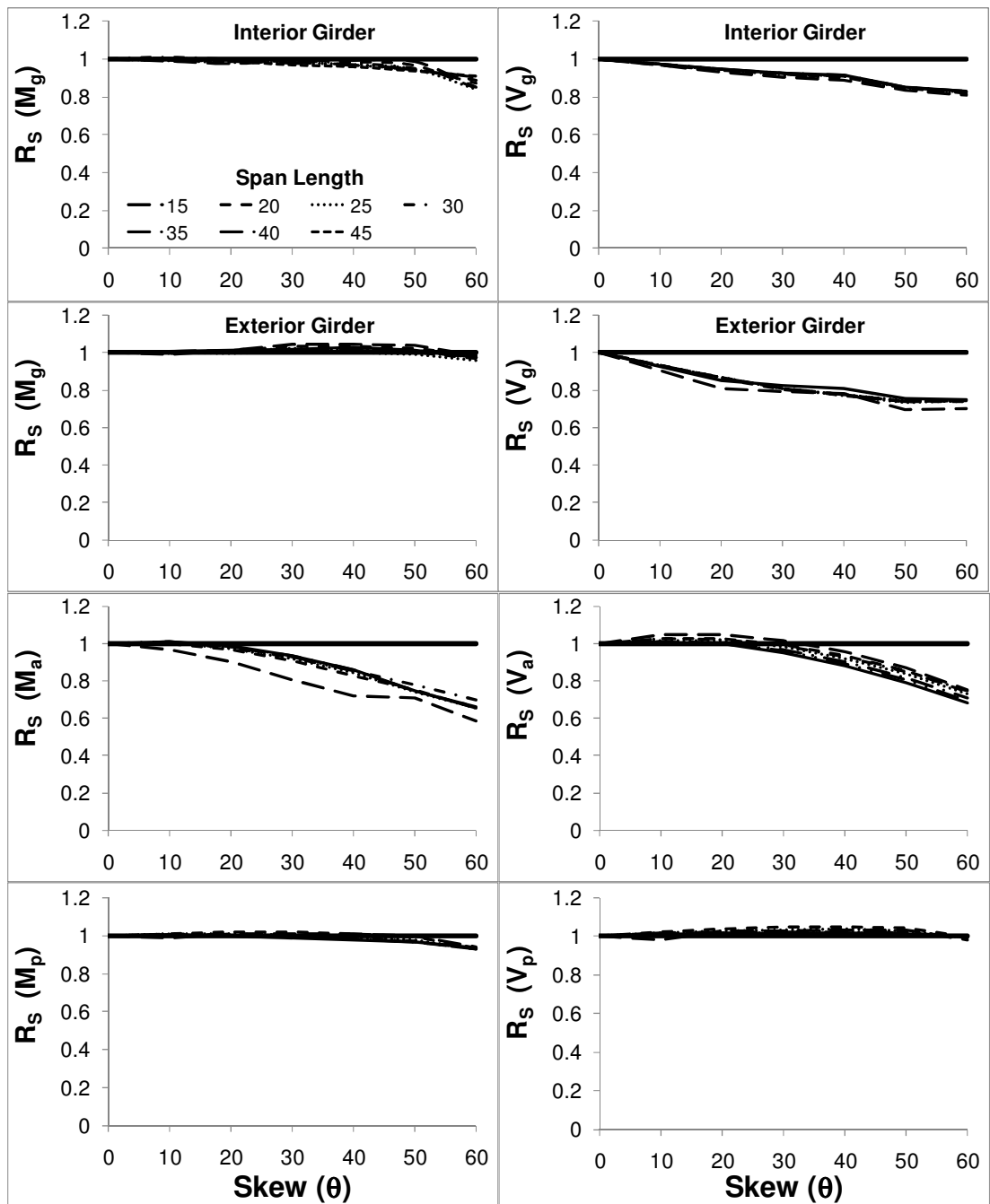


Figure 57. Effect of skew on  $R_s$  for Analysis Set 8 where two or more design lanes are loaded

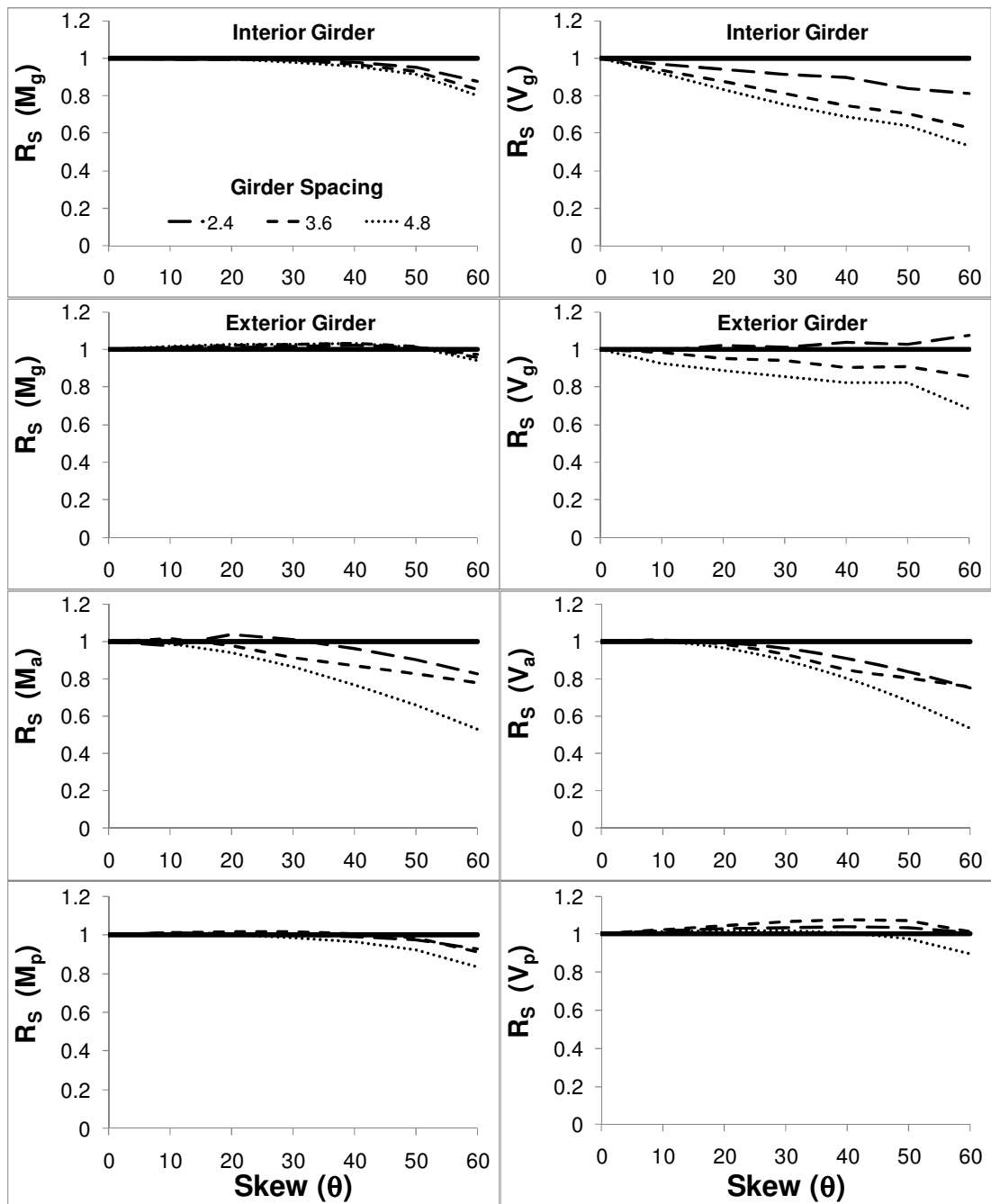


Figure 58. Effect of skew on  $R_s$  for Analysis Set 9 where two or more design lanes are loaded

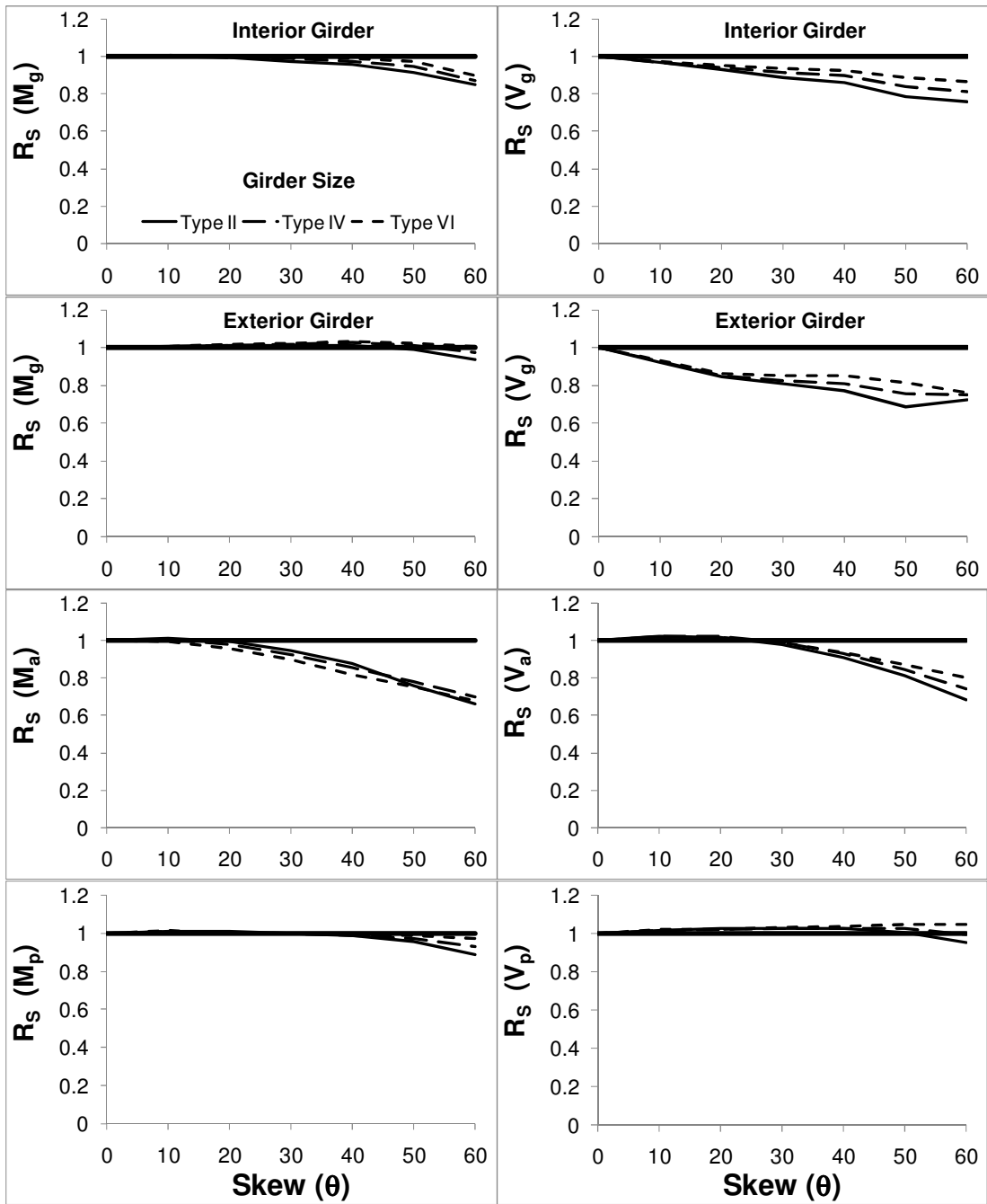


Figure 59. Effect of skew on  $R_s$  for Analysis Set 10 where two or more design lanes are loaded

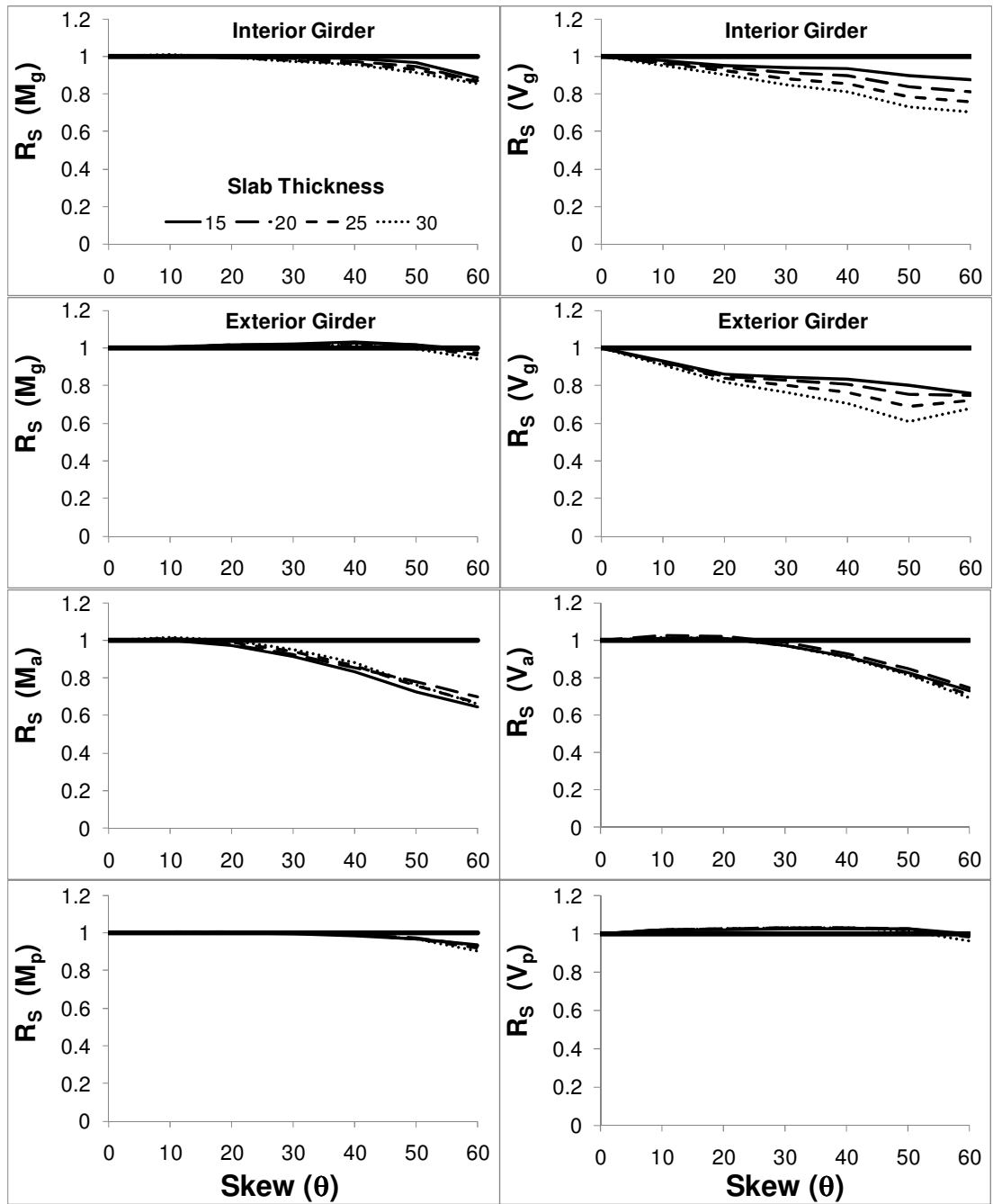


Figure 60. Effect of skew on  $R_s$  for Analysis Set 11 where two or more design lanes are loaded

Table 10. Effect of skew and selected parameters on  $R_s$  where two or more design lanes are loaded

	$M_{g-INT}$		$V_{g-INT}$		$M_{g-EXT}$		$V_{g-EXT}$		$M_a$		$V_a$		$M_p$		$V_p$	
	P	SA	P	SA	P	SA	P	SA	P	SA	P	SA	P	SA	P	SA
$N_b$	N	40	N	0	N	N	N	0	N	10	N	30	S	20	S	50
$c_u$	N	30	N	0	N	N	N	0	S	10	S	20	N	40	N	N
Pile S.	N	30	N	0	N	N	N	0	N	10	N	20	N	20	N	N
$S_p$	N	30	N	0	N	N	N	0	N	10	N	10	N	40	N	N
$H_a$	N	30	N	0	N	N	N	0	N	10	S	10	N	20	N	N
$w$	N	30	N	0	N	N	N	0	N	10	N	20	N	40	N	N
$\gamma$	N	30	N	0	N	N	N	0	N	10	N	20	N	40	N	N
$L$	N	30	N	0	N	N	S	0	S	10	S	20	N	N	N	N
$S$	S	30	S	0	N	N	S	0	S	10	S	20	S	30	S	N
GT	S	30	S	0	N	N	S	0	N	10	S	20	S	40	S	N
$t$	N	30	S	0	N	N	S	0	N	10	N	20	N	40	N	N

P: parameter effect

SA: the skew angle where the effect becomes pronounced

S: Significant

N: Negligible

## 6.2 Formulation of SCFs for SIBs

In this section, SCFs are developed to accurately calculate the LLDFs for the girders and abutments and piles of SIBs, for the cases where two or more design lanes are loaded and only one design lane is loaded. The ratio ( $R_s$ ) of the LLDFs for various skew angles to that of the case where skew angle is zero is used in the formulation of the SCFs. These SCFs will be used with the LLDEs developed by Dicleli and Erhan (2009a, 2009b) for IBs with zero skew to obtain the LLDFs for SIBs. LLDEs for straight IBs are presented in Appendix. In the developed SCFs all the parameters are measured in mm.

### 6.2.1 SCFs for Interior Girders

#### Girder Moment - Two or More Design Lanes Loaded:

To calculate the LLDFs for the girder moment of SIBs, results obtained from SIB models with zero skew angle (LLDF<sub>0</sub>) is simply multiplied by a correction factor, SCF<sub>1</sub>. Accordingly, LLDFs (LLDF<sub>θ</sub>) for the girder moment of SIBs is expressed as;

$$LLDF_{\theta} = SCF_1 \times LLDF_0 \quad (8)$$

The FEAs results reveal that the variation of R<sub>s</sub> (the ratio of the LLDFs for various skews to that for zero skew angle) for the interior girders of SIBs is a function of the skew angle, θ, girder spacing, S and girder type (Table 10). Accordingly the SCF is assumed to have the following form;

$$SCF_1 = a (b_1 + b_2 \tan \theta) \left( \frac{S}{N_b} \right)^{b_3} K_g^{b_4} \quad (9)$$

where a, b<sub>1</sub>, b<sub>2</sub>, b<sub>3</sub> and b<sub>4</sub> = constants to be determined via regression analyses using the ratio R<sub>s</sub> obtained from FEA results, S/N<sub>b</sub>= a parameter representing both the effect of the girder spacing (S) and the number of girder (N<sub>b</sub>) (Dicleli and Erhan 2009b). In the above equation, the effect of girder type is included by the parameter K<sub>g</sub> representing the longitudinal stiffness of the composite slab-on-girder section of the bridge expressed as (AASHTO 2007);

$$K_g = n(I + Ae_g^2) \quad (10)$$

In the above equation, n = the ratio of the modulus of elasticity of the girder material to that of the slab material, I = the moment of inertia of the girder, A = cross-sectional area of the girder and e<sub>g</sub> = distance between the centers of gravity of the girder and the slab.

To obtain these constants, first, the calculated  $R_s$  values are plotted as a function of the tangent of the skew angle, ( $\tan\theta$ ), as shown in Figure 61. Note that, the plot only includes the data beyond the skew angle where the effect of skew becomes noticeable (see Table 10).  $\tan\theta$  is used instead of “ $\theta$ ” to produce SCFs compatible with those presented in AASHTO for conventional jointed bridges and to obtain a more normalized representation of the skew angle. Then, a minimum least square fit of the logarithm of the  $\tan\theta$ - $R_s$  data is performed to obtain the following equation;

$$R_1 = 1.0606 - 0.1042 \tan \theta \quad (11)$$

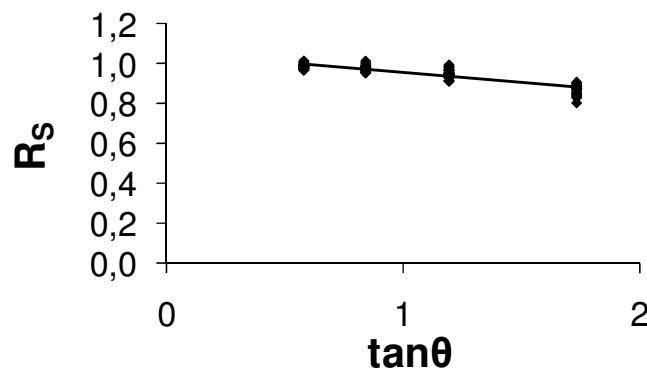


Figure 61.  $R_s$  versus  $\tan\theta$

The above equation, which is plotted using a solid line in Figure 61, gives the ratio of LLDF for various skew angles to those LLDFs for zero skew angle as a function of the skew angle. The term 1.0606 in Eqn. (11), represents the term  $b_1$  in Eqn. (9) and the term  $-0.1042 \times \tan\theta$  in Eqn. (11) represents the term  $b_2 \times \tan\theta$  in Eqn. (9). Thus,  $b_1=1.0606$  and  $b_2=-0.1042$ . The scatter present in Figure 61 with respect to the plot of Eqn. (11) is mainly due to the error introduced by the absence of the other parameters,  $S/N_b$  and  $K_g$  in the equation. This error will be corrected by involving the effect of these remaining parameters in the equation. For this purpose, a new ratio,  $R_2$ , is first calculated as;

$$R_2 = \frac{R_s}{R_1} \quad (12)$$

In the above equation,  $R_2$  represents the ratio  $R_s$ , corrected with respect to the skew angle,  $\theta$ . Then, the ratio  $R_2$  is plotted as a function of the  $S/N_b$  in Figure 62. Next, the minimum least square fit of the logarithm of the data is performed to obtain the following equation;

$$R_2 = 1.2583 \left( \frac{S}{N_b} \right)^{-0.04} \quad (13)$$

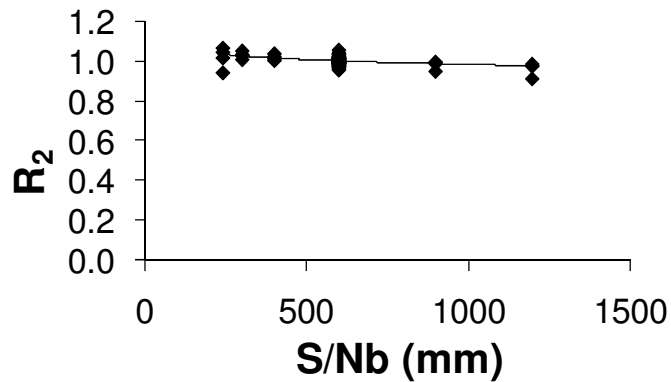


Figure 62.  $R_2$  versus  $S/N_b$

The above equation is plotted using a solid line as shown in Figure 62. The term  $(S/N_b)^{-0.04}$  in Eqn. (13), represents the term  $(S/N_b)^{b3}$  in Eqn. (9). Thus,  $b3 = -0.04$ . Following a procedure similar to that described above, the parameter,  $b4$  is calculated as 0.02. The constant in Eqn. (9) is obtained as 50/61 by multiplying  $a$  by  $b1$ . The coefficient of  $\tan\theta$  in Eqn. (9) is obtained as 2/25 by multiplying  $a$  by  $b2$ . Accordingly, the final form of the SCF becomes;

$$SCF_1 = 1 \quad \text{for } \theta \leq 30 \quad (14)$$

$$SCF_1 = \left( \frac{50}{61} - \frac{2}{25} \tan \theta \right) \left( \frac{N_b}{S} \right)^{0.04} K_s^{0.02} \quad \text{for } 30 < \theta \leq 60$$

For the remainder of the cases except the girder shear, a similar analytical expression as given in Eqn. (9) but with either more or less number of variables is assumed for the SCFs. For the girder shear however, based on the observed correlation between the skew angle and girder spacing, the following analytical expression is assumed for the SCFs.

$$SCF = a \left( b_1 + b_2 \left( \frac{S}{2400} \right)^{b_3} \tan \theta \right) \left( \frac{S}{N_b} \right)^{b_4} K_g^{b_5} L^{b_6} t^{b_7} \quad (15)$$

A procedure similar to that outlined above for the interior girder moment is followed to calculate the constants given in the SCFs for the shear and moment LLDFs of each particular component of SIBs for the cases where two or more design lanes are loaded and only one design lane is loaded.

*Girder Moment - One Design Lane Loaded:*

$$SCF_2 = 1 \quad \text{for } \theta \leq 30 \quad (16)$$

$$SCF_2 = \left( \frac{43}{50} - \frac{3}{50} \tan \theta \right) \left( \frac{N_b}{S} \right)^{0.03} K_g^{0.014} \quad \text{for } 30 < \theta \leq 60$$

*Girder Shear - Two or More Design Lanes Loaded:*

$$SCF_3 = 1 \quad \text{for } \theta < 10 \quad (17)$$

$$SCF_3 = \left( \frac{53}{25} - \frac{13}{50} \left( \frac{S}{2400} \right)^{1.2} \tan \theta \right) \left( \frac{N_b}{S} \right)^{0.07} \frac{K_g^{0.018}}{t^{0.15}} \quad \text{for } 10 \leq \theta \leq 60$$

### 6.1.2 SCFs for Exterior Girders

Girder Shear - Two or More Design Lanes Loaded:

$$SCF_4 = 1 \quad \text{for } \theta < 10 \quad (18)$$

$$SCF_4 = \left( \frac{17}{25} - \frac{1}{10} \left( \frac{S}{2400} \right)^{0.1} \tan \theta \right) \left( \frac{S}{N_b} \right)^{0.06} \frac{K_g^{0.02} L^{0.03}}{t^{0.17}} \quad \text{for } 10 \leq \theta \leq 60$$

Girder Shear - One Design Lane Loaded:

$$SCF_5 = 1 \quad \text{for } \theta < 10 \quad (19)$$

$$SCF_5 = \left( \frac{16}{25} - \frac{17}{200} \left( \frac{S}{2400} \right) \tan \theta \right) \left( \frac{S}{N_b} \right)^{0.04} \frac{K_g^{0.012} L^{0.064}}{t^{0.17}} \quad \text{for } 10 \leq \theta \leq 60$$

### 6.2.3 SCFs for Substructure

A similar procedure to that described in the previous sections is used to obtain SCFs for the shear and moment LLDFs of substructure components of SIBs for the cases where two or more design lanes are loaded and only one design lane is loaded.

Abutment Moment - Two or More Design Lanes Loaded:

$$SCF_6 = 1 \quad \text{for } \theta \leq 10 \quad (20)$$

$$SCF_6 = \left( \frac{9}{25} - \frac{2}{25} \tan \theta \right) \left( \frac{S}{N_b} \right)^{0.03} \mu^{0.01} L^{0.07} \quad \text{for } 10 < \theta \leq 60$$

Abutment Moment - One Design Lane Loaded:

$$SCF_7 = 1 \quad \text{for } \theta \leq 10 \quad (21)$$

$$SCF_7 = \left( \frac{19}{50} - \frac{1}{10} \tan \theta \right) \left( \frac{S}{N_b} \right)^{0.04} \mu^{0.01} L^{0.06} \quad \text{for } 10 \leq \theta \leq 60$$

Abutment Shear - Two or More Design Lanes Loaded:

$$SCF_8 = 1 \quad \text{for } \theta \leq 20 \quad (22)$$

$$SCF_8 = \left( 3 - \frac{3}{5} \tan \theta \right) \left( \frac{N_b}{S} \right)^{0.09} \frac{K_g^{0.017} \mu^{0.03}}{L^{0.07} H_c^{0.08}} \quad \text{for } 20 < \theta \leq 60$$

Abutment Shear - One Design Lane Loaded:

$$SCF_9 = 1 \quad \text{for } \theta \leq 20 \quad (23)$$

$$SCF_9 = \left( 2 - \frac{19}{50} \tan \theta \right) \left( \frac{N_b}{S} \right)^{0.09} \frac{K_g^{0.018} \mu^{0.034}}{L^{0.045} H_c^{0.07}} \quad \text{for } 20 < \theta \leq 60$$

Pile Moment - Two or More Design Lanes Loaded:

$$SCF_{10} = 1 \quad \text{for } \theta \leq 30 \quad (24)$$

$$SCF_{10} = \left( \frac{27}{50} - \frac{1}{25} \tan \theta \right) \left( \frac{S}{N_b} \right)^{0.06} K_g^{0.01} \quad \text{for } 30 < \theta \leq 60$$

Pile Moment - One Design Lane Loaded:

$$SCF_{11} = 1 \quad \text{for } \theta \leq 30 \quad (25)$$

$$SCF_{11} = \left( \frac{17}{25} - \frac{3}{100} \tan \theta \right) \left( \frac{S}{N_b} \right)^{0.07} \quad \text{for } 30 < \theta \leq 60$$

## 6.2 Comparison and Verification of SCFs

In this section, the SCFs developed for girders and substructure components of SIBs are verified against the available FEA results. For this purpose, the SCFs for the girders and substructure components of SIBs are calculated using the developed equations. Then, the calculated SCFs and FEA results are plotted as a function of the skew angle,  $\theta$  in Figures 63-73 for various parameters which are observed to significantly affect the SCF. These parameters are; girder spacing, S, span length, L and girder type. AASHTO skew correction factors which are originally developed for conventional jointed bridges are also included in the plots for the interior and exterior girders for comparison purposes. As observed from the Figures, the derived equations produce reasonable estimates of the SCFs calculated from FEAs results for girders and substructure components of SIBs. It is also observed that AASHTO SCFs are generally unconservative or smaller (smaller SCFs results in smaller live load effects in bridge components when multiplied with LLDFs obtained for straight bridges) especially for SIBs with larger skew ( $\theta > 30^\circ$ ). This is mainly due to the torsional rotational rigidity provided by the monolithic abutments to the girders and the slab of SIBs which enhances the distribution of live load among the bridge components when compared to conventional jointed bridges.

Furthermore, for the entire data used in the development of the SCFs, the averages and standard deviations of the ratios of the SCFs obtained from the derived equations to those from FEA are calculated for the girders and substructure components of SIBs and presented in Table 11. As observed from the table, the calculated average values of the ratios range between 0.99 and 1.02 while the standard deviations are between 0.02 and 0.06. The small deviations of the values of the calculated average ratios from 1.0 and

relatively small standard deviations also indicate that the derived correction factors produce reasonably good estimates of the SCFs calculated from FEAs results for girders and substructure components of SIBs for the range of parameters considered in this research study.

*Table 11. Averages and standard deviations for developed SCFs*

<b>Number of Design Lanes Loaded</b>	<b>Statistical Parameters</b>	<b>Mg Int.</b>	<b>Vg Int.</b>	<b>Vg Ext.</b>	<b>Ma</b>	<b>Va</b>	<b>Mp</b>
Two or More	Mean	1.01	1.01	1.02	0.99	1.00	1.00
	Std. Dev.	0.02	0.03	0.06	0.04	0.03	0.02
	Min.	0.98	0.91	0.67	0.77	0.92	0.94
	Max.	1.13	1.13	1.20	1.22	1.26	1.19
One	Mean	0.99	-	0.99	1.02	1.00	1.01
	Std. Dev.	0.01	-	0.05	0.03	0.03	0.03
	Min.	0.93	-	0.71	0.83	0.92	0.96
	Max	1.05	-	1.08	1.14	1.14	1.21

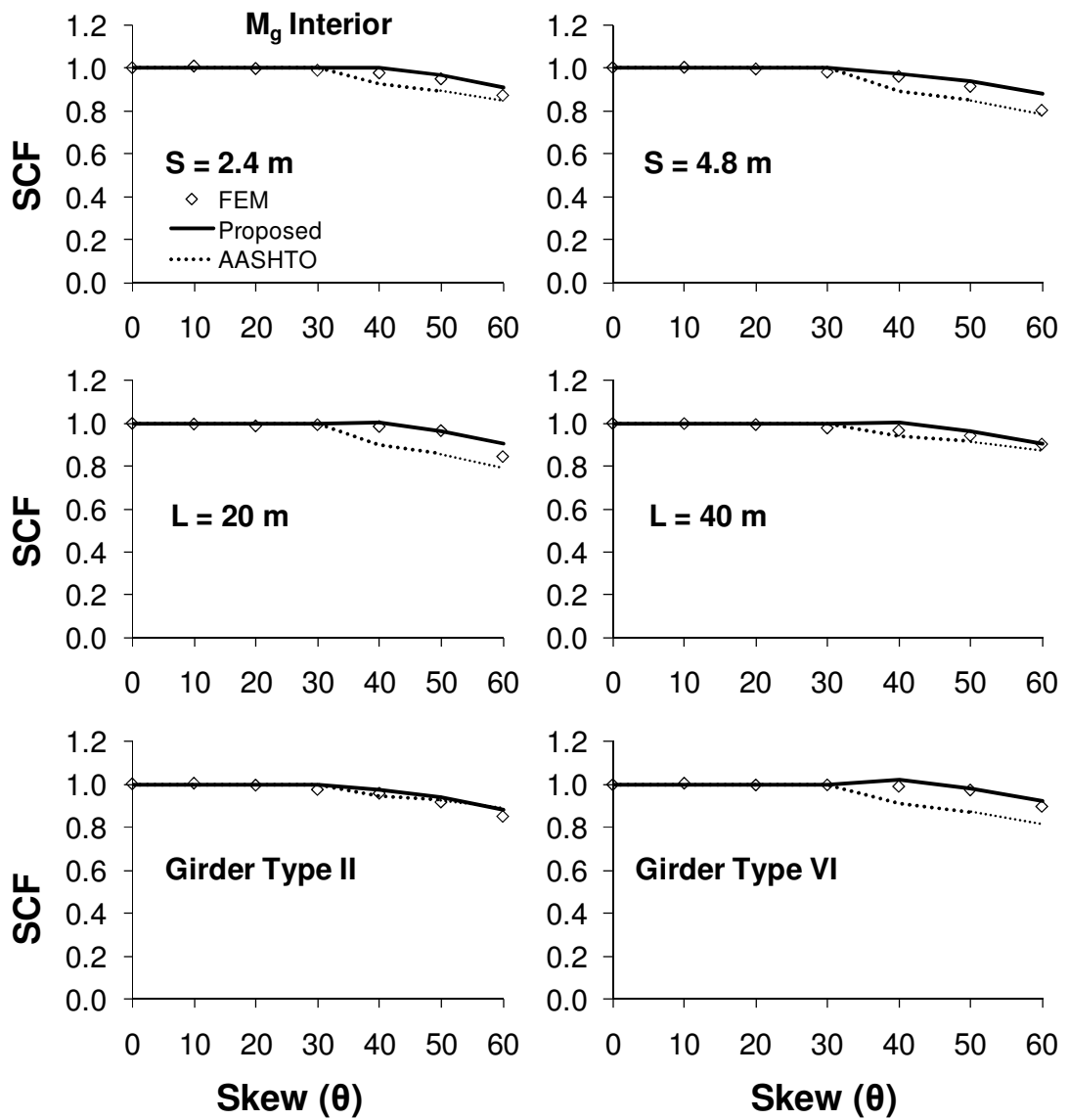


Figure 63. Plot of FEAs results, proposed SCFs and AASHTO SCFs for interior girder moment of selected models where two or more lanes are loaded

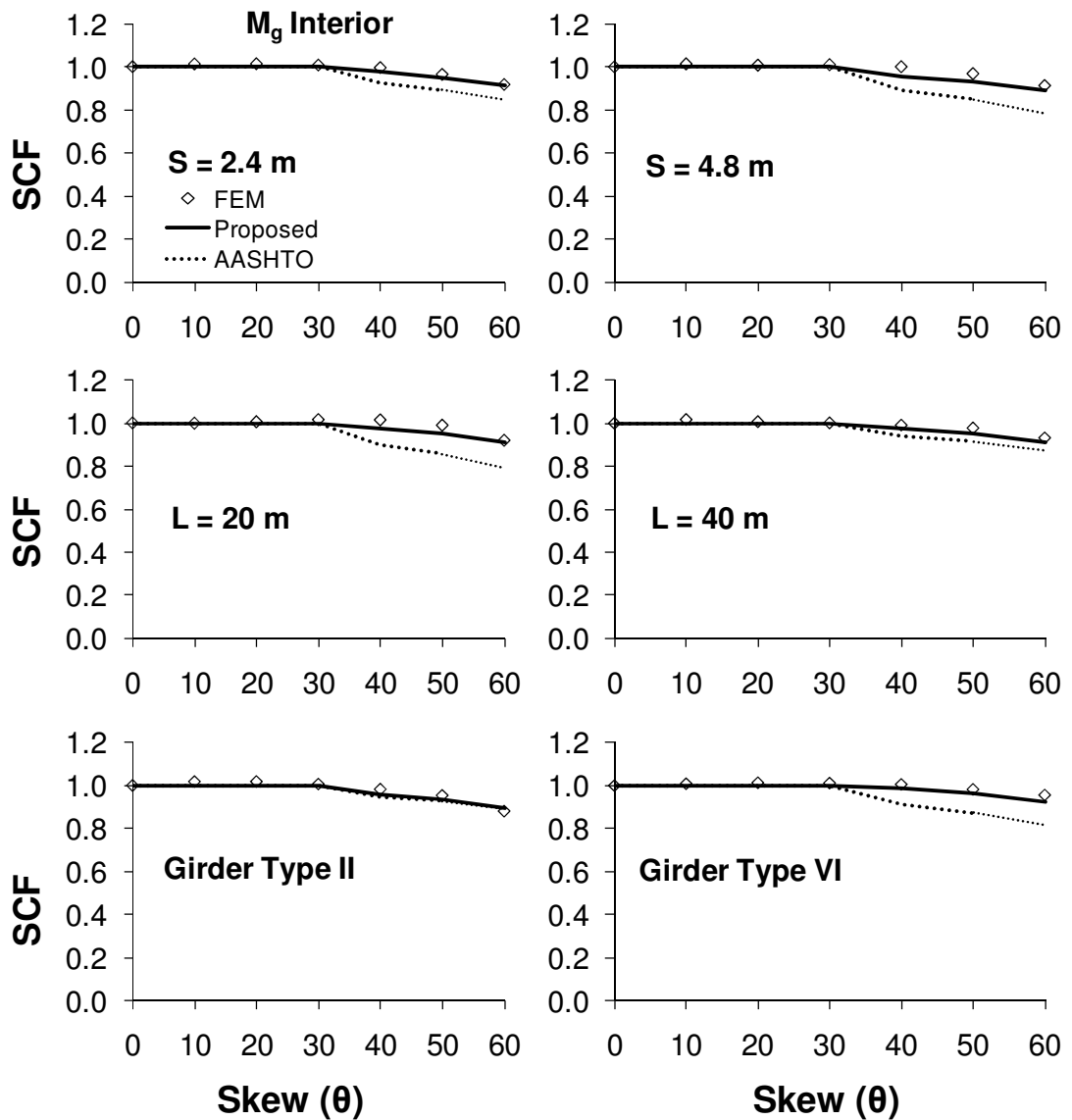


Figure 64. Plot of FEAs results, proposed SCFs and AASHTO SCFs for interior girder moment of selected models where only one design lane is loaded

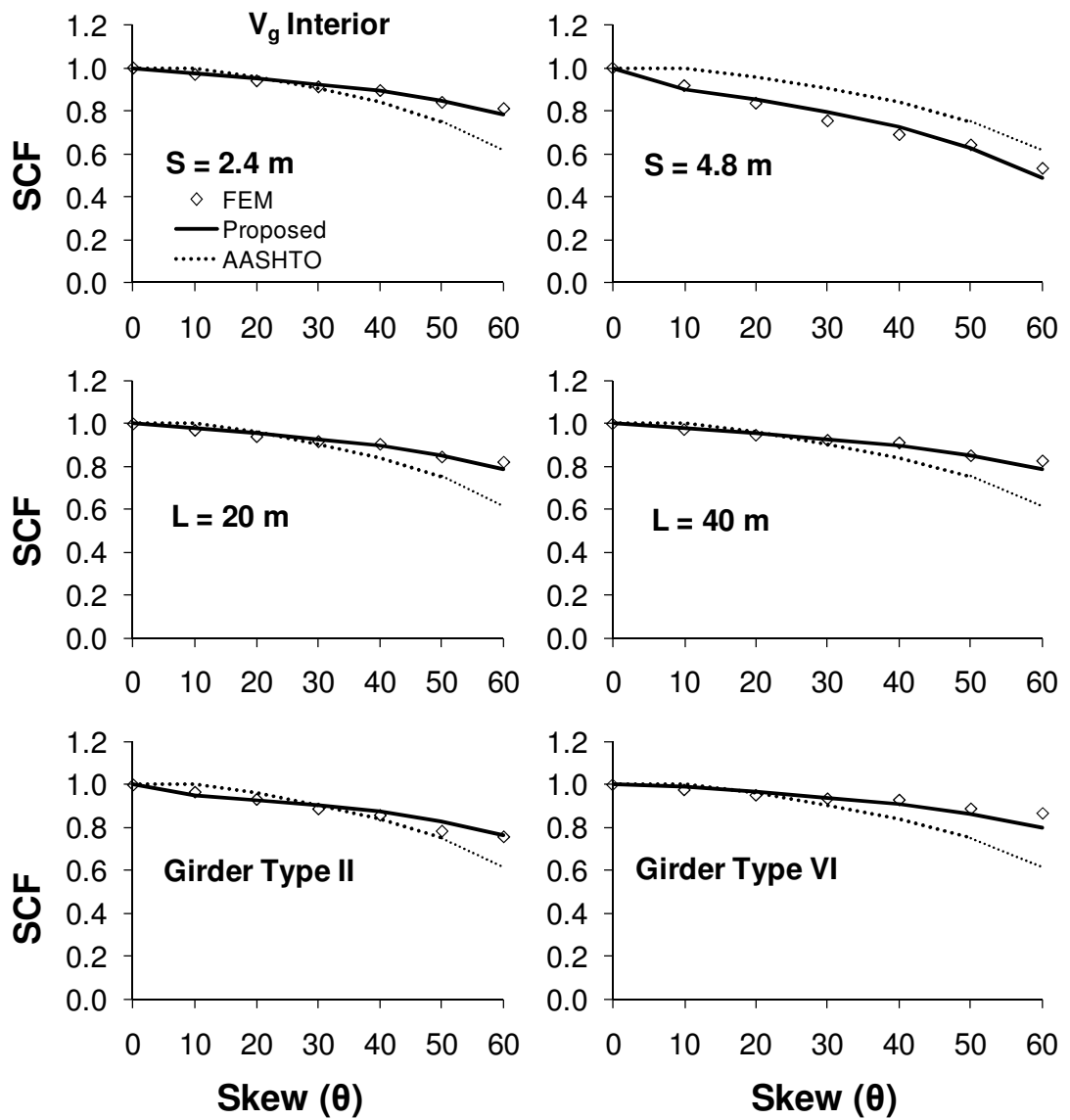


Figure 65. Plot of FEAs results, proposed SCFs and AASHTO SCFs for interior girder shear of selected models where two or more lanes are loaded

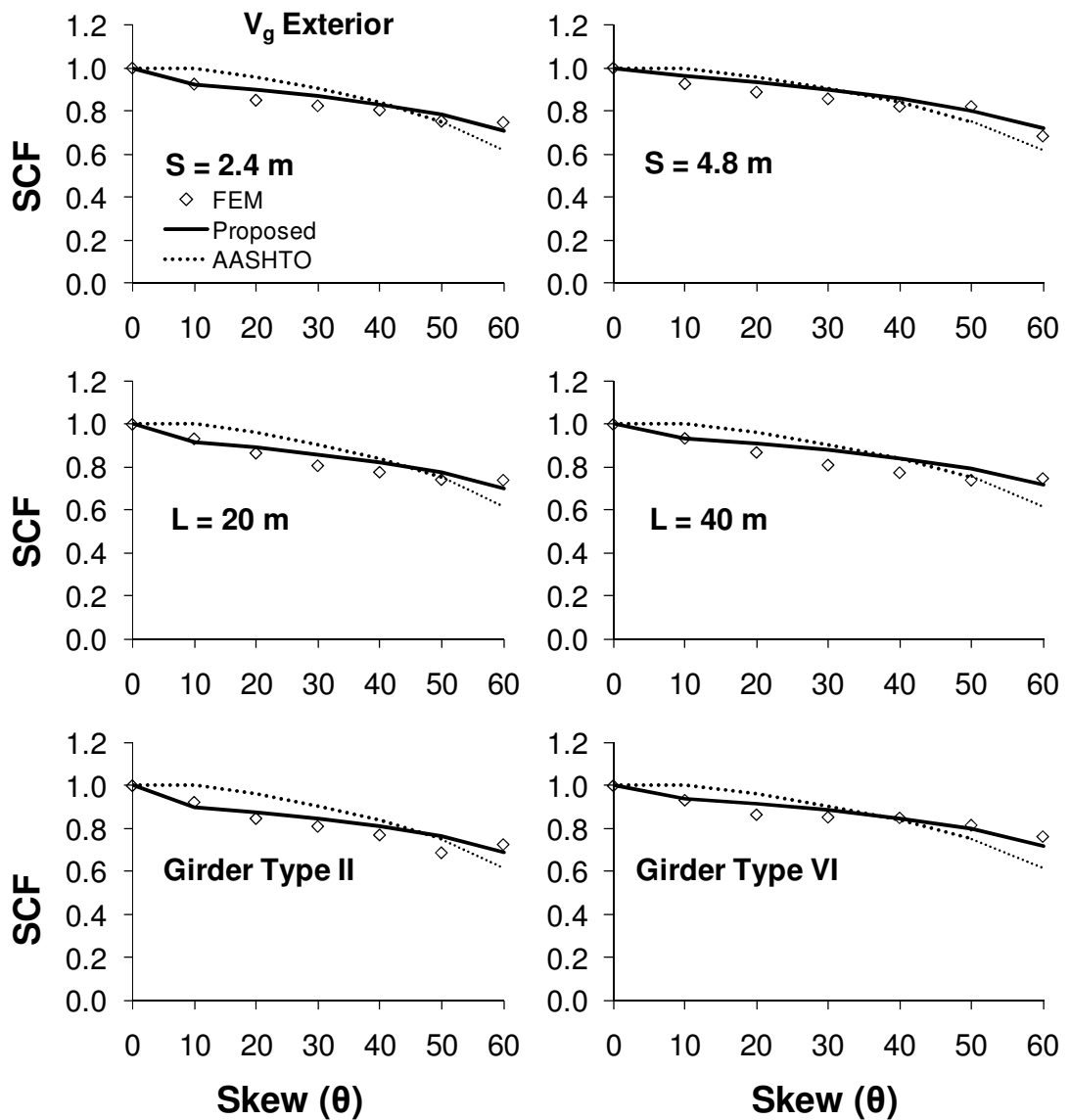


Figure 66. Plot of FEAs results, proposed SCFs and AASHTO SCFs for exterior girder shear of selected models where two or more lanes are loaded

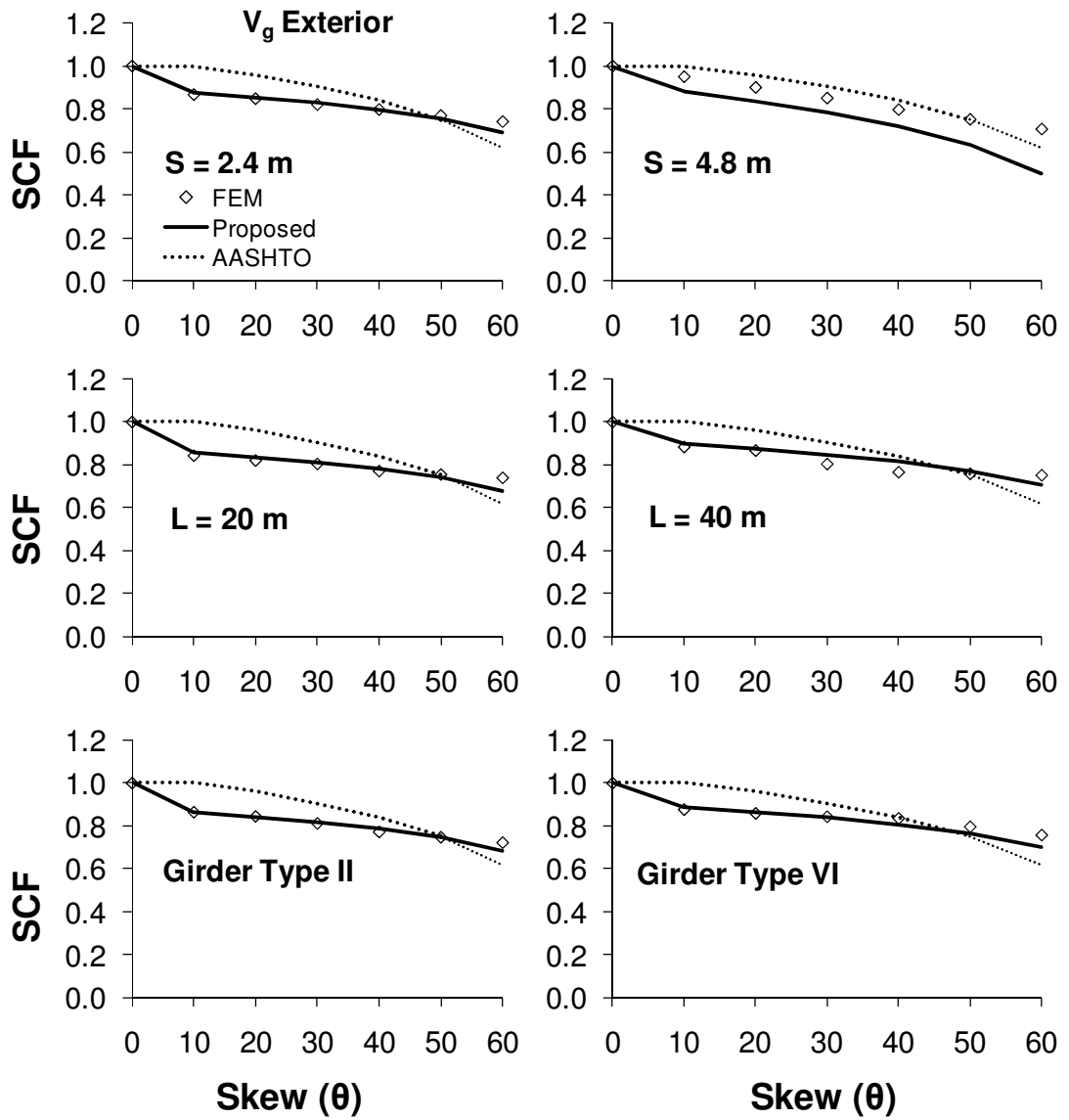


Figure 67. Plot of FEAs results, proposed SCFs and AASHTO SCFs for exterior girder shear of selected models where only one design lane is loaded

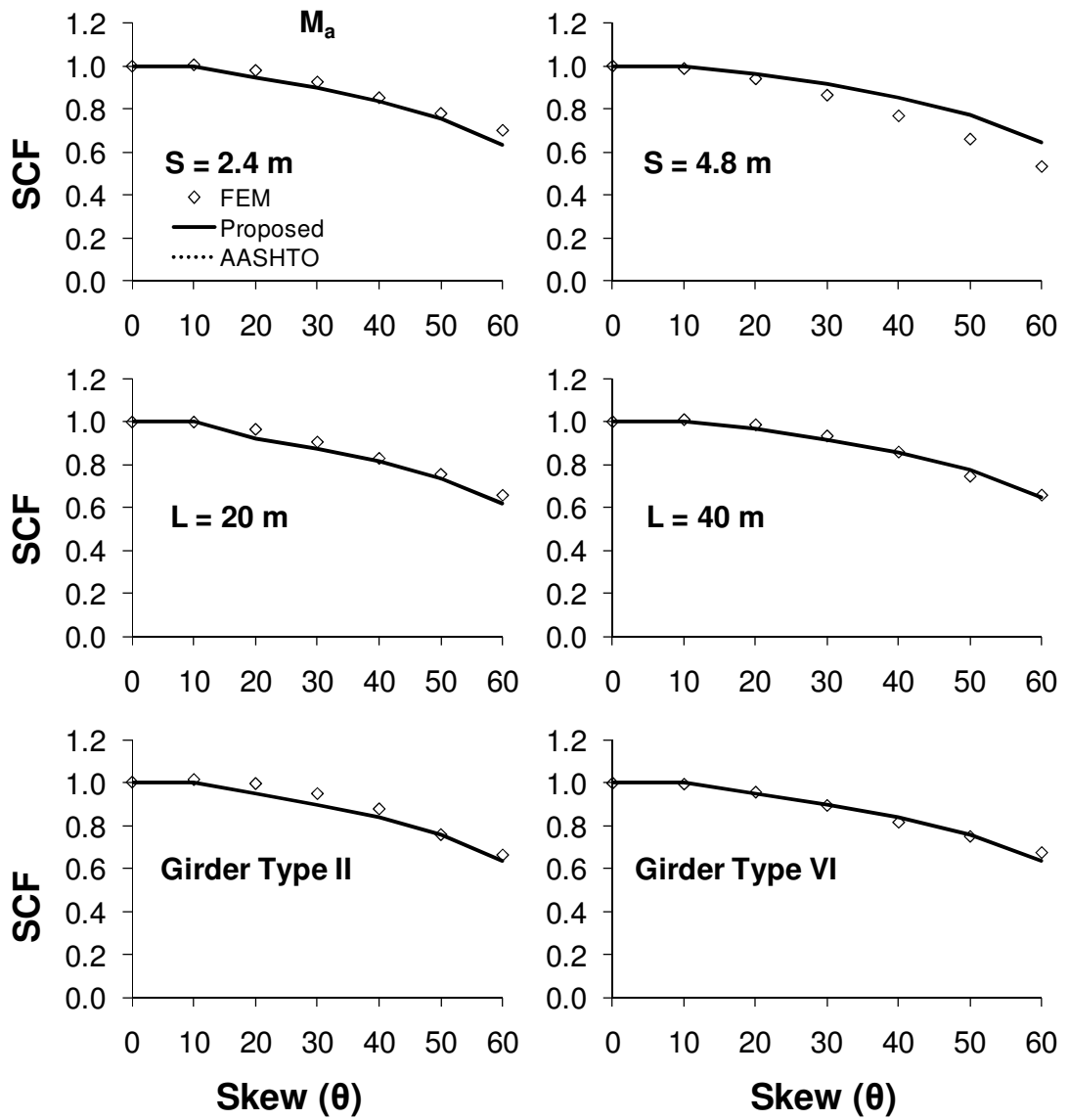


Figure 68. Plot of FEAs results, proposed SCFs and AASHTO SCFs for abutment moment of selected models where two or more lanes are loaded

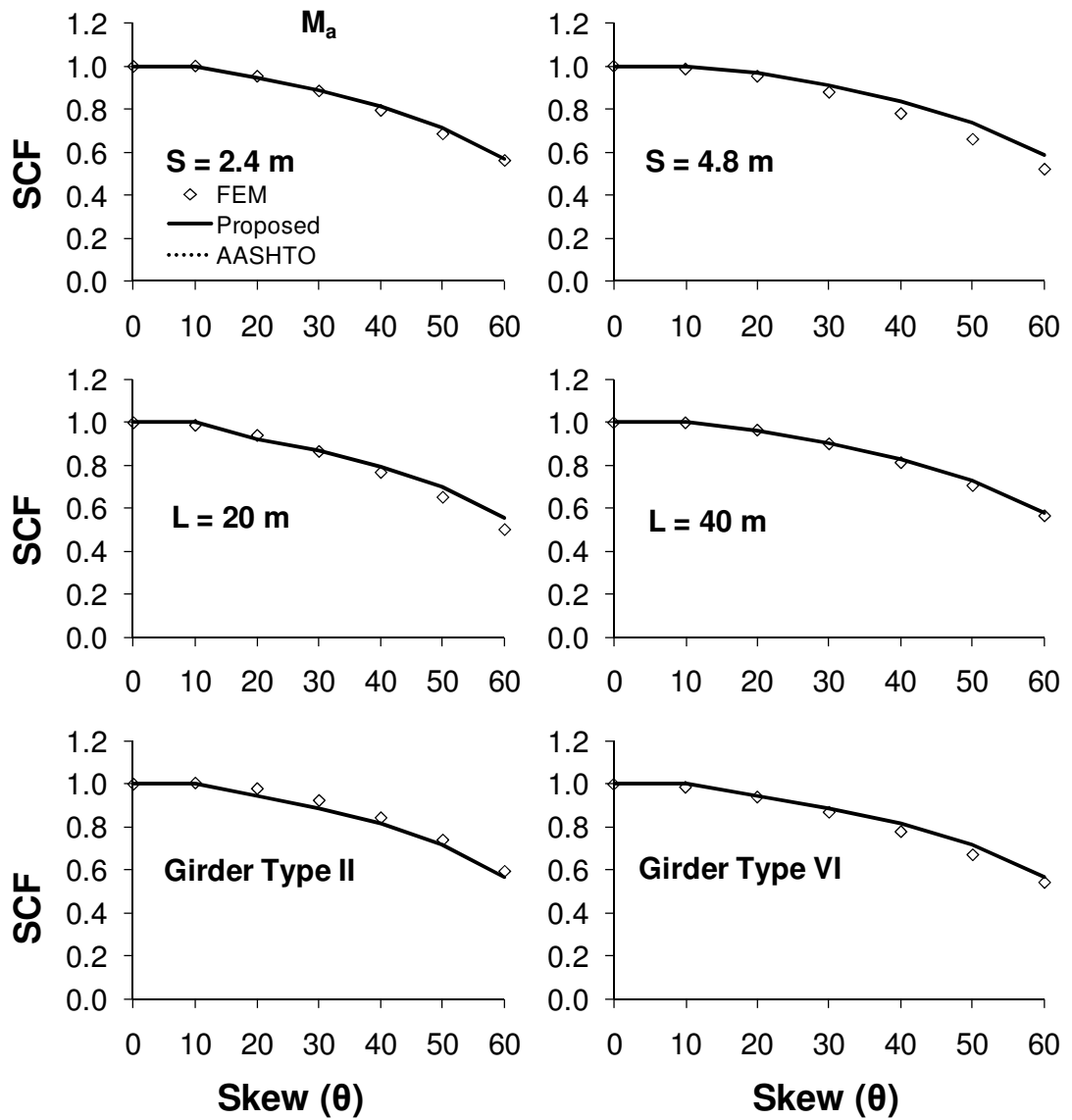


Figure 69. Plot of FEAs results, proposed SCFs and AASHTO SCFs for abutment moment of selected models where only one design lane is loaded

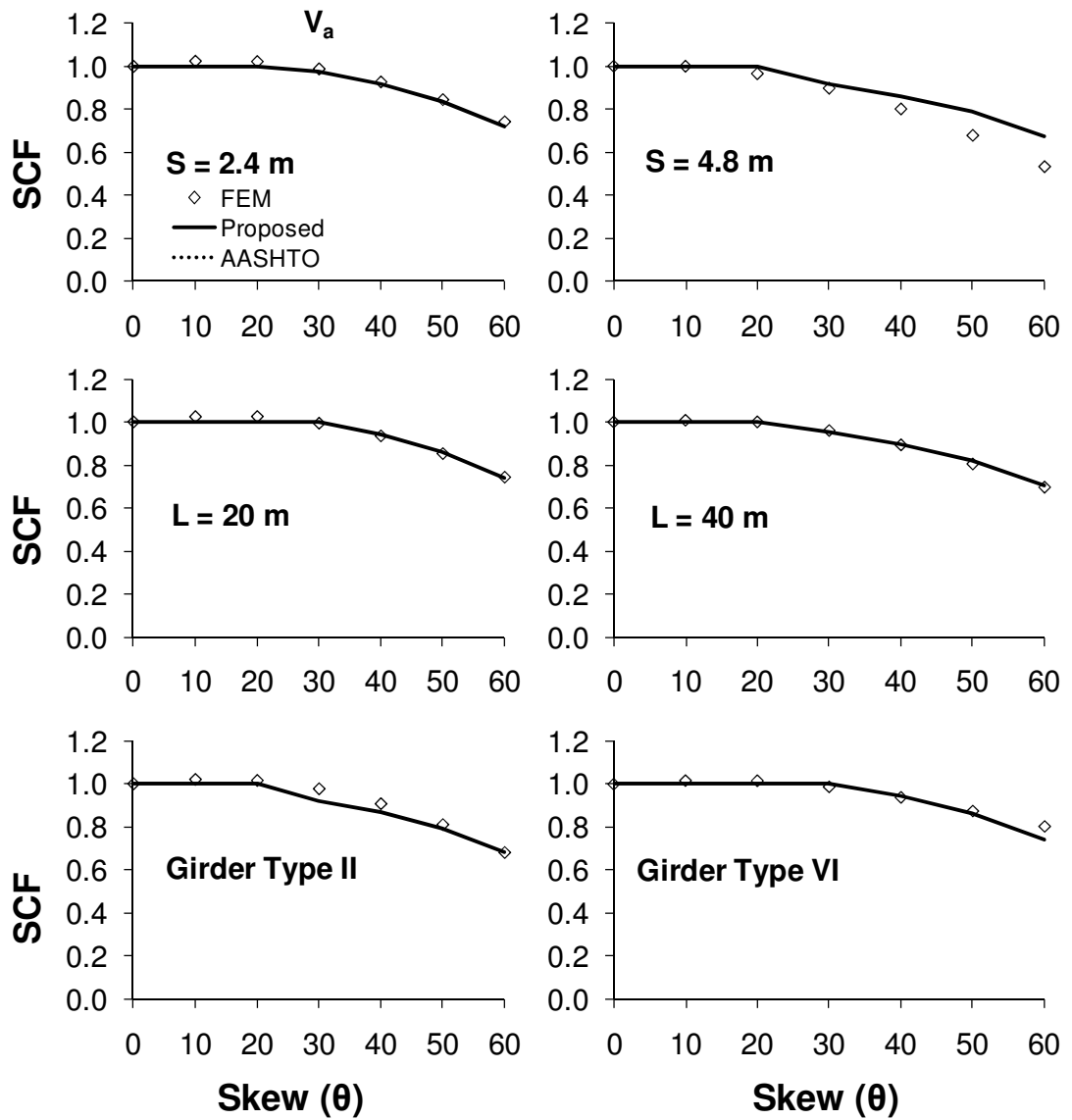


Figure 70. Plot of FEAs results, proposed SCFs and AASHTO SCFs for abutment shear of selected models where two or more lanes are loaded

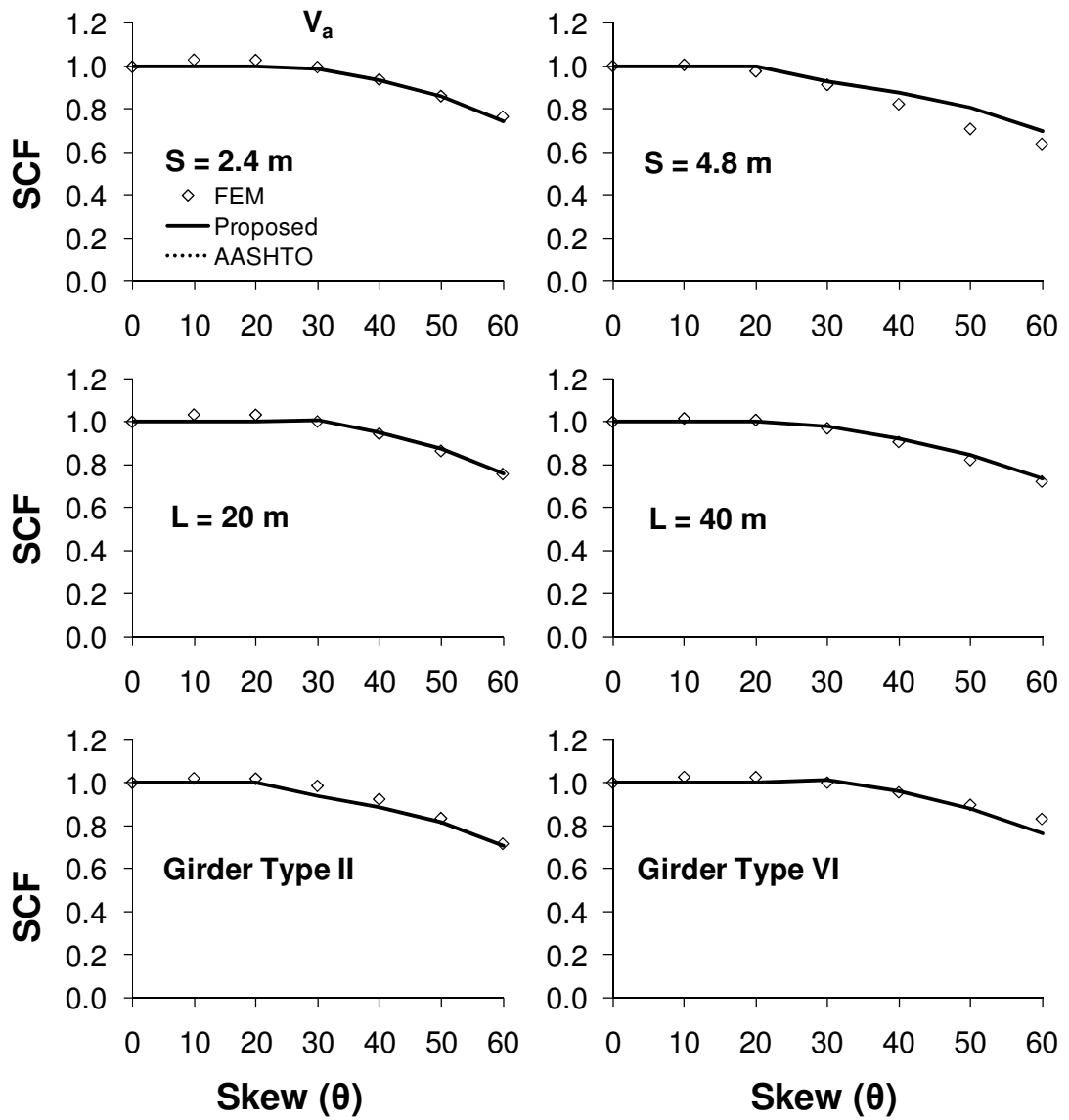


Figure 71. Plot of FEAs results, proposed SCFs and AASHTO SCFs for abutment shear of selected models where only one design lane is loaded

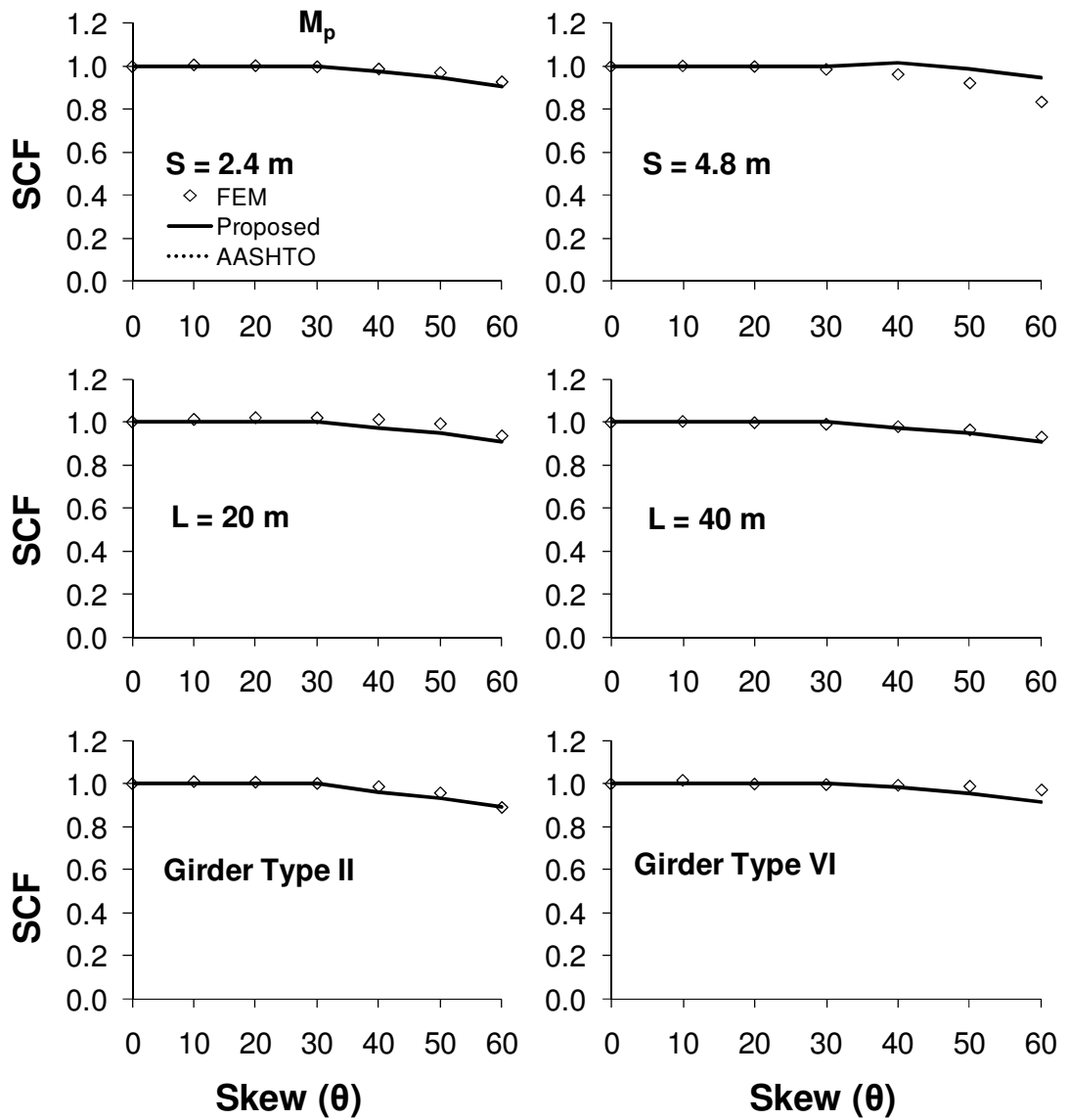


Figure 72. Plot of FEAs results, proposed SCFs and AASHTO SCFs for pile moment of selected models where two or more lanes are loaded

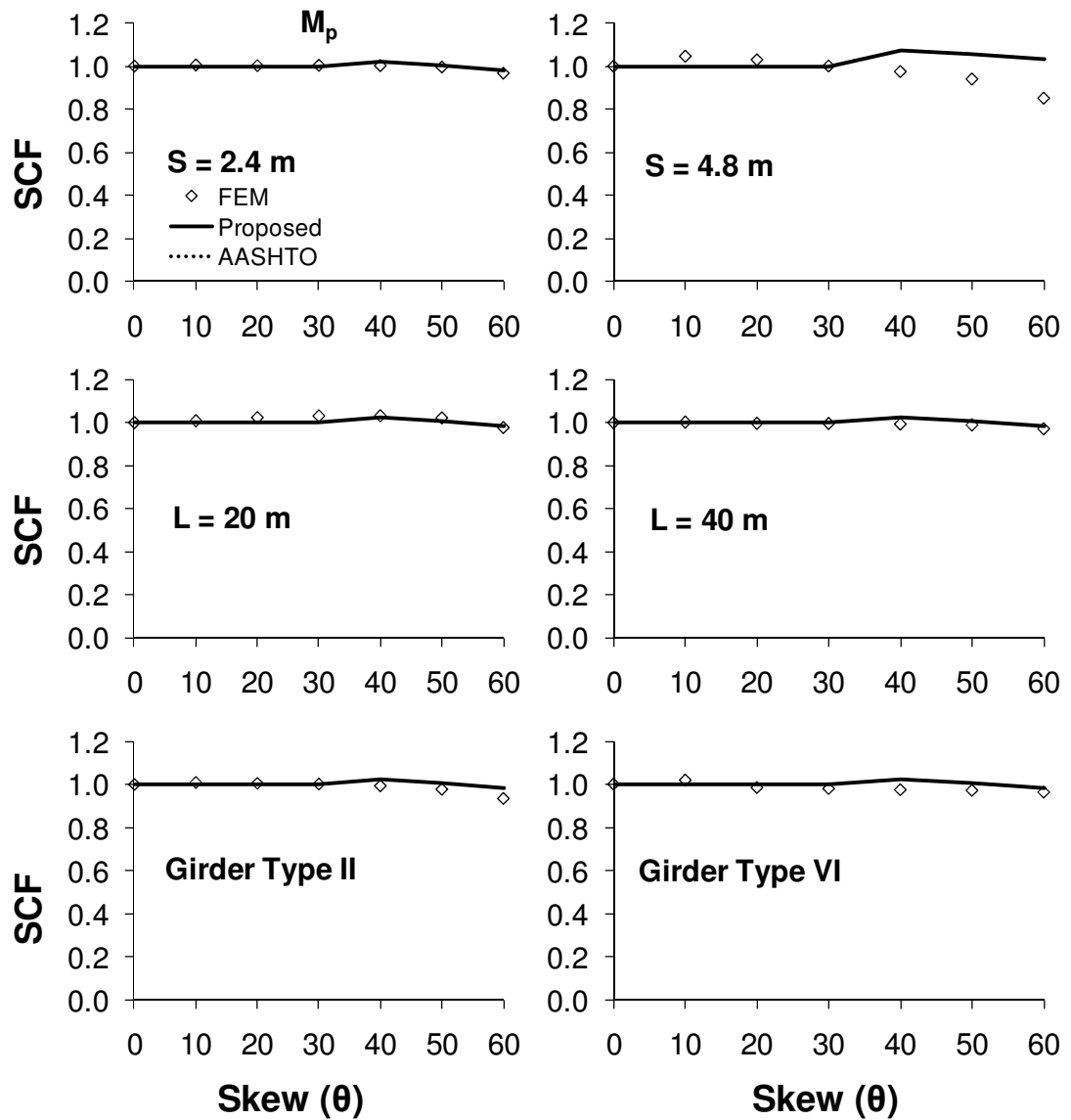


Figure 73. Plot of FEAs results, proposed SCFs and AASHTO SCFs for pile moment of selected models where only one design lane is loaded

To further verify the SCFs developed as part of this study, the LLDEs developed by Dicleli and Erhan (2009a, 2009b) for straight IBs (skew effect was totally neglected) are plotted as a function of the skew angle together with FEAs results and the results obtained by multiplying these LLDEs by the developed SCFs. The results are presented in Figures 74-79 for the case

where two or more design lanes are loaded. The plots for the case where only one design lane is loaded are similar. As observed from the figures, using the SCFs together with the LLDEs developed by Dicleli and Erhan (2009a, 2009b) resulted in a considerable improvement in the prediction of live load effects in SIB components.

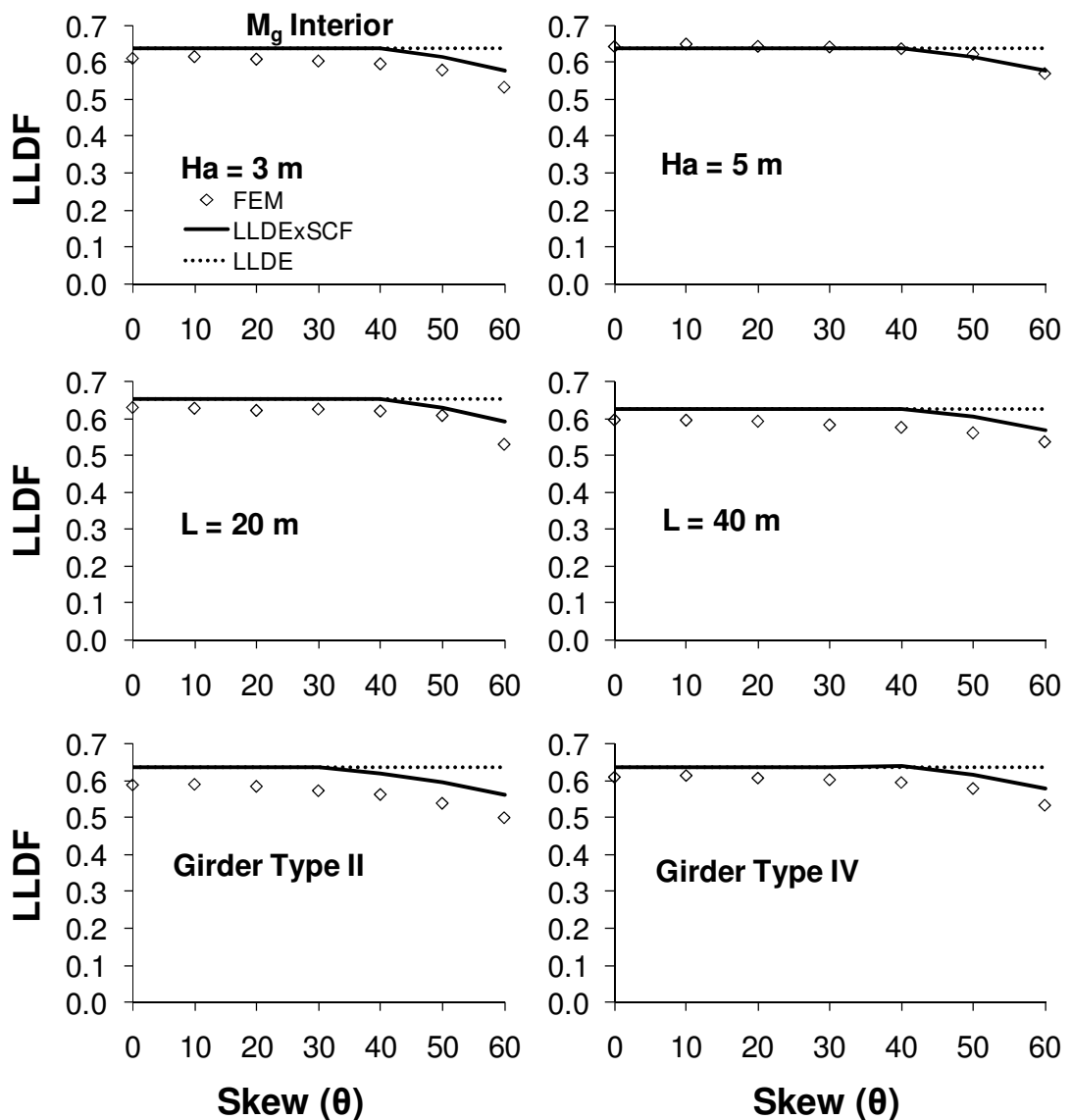


Figure 74. Plot of FEAs results, LLDEs and LLDEs multiplied by SCFs for interior girder moment of selected models where two or more lanes are loaded

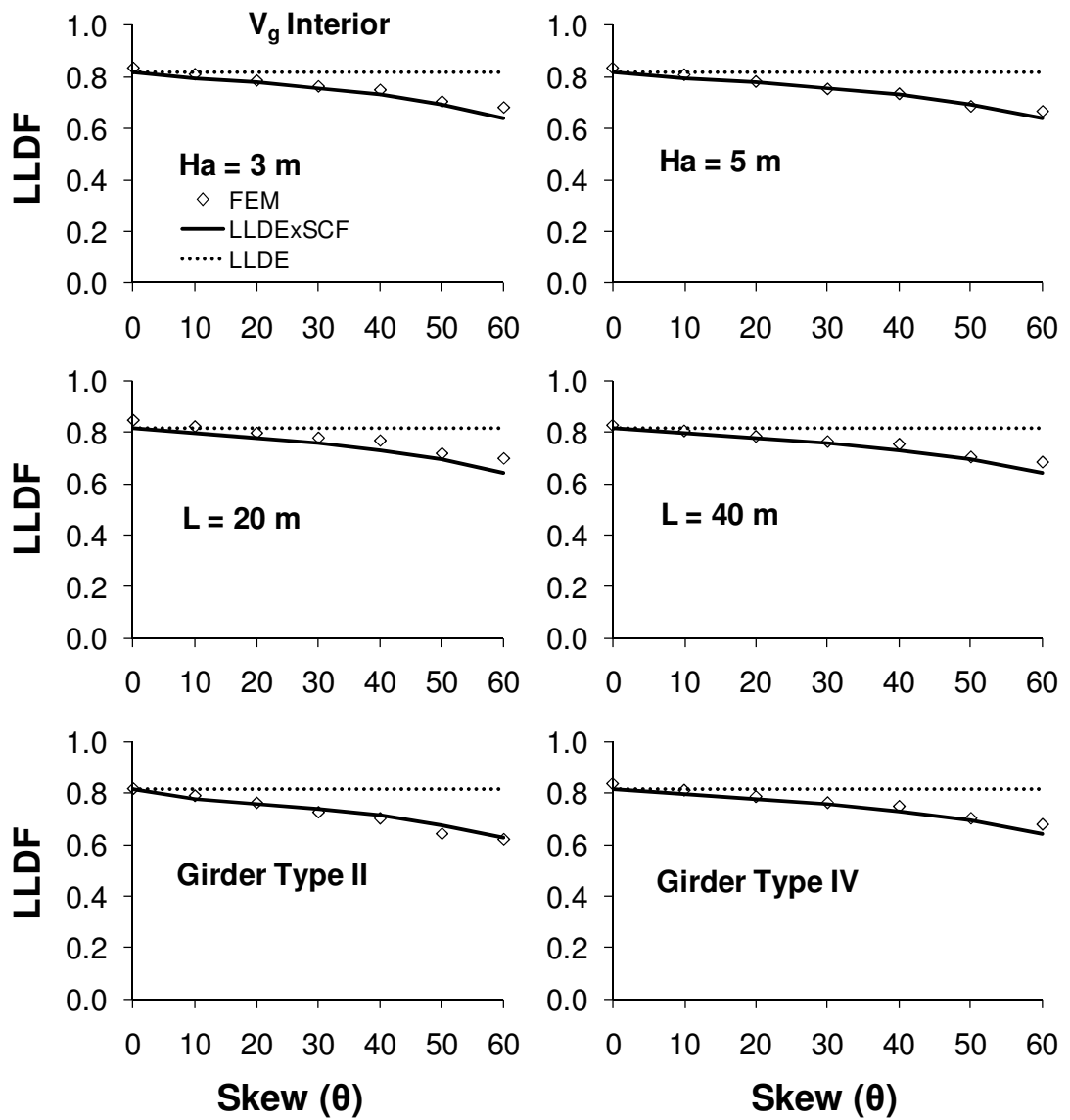


Figure 75. Plot of FEAs results, LLDEs and LLDEs multiplied by SCFs for interior girder shear of selected models where two or more lanes are loaded

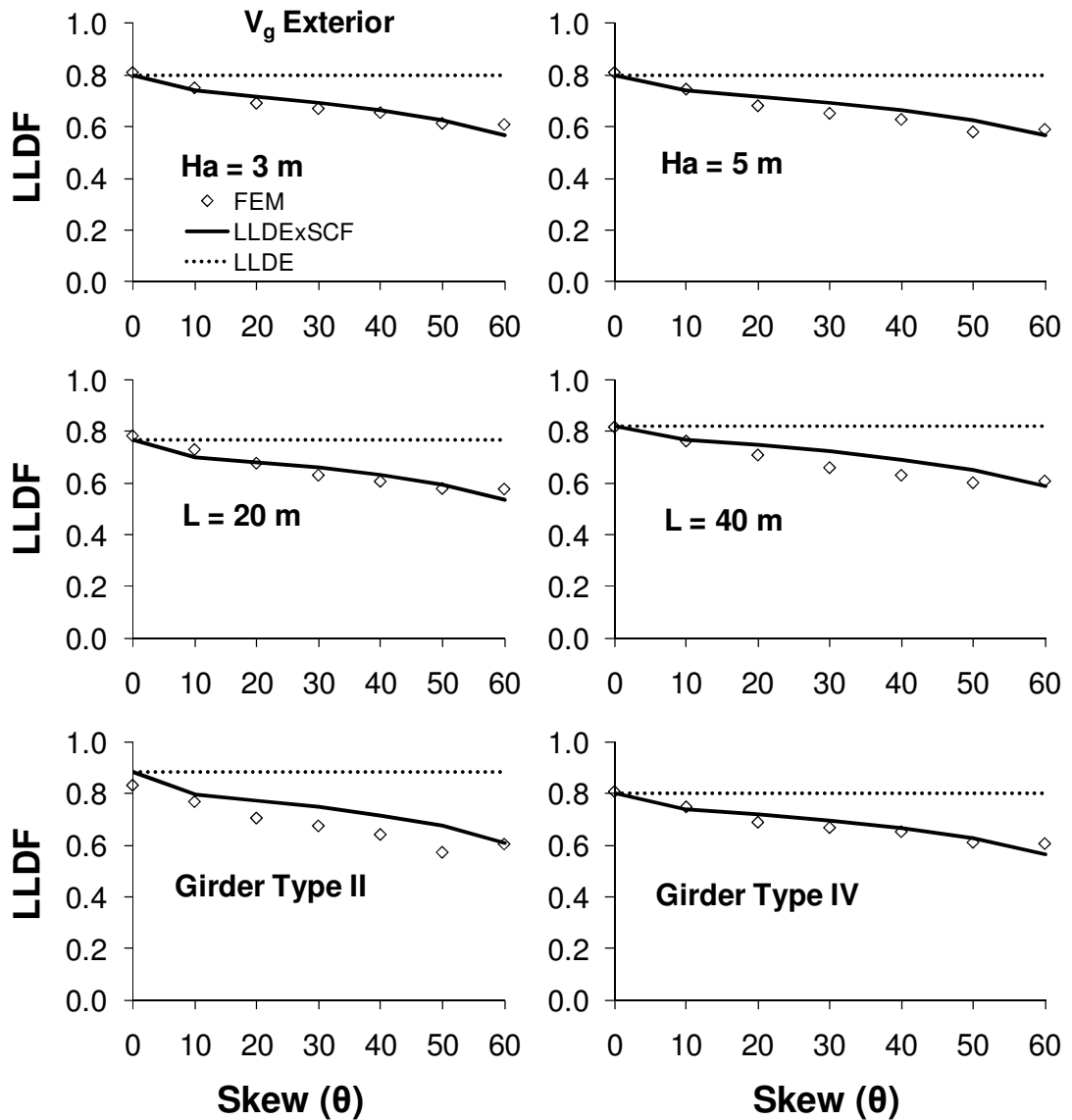


Figure 76. Plot of FEAs results, LLDEs and LLDEs multiplied by SCFs for exterior girder shear of selected models where two or more lanes are loaded

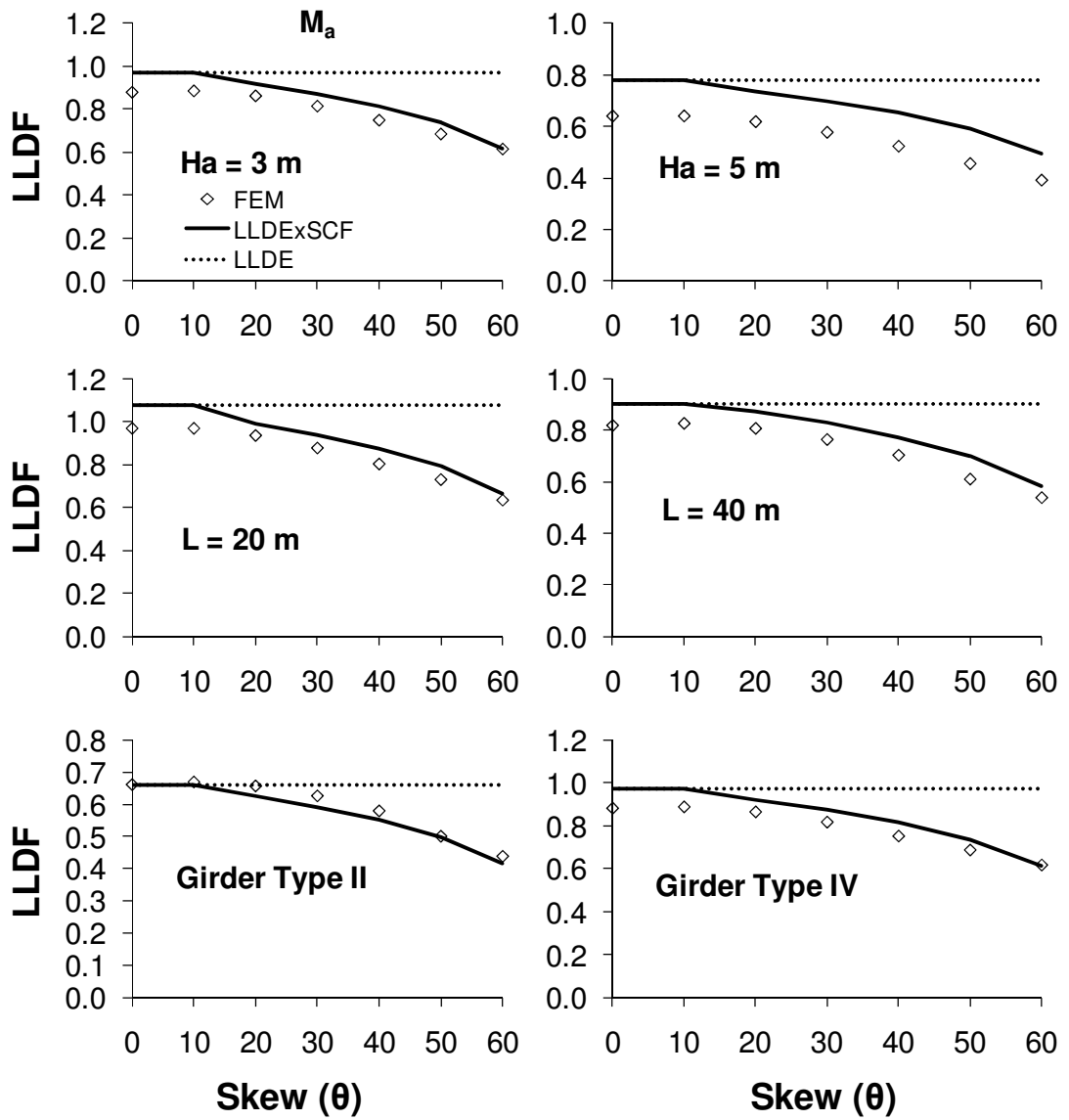


Figure 77. Plot of FEAs results, LLDEs and LLDEs multiplied by SCFs for abutment moment of selected models where two or more lanes are loaded

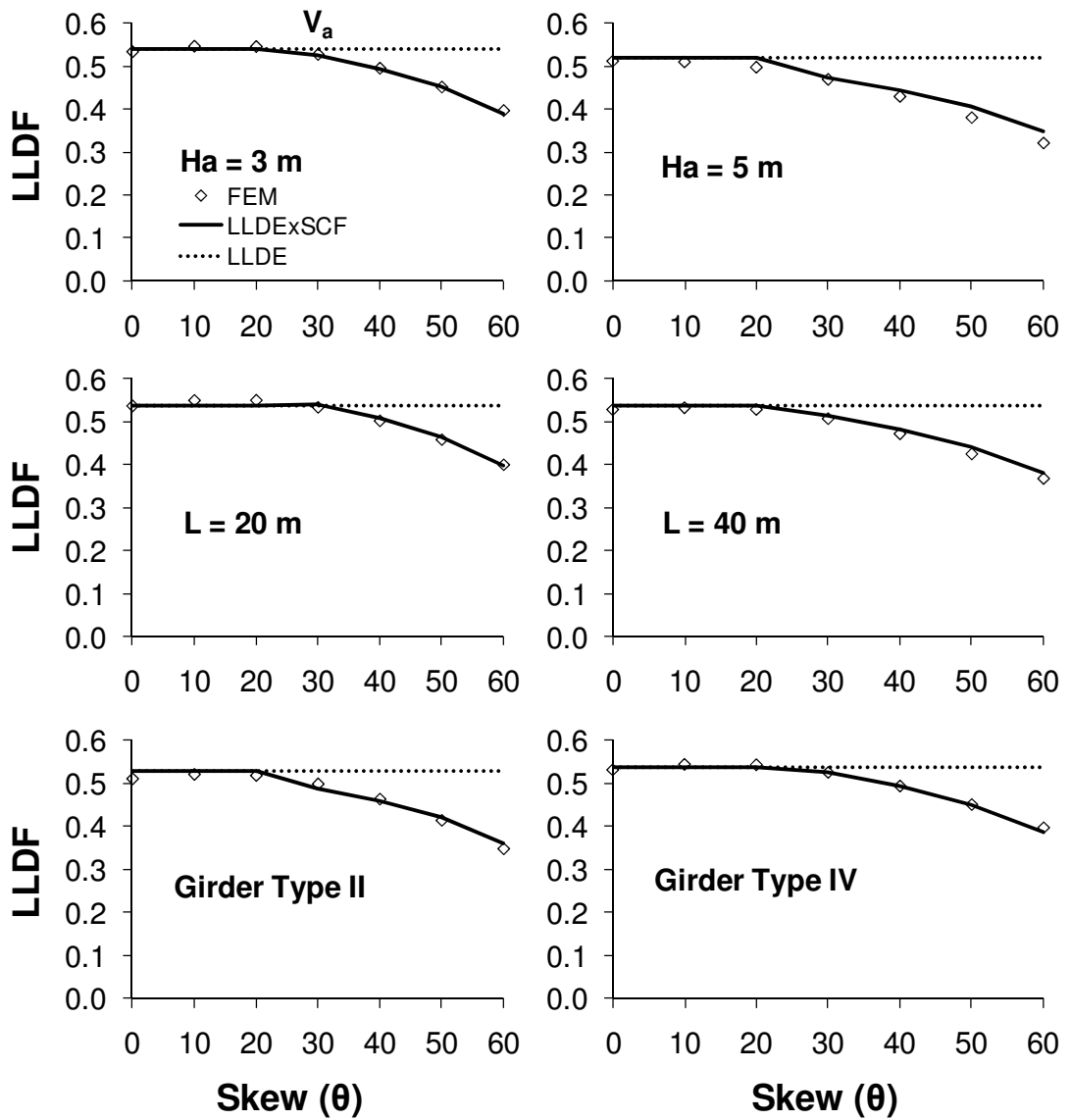


Figure 78. Plot of FEAs results, LLDEs and LLDEs multiplied by SCFs for abutment shear of selected models where two or more lanes are loaded

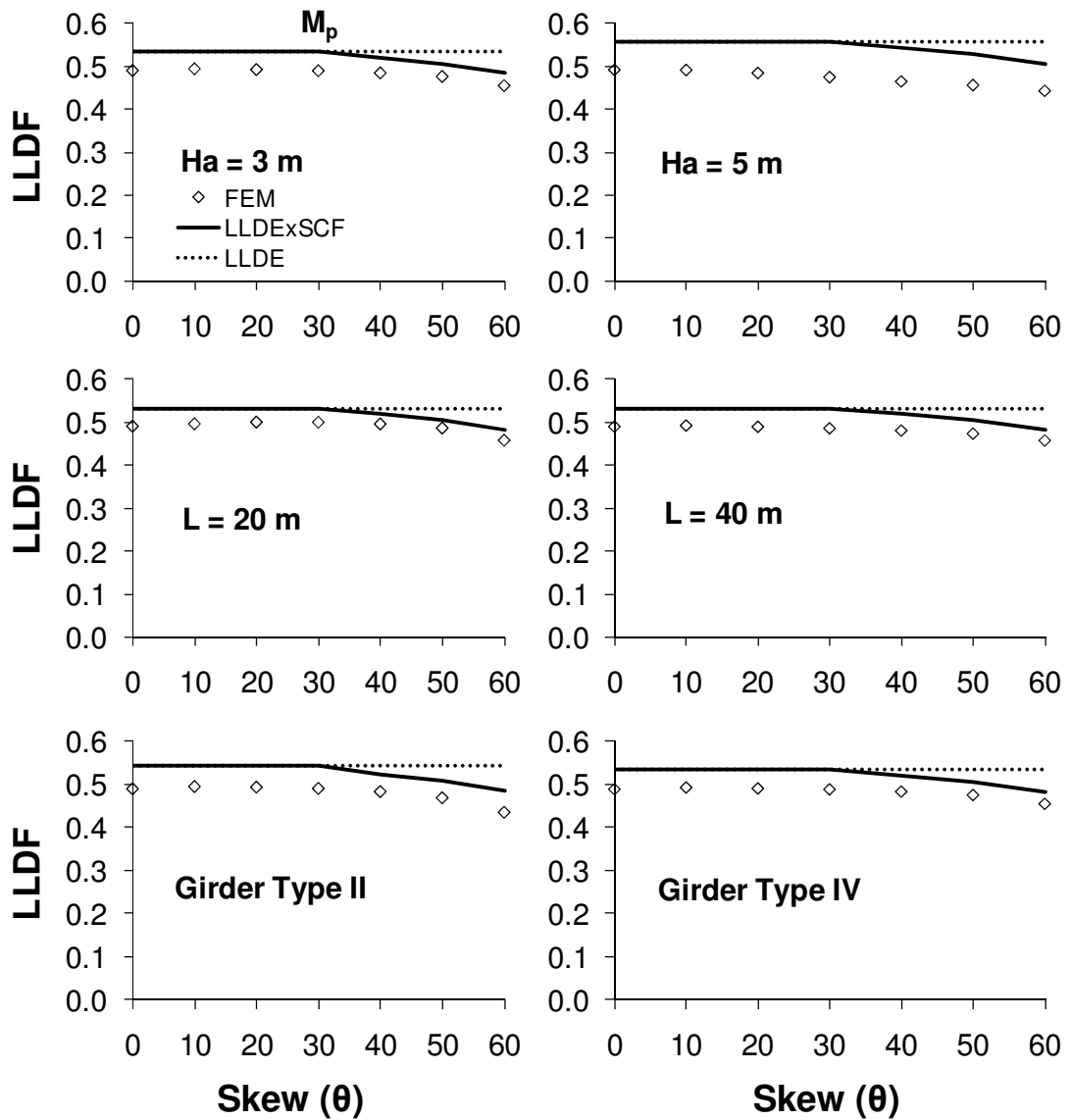


Figure 79. Plot of FEAs results, LLDEs and LLDEs multiplied by SCFs for pile moment of selected models where two or more lanes are loaded

## CHAPTER 7

### CONCLUSIONS

This research study is conducted to study the effect of skew on live load distribution in SIB components and to obtain SCFs for SIB girders and substructure components. Followings are the conclusions deduced from this research study:

1. The analyses results reveal that for the case of SIBs, different truck loading patterns arise when compared to conventional jointed bridges due to the presence of skew. Trucks, which are placed diagonally across the width of the bridge, are observed to produce the most unfavorable live load effects in bridge components.
2. It is observed that the effect of skew angle on LLDFs for exterior girder moment and pile shear is negligible both for the case where two or more design lanes are loaded and only one design lane is loaded. The effect of skew angle on LLDFs for interior girder shear for the case where only one design lane is loaded is also negligible.
3. The analyses results reveal that the effect of skew on the distribution of live load moment and shear is significant (excluding the above mentioned live load responses in the girders and piles). Skew generally tends to decrease live load effects in girders and substructure components of SIBs.
4. It observed that the LLDFs and hence, the SCFs for the interior girder moment, abutment moment and shear as well as pile moment are generally constant up to skew angles of 30°, 10°, 20° and 30°

respectively (i.e. skew has no effect on live load distribution). Beyond these skew angles the LLDFs and hence, the SCFs decrease as the skew angle becomes larger.

5. It is also noted that interior and exterior girder SCFs for live load shears for the case where two or more design lanes are loaded decrease nearly linearly as the skew angle increases for the range of skew angles considered.
6. It is observed that effect of bridge parameters, such as slab thickness and girder spacing, on LLDFs for girders and substructure components of SIBs becomes more pronounced as the skew angle increases.
7. SCFs are developed to accurately estimate the reduction in LLDFs for the girders and substructure components of SIBs as a function of the skew angle. The developed SCFs are compared with FEAs results and those of AASHTO, which are originally developed for conventional jointed bridges. This comparison revealed that the developed SCFs yield a reasonably good estimate of the reduction in live load effects in SIBs while AASHTO SCFs generally produce unconservative estimates of live load effects in SIB girders.

## REFERENCES

AASHTO (2007). American Association State Highway Transportation Officials Load and Resistance Factor Design Bridge Design Specifications. 4<sup>th</sup> Edition; Washington, D.C., USA.

ANSYS (2007). Computer-aided engineering design and analysis software. SAS IP Inc., Canonsburg, Pa.

Bakht B, Moses F (1988). Lateral distribution factors for highway bridges. Journal of Structural Engineering; 114(8): 1785-1803.

Barker RM, Puckett JA (1997). Design of highway bridges. John Wiley & Sons, New York.

Barr PJ, Eberhard MO, Stanton F (2001). Live-load distribution factors in prestressed concrete girder bridges. Journal of Bridge Engineering; 6(5): 298-306.

Brockenbrough RL (1986). Distribution factors for curved I-girder bridges. Journal of Structural Engineering; 112(10): 2200-2215.

Burke MP Jr (1988). Bridge deck joints. NCHRP Synthesis of Highway Practice, No 141. Transportation Research Board, National Research Council; Washington, D.C., USA

Burke MP Jr (1990a). Integral bridge design is on the rise. *AISC Modern Steel Construction*; 30(4): 9-11.

Burke, MP Jr (1990b). Integral bridges. *Transportation Research Record*, No 1275, Transportation Research Board, National Research Council, Washington, D.C., USA.

Burke, MP J (1994). Semi-Integral Bridges: Movements and Forces. *Transportation Research Record*, No 1460, Transportation Research Board, National Research Council, D.C., USA.

CHBDC (2006). *Canadian Highway Bridge Design Code*.

Cai CS (2005). Discussion of AASHTO LRFD load distribution factors for slab-on-girder bridges. *Pract. Period Struct Des Constr*; 10(3): 171-176.

Chen Y, Aswad A (1996). Stretching span capability of prestressed concrete bridges under AASHTO LRFD. *Journal of Bridge Engineering*; 1(3): 112-120.

Clough GM, Duncan JM (1991). *Foundation Engineering Handbook*. Second Edition Edited by Fang HY, Van Nostrand Reinhold, New York, USA.

Cook RD (1995). *Finite element modeling for stress analysis*. John Wiley & Sons. New York, NY.

Cross H (1930). Analysis of continuous frames by distributing fixed-end moments. *Proceedings of the American Society of Civil Engineers (ASCE)*: 919–928.

Dicleli M (2000). A rational design approach or prestressed-concrete-girder integral bridges. *Engineering Structures*; 22(3): 230-245.

Dicleli M (2005). Integral abutment-backfill behavior on sand soil - pushover analysis approach. *Journal of Bridge Engineering*; 10(3): 354-364.

Dicleli M, Albhaisi SM (2003). Maximum length of integral bridges supported on steel H-piles driven in sand. *Engineering Structures*; 25(12): 1491-1504.

Dicleli M, Albhaisi SM (2004). Performance of abutment-backfill system under thermal variations in integral bridges built on clay. *Engineering Structures*; 26(7): 949-962.

Dicleli M, Erhan S (2008a). Effect of superstructure-abutment continuity on live load distribution in integral abutment bridge girders. *Engineering Structures*. In-print.

Dicleli M, Erhan S (2008b). Effect of soil and substructure properties on live load distribution in integral abutment bridges. *Journal of Bridge Engineering*; 13(5): 527-539.

Dicleli M, Erhan S (2009a). Live load distribution equations for integral bridge substructures. *Engineering Structures*; 31(5): 1250-1264.

Dicleli M, Erhan S (2009b). Live load distribution formulas for single-span prestressed concrete integral abutment bridge girders. *Journal of Bridge Engineering*; 14(6): 472-486.

Dicleli M, Erhan S (2009c). Investigation of the applicability of AASHTO LRFD live load distribution equations for integral bridge substructures. *Advances in Structural Engineering*; 12(4): 559-578.

Dicleli M, Erhan S (2010). Effect of soil-bridge interaction on the magnitude of internal forces in integral abutment bridge components due to live load effects. *Engineering Structures*; 32(1): 129-145.

Duncan JM, Arsoy S (2003). Effect of bridge-soil interaction on behavior of piles supporting integral bridges. *Transportation Research Record*, No 1849, Transportation Research Board of the National Academies: 91-97

Evans LT (1982). Simplified analysis of laterally loaded piles. Ph.D. Thesis; UC: Berkeley, California; 211.

Faraji S, Ting JM, Crovo DS, Ernst H (2001). Nonlinear analysis of integral bridges: finite element model. *J. Geotech. and Geoenv. Eng*; 127(5): 454-462.

Hays CO. Sessions LM. Berry AJ (1986). Further studies on lateral load distribution using a finite element method. *Transportation Research Record* 1072, Transportation Research Board: 6-24, Washington D.C.

Hindi R, Yousif Z (2006). Live load distribution factor for highway bridges based on AASHTO-LRFD and finite element analysis. *Proceedings of the Structures Congress*, ASCE: St. Louis (MI).

Husain I, Bagnariol D (1996). Integral abutment bridges. Report SO-96-01, Ontario Ministry of Transportation, St. Catharines, Ontario, Canada.

Imbsen RA, Nutt RV (1978). Load distribution study on highway bridges using STRUDL finite element analysis capabilities. Conference on Computing in Civil Engineering, New York.

Khan MA (2004). Modeling and seismic analysis of integral abutments. structures - building on the past: securing the future, Conference Proceeding Paper: 1-9.

Khodair YA, Hassiotis S (2005). Analysis of soil–pile interaction in integral abutment. Computers and Geotechnics, 32(3): 201–209.

Law SS, Bu JQ, Zhu XQ, Chan SL (2004). Vehicle axle loads identification using finite element method. Engineering Structures; 26(8): 1143-1153.

Mabsout ME, Tarhini KM, Frederick GR, Tayar C (1997). Finite element analysis of steel girder highway bridges. Journal of Bridge Engineering; 2(3): 83-87.

Mourad S, Tabsh SW (1999). Deck slab stresses in integral abutment bridges. Journal of Bridge Engineering; 4(2): 125-130.

Mourad S, Tabsh SW (1998). Pile forces in integral abutment bridges subjected to truck loads. Transportation Research Record, No 1633: 77-83, Transportation Research Board of the National Academies.

Newmark NM (1948). Design of I-beam bridges. J. Struct. Div.; 74(1): 305-330.

Patrick MD, Huo XS, Puckett JA, Jablin M, Mertz D (2006). Sensitivity of live load distribution factors to vehicle spacing. *Journal of Bridge Engineering*; 11(1): 131-134.

Puckett JA, Huo XS, Patrick MD, Jablin MC, Mertz D, Peavy MD (2005). Simplified live load distribution factor equations for bridge design. *Transportation Research Board of the National Academies, Special Volume 11-S*: 67-78.

SAP2000 (2007). *Integrated finite element analysis and design of structures*. Computers and Structures Inc.; Berkeley (CA).

Skempton AW (1951). The bearing capacity of clays. *Building Research Congress; Division I, Part 3*: 180-189.

Soltani AA, Kukreti AR (1992). Performance evaluation of Integral abutment Bridges. *Transportation Research Record, No 1371*: 17-25, *Transportation Research Board, National Research Council, Washington, D.C., USA*

Sriharan S, Werf JV, Abendroth RE, Wassef WG, Greimann LF (2005). Seismic behavior of a concrete/steel integral bridge pier system. *Journal of Structural Engineering*; 131(7): 1083-1094.

Steiger DJ (1993). Jointless bridges provide fuel for controversy. *Roads and Bridges*; 31(11):48-54.

Steinberg E, Sargand SM, Bettinger C (2004). forces in wingwalls of skewed semi-integral bridges. *Journal of Bridge Engineering*; 9(6): 563-571.

Tarhini KM, Frederick GR (1992). Wheel load distribution in I-girder highway bridges. *Journal of Structural Engineering*; 118(5): 1285-1295.

Westergaard HM (1930). Computation of stresses in bridge slabs due to wheel loads. *Public Roads*; 11(1): 1-23.

Wolde-Tinsae AM, Klinger JE, Mullangi R (1988a). Bridge deck joint rehabilitation or retrofitting - Final Report. Department of Civil Engineering; Maryland University, College Park, MD, USA.

Wolde-Tinsae AM, Klinger JE, White EJ (1988b). Performance of jointless bridges. *asce journal of performance of constructed facilities*: 111-128.

Yalcin OF, Dicleli M (2009). Comparative Study on the Effect of Number of Girders on Live Load Distribution in Integral Abutment and Simply Supported Bridge Girders, *Engineering Structures*, under review.

Yousif Z, Hindi R (2007). AASHTO-LRFD live load distribution for beam-and-slab bridges: Limitations and applicability. *Journal of Bridge Engineering*; 12(6): 765-773.

Zhang Y, Cai CS (2007). Load distribution and dynamic response of multi-girder bridges with FRP decks. *Engineering Structures*; 29(8): 1676-1689.

Zokaie T, Mish KD, Imbsen RA (1993). Distribution of wheel loads on highway bridges. Phase III; NCHRP Final Report 12-26 (2).

Zokaie T, Osterkamp TA, Imbsen RA (1991). Distribution of wheel loads on highway bridges. NCHRP 12-26, National cooperative highway research program; Washington D.C.

## APPENDIX

### A LLDEs for Straight Integral Bridges

#### A.1 LLDEs for Interior Girders

Girder Moment - Two or More Design Lanes Loaded:

$$LLDE_{IB} = \frac{S^{0.82}}{500L^{0.06}} \quad (26)$$

Girder Moment - One Design Lane Loaded:

$$LLDE_{IB} = \frac{3S^{0.72}}{500L^{0.13}} \quad (27)$$

Girder Shear - Two or More Design Lanes Loaded:

$$LLDE_{AASHTO} = 0.36 + \frac{S}{7600} \quad (28)$$

Girder Shear - One Design Lane Loaded:

$$LLDE_{AASHTO} = 0.2 + \frac{S}{3600} - \left( \frac{S}{10700} \right)^2 \quad (29)$$

#### A.2 LLDEs for Exterior Girders

Girder Moment - Two or More Design Lanes Loaded:

$$LLDE_{IB} = \frac{L^{0.09} S^{0.53} t^{0.06}}{80 K_g^{0.04}} \left( 0.5 + \frac{d_e}{5000} \right) \quad (30)$$

Girder Moment - One Design Lane Loaded:

$$LLDE_{IB} = \frac{L^{0.06} S^{0.45}}{18 t^{0.02} K_g^{0.04}} \left( 0.4 + \frac{d_e}{6000} \right) \quad (31)$$

Girder Shear - Two or More Design Lanes Loaded:

$$LLDE_{IB} = \frac{L^{0.10} S^{0.43} t^{0.03}}{14 K_g^{0.07}} \left( 0.4 + \frac{d_e}{3000} \right) \quad (32)$$

Girder Shear - One Design Lane Loaded:

$$LLDE_{IB} = \frac{2L^{0.05} S^{0.34}}{15t^{0.01} K_g^{0.04}} \left( 0.5 + \frac{d_e}{3000} \right) \quad (33)$$

### **A.3 LLDEs for Substructure**

Abutment Moment - Two or More Design Lanes Loaded:

$$LLDE_{IB} = \frac{S^{0.5} \cdot K_g^{0.2}}{7 \cdot N_b^{0.44} \cdot H_c^{0.25} \cdot L^{0.25} \cdot I_p^{0.08} \cdot \mu^{0.06} \cdot N_p^{0.06}} \quad (34)$$

Abutment Moment - One Design Lane Loaded:

$$LLDE_{IB} = \frac{S^{0.33} \cdot K_g^{0.3}}{2 \cdot N_b^{0.25} \cdot H_c^{0.3} \cdot L^{0.53} \cdot I_p^{0.08} \cdot \mu^{0.06} \cdot N_p^{0.08}} \quad (35)$$

Abutment Shear - Two or More Design Lanes Loaded:

$$LLDE_{IB} = \frac{S^{0.54}}{44 \cdot N_b^{0.54} \cdot H_c^{0.04}} \quad (36)$$

Abutment Shear - One Design Lane Loaded:

$$LLDE_{IB} = \frac{S^{0.52}}{90 \cdot N_b^{0.52} \cdot H_c^{0.02}} \quad (37)$$

Pile Moment - Two or More Design Lanes Loaded:

$$LLDE_{IB} = \frac{1}{66} \left( \frac{S}{N_b} \right)^{0.5} H_c^{0.05} \quad (38)$$

Pile Moment - One Design Lane Loaded:

$$LLDE_{IB} = \frac{1}{160} \left( \frac{S}{N_b} \right)^{0.5} H_c^{0.07} \quad (39)$$

Pile Shear - Two or More Design Lanes Loaded:

$$LLDE_{IB} = \frac{1}{60} \left( \frac{S}{N_b} \right)^{0.5} H_c^{0.04} \quad (40)$$

Pile Shear - One Design Lane Loaded:

$$LLDE_{IB} = \frac{1}{145} \left( \frac{S}{N_b} \right)^{0.5} H_c^{0.06} \quad (41)$$

#### **A.4 An Example for the Calculation of LLDF Including Skew Effects**

The reference model employed in this study used as an example to demonstrate the calculation of LLDF including skew effect (L=30 m, S=2.4 m, t=20 cm,  $\theta=60$ , detailed information can be found in Table 1). Corresponding 2-D view and 3-D plan view of the model is shown in Figure 10 (b) (not to scale). The interior girder moment, where two or more design lanes are loaded, is calculated in this example. Remaining component responses can be calculated with a similar procedure.

For the calculation of interior girder moment for straight IB, first, interior girder moment of 2-D model is obtained as 1725.38 kNm. Then, Eqn. 26 (LLDE developed by Dicleli and Erhan (2009a)) is used to calculate the corresponding LLDF for straight IB as 0.637.

$$LLDE_{IB} = \frac{S^{0.82}}{500L^{0.06}} = \frac{2400^{0.82}}{500 \times 30000^{0.06}} = 0.637$$

Then, the interior girder moment due to live load is obtained as the moment of a 2-D model multiplied by the LLDF and found as 1099.07 kNm.

$$M_{g-INT-3D} = M_{g-INT-2D} LLDE_{IB} = 1725.38 \times 0.637 = 1099.07 \text{ kNm}$$

Results of FEAs for this response is 1052.344 kNm which shows that the LLDE predicts the interior girder moment quite accurate. However, this

moment is only for straight IB. For the case of SIB, a SCF (Eqn. 24) is calculated as 0.907.

$$SCF_1 = \left( \frac{50}{61} - \frac{2}{25} \tan \theta \right) \left( \frac{N_b}{S} \right)^{0.04} K_g^{0.02} \quad \text{for } 30 < \theta \leq 60$$

$$\text{for } \theta = 60 \quad SCF_1 = \left( \frac{50}{61} - \frac{2}{25} \times \tan 60 \right) \left( \frac{4}{2400} \right)^{0.04} 6.07E + 11^{0.02} = 0.907$$

Then moment found for straight IB is multiplied with SCF to obtain the interior girder moment of SIB due to live load as 996.86 kNm.

$$M_{g-INT-3D-\theta=60} = M_{g-INT-3D} SCF_1 = 1099.07 \times 0.907 = 996.86 \text{ kNm}$$

Results of FEAs for this response is 919.58 kNm which shows that the LLDE and SCF predicts the interior girder moment quite accurate.